NAVAL POSTGRADUATE SCHOOL
Monterey, California

AD-A267 465

DTIC
SELECTED
JUL 27 1993
S B D

THESIS

EVALUATION OF SITE EFFECTS ON A
HIGH FREQUENCY DIRECTION FINDING
SINGLE SITE LOCATION SYSTEM

by

Gerasimos Dionisios Milatos

March, 1993

Thesis Advisor: Richard W. Adler

93-16786

REPORT DOCUMENTATION PAGE

Report Security Classification: Unclassified			1b Restrictive Markings			
Security Classification Authority			3 Distribution/Availability of Report			
Declassification/Downgrading Schedule			Approved for public release; distribution is unlimited.			
erforming Organization Report Number(s)			5 Monitoring Organization Report Number(s)			
Name of Performing Organization val Postgraduate School		6b Office Symbol *(if applicable)* EC/AB	7a Name of Monitoring Organization Naval Postgraduate School			
Address *(city, state, and ZIP code)* nterey CA 93943-5000			7b Address *(city, state, and ZIP code)* Monterey CA 93943-5000			
Name of Funding/Sponsoring Organization		6b Office Symbol *(if applicable)*	9 Procurement Instrument Identification Number			
Iress *(city, state, and ZIP code)*			10 Source of Funding Numbers			
			Program Element No	Project No	Task No	Work Unit Accession No
Title *(include security classification)* EVALUATION OF SITE EFFECTS ON A HIGH FREQUENCY DIRECTION FINDING SINGLE SITE LOCATION STEM						
Personal Author(s) MILATOS, Gerasimos Dionisios						
Type of Report ster's Thesis		13b Time Covered From To	14 Date of Report *(year, month, day)* March 1993		15 Page Count 128	
Supplementary Notation The views expressed in this thesis are those of the author and do not reflect the official policy or position the Department of Defense or the U.S. Government.						
Cosati Codes			18 Subject Terms *(continue on reverse if necessary and identify by block number)* Single Site Location systems, ionospheric propagation, High Frequency Direction Finding			
d	Group	Subgroup				

Abstract *(continue on reverse if necessary and identify by block number)*

An important resource for Signal Intelligence activity in High Frequency Direction Finding (HFDF) is the use of Single Site :ation (SSL) systems. Present research and development is aimed at developing tactical, mobile, easy to deploy SSL systems for ating hostile transmitters. These systems can detect, determine azimuth and elevation angles of incoming signals, and using ospheric height information can calculate emitter location. The success or failure of SSL systems is dependent on many ferent factors, some of which are associated with site effects. System operation over different ground parameters can affect : accuracy of locating emitters. In this thesis, the performance of an "X"-shaped interferometer HF SSL system is examined ng the Numerical Electromagnetic Code (NEC). Performance in the presence of two different types of lossy ground conditions : investigated.

)istribution/Availability of Abstract unclassified/unlimited __ same as report __ DTIC users	21 Abstract Security Classification Unclassified	
Name of Responsible Individual hard W. Adler	22b Telephone *(include Area Code)* (408) 656-2352	22c Office Symbol EC/AB

'ORM 1473,84 MAR   83 APR edition may be used until exhausted   security classification of this page

All other editions are obsolete   Unclassified

Evaluation of Site Effects on a
High Frequency Direction Finding
Single Site Location System

by

Gerasimos Dionisios Milatos
Lieutenant, Hellenic Navy
B.S.E.E., Hellenic Naval Academy, 1984

Submitted in partial fulfillment
of the requirements for the degree of

MASTER OF SCIENCE IN ELECTRICAL ENGINEERING

from the

NAVAL POSTGRADUATE SCHOOL
March 1993

Author: _____
Gerasimos Dionisios Milatos

Approved by: _____
Richard W. Adler, Thesis Advisor

_____
Wilbur R. Vincent, Second Reader

_____
Michael A. Morgan, Chairman
Department of Electrical and Computer Engineering

ii

ABSTRACT

An important resource for Signal Intelligence activity in High Frequency Direction Finding (HFDF) is the use of Single Site Location (SSL) systems. Present research and development is aimed at developing tactical, mobile, easy to deploy SSL systems for locating hostile HF transmitters. These systems can detect, determine azimuth and elevation angles of incoming signals, and using ionospheric height information can calculate emitter location. The success or failure of SSL systems is dependent on many different factors, some of which are associated with site effects. System operation over different ground parameters can affect the accuracy of locating emitters. In this thesis, the performance of an "X"-shaped interferometer HF SSL system is examined using the Numerical Electromagnetics Code (NEC). Performance in the presence of two different types of lossy ground conditions are investigated.

DTIC QUALITY INSPECTED 3

Accession For		
NTIS CRA&I	☑	
DTIC TAB	☐	
Unannounced	☐	
Justification		
By		
Distribution/		
Availability Codes		
Dist	Avail and/or Special	
A-1		

TABLE OF CONTENTS

LIST OF TABLES

LIST OF FIGURES

I. INTRODUCTION

A. OVERVIEW

Passive electronic warfare (EW) examines spectrum use by hostile emitters and exploits their emissions to provide intelligence about emitter locations and capabilities. Electronic support measures (ESM) accomplish search, interception, location, and identification of hostile radiations.

Radio direction finding (DF) is the part of ESM whose goal is to fix the geographical position of a targeted transmitter. The most common DF technique uses more than one DF station and employs azimuth triangulation. An ideal DF system is capable of measuring both azimuth and elevation angles of arrival of incoming signals, using the smallest possible number of stations.

Once the propagation path and ionospheric height are known and azimuth and elevation angles measured, it is possible to determine the location of an emitter using a single DF station. This technique is called Single Site Location (SSL).

A simplified SSL analysis uses vertical triangulation and a mirror-like ionospheric reflecting surface at an assumed or measured height. Each of the above assumptions have inherent sources of error [Ref. 11:p. 61]. Incorrect angle of arrival

(AOA) measurements, misidentification of the path, or inaccurate ionospheric parameters produce estimation errors in emitter location. Multipath transmission and DF site errors add to these errors.

This thesis investigates the effects of inter-element mutual coupling and finite ground on the accuracy of a specific Navy Single Site Location system. The Numerical Electromagnetics Code (NEC-3) is used to calculate errors from these sources.

B. DIRECTION FINDING TECHNIQUES

The function of a direction finding system is to determine the direction of arrival of an incident signal relative to the coordinates of the High Frequency Direction Finding (HFDF) site. Using a network of at least three DF stations, it is possible to determine emitter location to within an acceptable error (using the horizontal triangulation technique).

A general assumption in DF systems is that the received field exhibits far-field plane-wave behavior with linear polarization. In reality, incident fields are often non-planar with phase-front distortion caused by multipath and scattering.

Typical DF system techniques assume that only a single signal source is received. Because of multipath ionospheric propagation, wave scattering by objects close to the DF site, or co-channel transmitting stations, signals from multiple

2

paths and sources are often received at DF sites. A DF system designed to handle one source at a time can work in a multiple source environment if other signals are well separated in frequency, time, or direction of arrival. In practice, DF stations often receive signals from several sources in the same frequency range, at the same time, and from many different angles of arrival [Ref. 20:pp. 281-290]. To resolve multicomponent wavefields, modern techniques of spectral estimation methods are used. These methods include linear prediction, maximum likelihood, eigenanalysis, and maximum entropy techniques. [Ref. 19:p. 985]

There are five different basic DF techniques for determining angle of arrival (AOA): a) relative amplitude, b) relative phase, c) time of arrival, d) Doppler, and e) correlation technique.

1. Relative Amplitude Technique

The relative amplitude method employs directional antennas whose patterns are rotated mechanically or electronically. Alternatively direct amplitude comparison can be obtained from multiple receivers. Accuracy depends on the directionality of antenna patterns. The major limitation of this technique lies in the ability to locate the required antenna system within the physical space available. Three different relative amplitude techniques [Ref. 14: pp. 13-18]

are used: a) rotatable antenna systems, b) rotatable fixed-pattern antenna systems, and c) instantaneous systems.

a. Rotatable Antenna Systems

In rotatable antenna systems, the antenna structure, hence the radiation pattern, is rotated mechanically. The line of bearing to the emitter is determined by the angular position of the antenna at maximum or minimum response. Rotatable antennas system have good sensitivity, but the bearing accuracy for sky waves is generally poor [Ref. 15: p. 9].

b. Rotatable Fixed-Pattern Antenna Systems

Rotatable fixed-pattern antenna systems use antennas too large to be mechanically rotated at the desired rate, so electromechanical or electronic rotation of the pattern is used. These systems have the advantage of rapid bearing acquisition but are relatively complex. They also suffer poor accuracy on sky waves [Ref. 15: p. 9].

c. Instantaneous Systems

Instantaneous systems employ multiple antennas and receivers in a direct amplitude comparison of the signal, using the overlapping directional patterns of the antennas. The line of bearing is determined by comparing the relative signal strength in each pattern [Ref. 15: p. 9].

2. Relative Phase Technique

Relative phase systems use at least two separated non-directional antennas and determine angle of arrival by comparing phase from two or more different array elements. This technique uses the fact that the incoming signal wavefront arrives at two different elements at different times, producing a phase difference in the signal received by these elements. A phase comparator measures these phase differences. The bearing accuracy depends on the d/λ, where d is the element's separation distance and λ is the wavelength. Relative phase techniques lead to ambiguous data unless the element separation is less than half a wavelength. The accuracy is reduced as distance between elements decreases. (More information on this method will be given in the next chapter).[Ref. 14: pp 18-19]

3. Time of Arrival Technique

The time of arrival technique is similar to the relative phase technique except that the measured parameter is time instead of phase. This method requires accurate time measurement of a given, well defined, modulation event at two or more locations and works best for pulsed signals above 1000 MHz. Its performance rapidly deteriorates below 300 MHz because of the difficulty in precisely locating the same modulation event at each antenna element [Ref. 2: p. 17].

4. Doppler Technique

Doppler is a short wavelength technique which requires a circular array of many wavelengths. It relies on the principle that a receiving system in motion, relative to the incident wave front, will produce an output which is a modulated representation of the original signal. If motion is simulated by commutation, this technique is called pseudodoppler DF and is based on sequential phase measurements from a circular array of fixed antennas switched to a common receiver. The extraction of frequency modulation information or doppler shift from the signal determines the angle of arrival (AOA). The large size of the antenna system prevents the use of this method for lower frequency applications [Ref. 14: pp. 21-22].

II. HF SINGLE-SITE-LOCATION DIRECTION FINDING

A. THE IONOSPHERE

The ionosphere, ionized layers of the earth's atmosphere, allows long range, over the horizon, skywave propagation. The ionosphere is composed of different gases which are ionized by extreme ultraviolet (EUV) light from the sun [Ref. 1:p. 17]. Because a large number of atoms of different gases are present and the intensity of EUV radiation varies with wavelength and altitude, the ionosphere is modeled as a series of four different layers. These layers are named D, E, F_1, and F_2. The variability of formative parameters affects the structure of the ionospheric layers. Five main variations must taken into account in order to predict HF propagation conditions:

a) Diurnal (variations which change throughout the day). The ionosphere during daytime is formed of D, E, F_1, and F_2-layers but during nighttime the D, E, and F_1-layers almost disappear.

b) Seasonal (variations which depend on the position of the sun). In winter months, exposure to the sun's rays is much different than in the summer, so the ionospheric structure changes continuously during the year.

c) Location has a considerable effect on the ionospheric structure. Two extreme cases are the equatorial and the polar regions.

d) Solar activity as described by sunspot number and solar flux also affects the ionosphere.

e) The altitude of the layers affects their behavior. The lowest layer is called the D-layer and occurs from 50-90 Km above the earth. It exists only during the daytime, responds quickly to the diurnal variation of the sun's movement, and is an absorptive layer for MF and HF signals [Ref. 11:p. 58]. The E-layer is between 90 and 130 Km above the earth's surface and supports short to medium range propagation. It occurs mainly during the day; its presence is negligible at night. During daylight it attenuates lower HF frequencies and supports ray bending. The F-layer supports most HF propagation, is 150 to 600 Km above the earth's surface and is divided in two layers, F_1 and F_2. At night the F_1-layer almost completely disappears, but the F_2 survives. The F_2-layer supports reflection for long range communications.

Two of the most important layer characteristics are virtual height and critical frequency. Virtual height is the distance between the surface of the earth and the level of the ionosphere at which the wave appears to be reflected. Virtual height can be determined from a wave transmitted vertically upward where it is reflected by the ionosphere and returned to the receiver. The critical frequency for an ionized layer is

8

the maximum frequency returned for vertical incidence. By measuring the time delay, T, it is possible to determine the altitude of the ionosphere where the reflection appears to take place. This distance is called virtual height h' and is determined by:

$$h' = c \cdot \frac{T}{2} \qquad \qquad \textbf{(1)}$$

where: c= speed of light in free space

T= time delay between transmission and reception.

Sounders are used to measure the critical frequency and altitude of each layer. Three types of sounders are: vertical incidence, oblique incidence, and oblique incidence backscatter sounders. Sounder output is a plot of reflection height vs. frequency, called an ionogram.

B. SINGLE STATION LOCATION

HFDF systems determine the location of unknown transmitters by measuring the angle of arrival of the incoming signal. There are two main categories of HFDF systems. In the first, systems measure only the horizontal angle of arrival, and determine only the azimuth bearing. A network of more than one DF station can determine the transmitter bearing and distance using triangulation.

In the second category, systems measure both azimuth and elevation angles of arrival and, using information about the

ionosphere in the midpath area, can determine the transmitter location (SSL systems).

Current SSL systems use vertical ionospheric sounders to identify different propagated modes and provide reasonably accurate emitter position estimations. Some SSL system options are: signal monitoring and acquisition, spectral windowing for the reduction of co-channel interference, and sensitivity thresholds for the prosecution of very weak signals. Additional features include target file systems and geographic displays, fully automatic data communication interfaces, and local or remote command centers for network operation.

The first SSL system was designed in 1924 by Appleton and Barnett [Ref. 16:p. 26], but modern SSL systems were developed after 1950. Modern systems were designed to improve traditional DF system accuracy at high elevation angles where horizontal triangulation was not always possible.

The classical SSL method for determining location assumes the mirror reflection of signals from a flat ionosphere over a flat earth as shown in Figure 1.

The ground range, is given from [Ref. 1: p. 167]:

$$RT = \frac{2 \cdot h}{\tan \beta} \qquad \textbf{(2)}$$
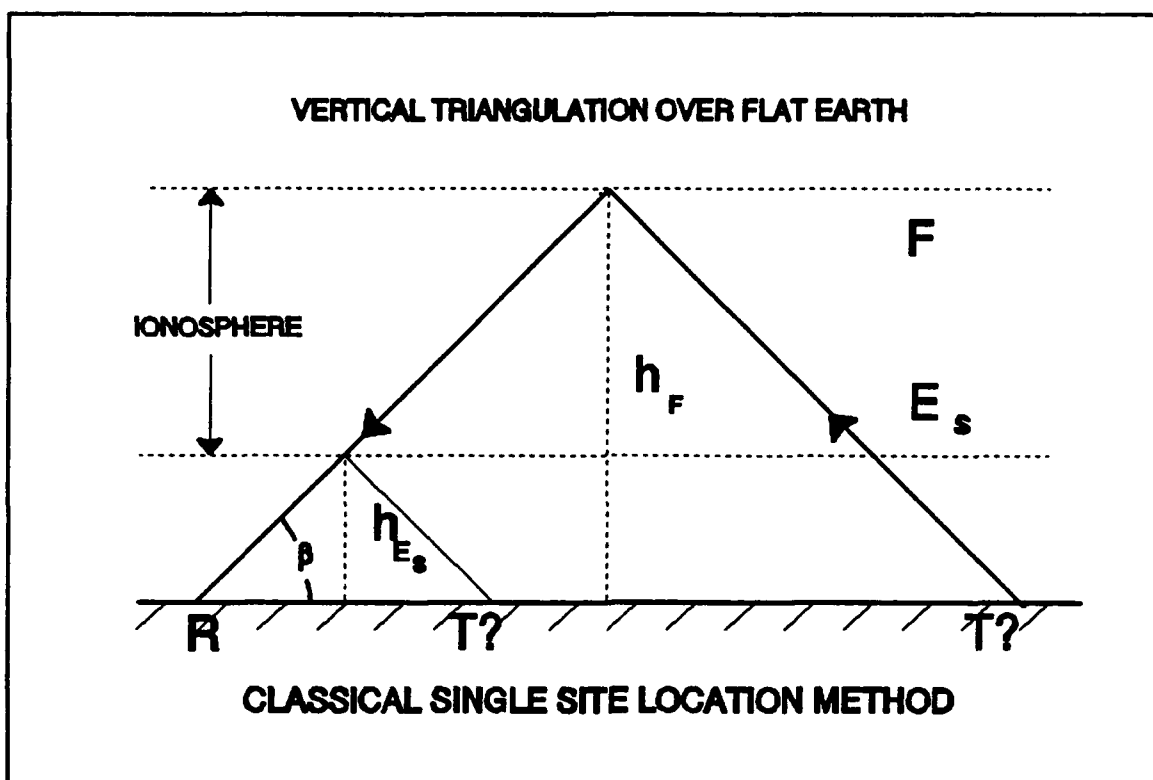
Figure 1. Classical Single Site Location Method.

where: RT = ground range from receiver R to transmitter T

h = height of the ionosphere

β = elevation angle.

For accurate range prediction, it is important to know the height of the ionosphere. For vertical triangulation it is assumed that reflection takes place at an altitude which is equal to the virtual height, h'(f_v). Virtual height is obtained from a local vertical incident ionogram at the critical frequency f_v. The secant law used is defined as [Ref. 1: p. 167]:

$$f_v = \frac{f}{\sec\beta} \qquad (3)$$

11

where: f_v= equivalent vertical frequency

f= operating frequency

β= elevation angle.

For accurate SSL measurements it is necessary to include the effects of earth curvature, ray refraction in the atmosphere, and as much information as possible about the ionospheric structure. Some modern SSL systems obtain long-term worldwide ionospheric layer height from prediction programs. For real time reflection heights, vertical or oblique sounders are used.

For the SSL system described in this thesis, a vertical sounder can be used to obtain ionospheric information and for measuring angles of arrival, a phase interferometer is employed.

C. PHASE INTERFEROMETER

A phase interferometer is a direction finding system that uses a number of spaced identical antennas to determine the direction of arrival of the incoming signal by measuring the phase differences between two or more elements. By combining the angle information with ionospheric data, it is possible to determine the propagation path and the location of the transmitter.

Interferometers accept all signals incident on the array and analyze them using two different approaches. The first is wave front testing (WFT), which is economical and easy and is

12

most often used. It is useful only on single mode, or on quasi uni-modal propagation when one mode is much stronger than the others. The second approach, called wave front analysis (WFA), measures and analyzes complex voltages appearing on each antenna [Ref. 1:p. 150]. This method is more accurate, but the system is far more complicated, so is not as popular.

D. INTERFEROMETER OPERATION

Antennas used in phase interferometers are generally omni-directional, vertical monopoles, or circularly polarized crossed loops. The crossed loops are used for short-range, low-frequency, high-elevation-angle circuits, and the monopoles for long-range, high-frequency, low-elevation-angle circuits. The line connecting two interferometer elements is called the baseline. If a system uses only two elements, it is called a single baseline interferometer; if it uses more than two, it is called a multiple baseline interferometer.

For a single baseline interferometer, the incident electric field at antenna 1 is [Ref. 5:p. 205]:

$$E_1 = E \cdot e^{j(\omega t - \kappa x)} \tag{4}$$

where: E_1 = incident electric field at antenna 1

E = magnitude of the electric field

$\kappa = 2\pi/\lambda$ = free space propagation constant

x = distance traveled by the wave.

13

The incident electric field at antenna 2 is:

$$E_2 = E \cdot e^{j(\omega t - kx - kd\cos\gamma)}$$ (5)

where: E_2 = incident electric field at antenna 2

E = magnitude of the electric field

d = distance between antenna 1 and 2

γ = angle between antennas' baseline and the ray path.
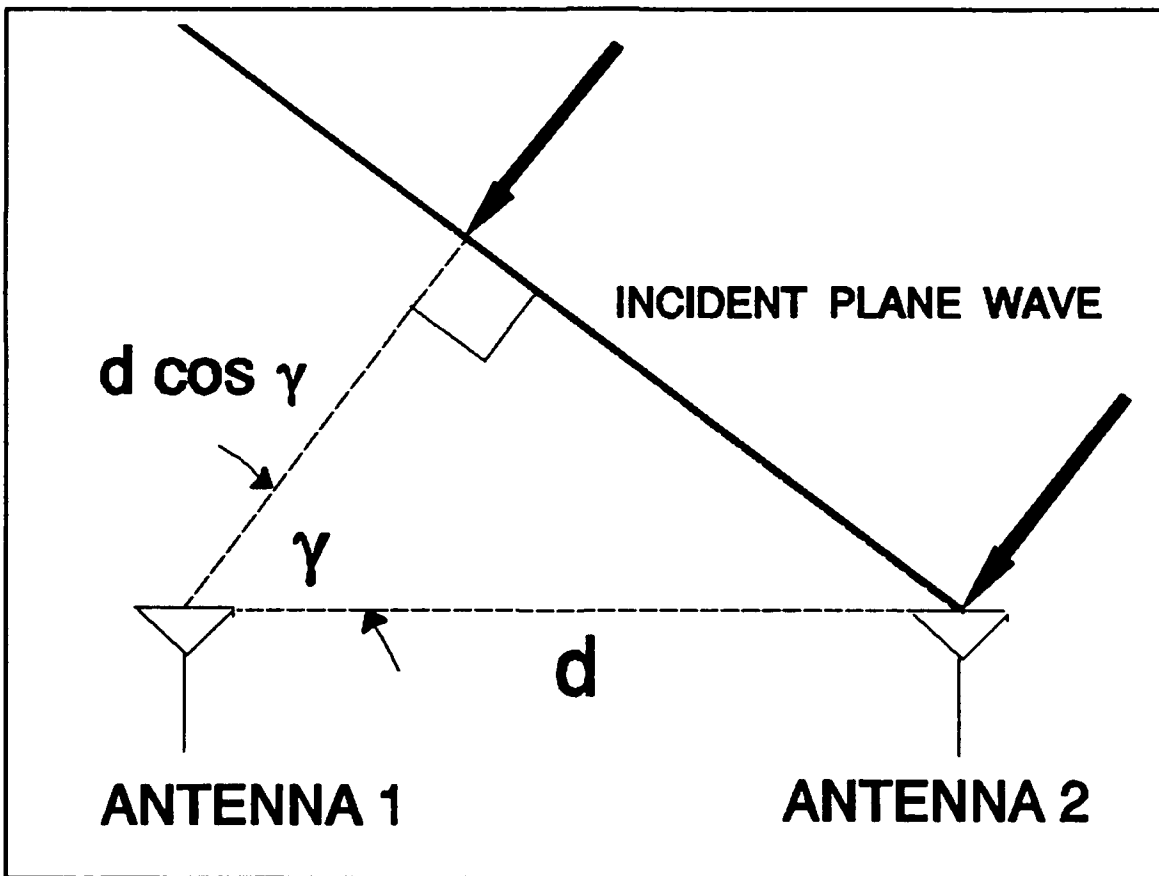
Figure 2. Two Element Interferometer.

The phase difference between antenna 1 and 2 is:

$$\Phi_{12} = \kappa \cdot d \cdot \cos\gamma \qquad\qquad (6)$$

where: Φ_{12} = phase difference between antenna 1 and 2

κ = free space propagation constant

d = distance between antennas 1 and 2

γ = angle between baseline and ray path.

From this equation the angle of arrival γ is given by:

$$\cos\gamma = \frac{\Phi_{12}}{\kappa \cdot d} = \frac{\Phi_{12}}{\frac{2\pi}{\lambda} \cdot d} \qquad\qquad (7)$$

where: λ = wavelength.

Fluctuations in the phase difference Φ_{12}, from moment to moment, produce corresponding fluctuations in the angle of arrival γ.

For a given angle of arrival γ, if the distance d increases, the effect of the phase difference measurement errors on Φ_{12} decreases, so the system accuracy increases. Also the number of ambiguities increase. The ambiguity problem is resolved by utilizing a more complicated array, with a number of additional elements between antenna 1 and 2. For a single baseline interferometer, when the antenna separation distance is more than half wavelength, an ambiguity of $\pm$ $\pi/2$ occurs, and if the distance becomes larger than one wavelength, the ambiguity becomes $\pm$ $n\pi$.

E. SSL INTERFEROMETER CONFIGURATIONS

For an SSL interferometer, a practical number of array elements is between nine and thirteen, and the array is most often an L, X, or T shaped orthogonal array. The spacing between the elements depends on desired coverage frequencies. Large element separation provides better frequency coverage of the HF band along with greater accuracy because of the narrow beamwidth and greater freedom from polarization and interference errors [Ref. 2:p. 121].

The L-shaped array interferometer is good for situations in which the general directions of transmitters are known with the array "V" opening pointing toward that direction. An L-shaped array has higher accuracy potential than the conventional cross, square, octagon and many other simple layouts, but it is not omni-directional. The X-shaped, or crossed interferometer, is a combination of two L-shaped interferometers, with nearly omni-directional coverage.

The system modeled in this thesis is an X-shaped orthogonal interferometer with nine array elements as shown in Figure 6. The center, or reference antenna and four outer antennas are used for phase measurements. Generally, the phase differences are in the form $n_i\pi+\Phi_i$, where Φ is phase difference between 0 and π, and the term $n\pi$ is the ambiguity in the measured phase difference. The use of four coarse antennas between the center and each one of the outer antennas resolves the ambiguity problem.

16

According to McNamara [Ref. 1:p. 150], for a three element interferometer which is shown in Figure 3, the angles of arrival of the incoming signal are:

$$\phi = \arctan\left[\frac{\Phi_{EW}}{\Phi_{NS}}\right] \tag{8}$$

$$K = \left[\frac{\lambda}{360 \cdot d}\right]^2 \cdot \left[\Phi^2_{NS} + \Phi^2_{EW}\right] \tag{9}$$

$$\Delta = \arctan\left[\sqrt{\frac{1}{K} - 1}\right] \tag{10}$$

where : ϕ = azimuth angle of the incoming wave

Δ = elevation angle of the incoming wave

Φ_{EW} = phase difference between antennas E-W

Φ_{NS} = phase difference between antennas N-S.

The elevation angle is measured upwards from the ground and the azimuth angle clockwise from the North.

F. ACCURACY

The accuracy of phase interferometer direction finding depends on many different factors, which are discussed in more detail in Chapters V and VI. The most important factors are:

a) antenna aperture size, b) instrument accuracy, c) ionospheric conditions, d) receiver S/N ratio, e) integration time, f) distance between transmitter and receiver, and g) ground characteristics.

17
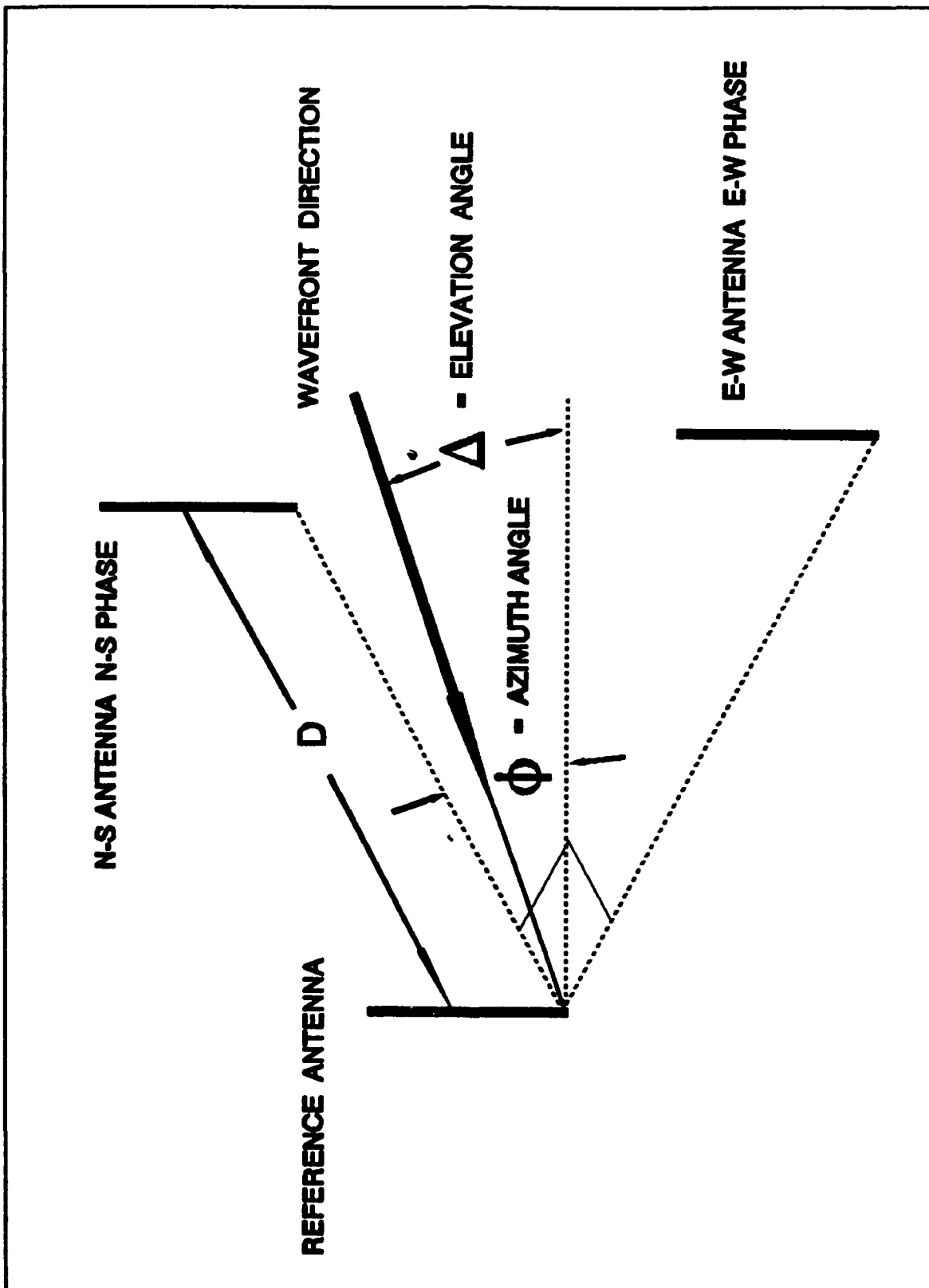
Figure 3. Three Element Interferometer.

18

III. NEC MODELING

A. BACKGROUND

The Numerical Electromagnetics Code was developed for analyzing the electromagnetic response of wire antennas and other metal structures in free space or over ground planes, using the Method of Moments. NEC combines an accurate integral equation for smooth, closed surfaces with one specialized to wires to provide for accurate modeling of a wide range of structures. A model may include nonradiating networks and transmission lines connecting parts of the structure, perfect or imperfect conductors, and lumped element loading. Also, the structure can be modeled over a ground plane that may be either a perfect or imperfect conductor [Ref. 3:pp. 1-2].

The excitation may be either voltage sources on the structure or an incident plane wave of linear or elliptic polarization. The output may include induced currents, charge density on wires, input impedance and admittance, input and radiated power, ohmic loss and efficiency, average and directive gain. Also it may include near electric or magnetic fields, maximum coupling for matched source and load, receiving patterns for antenna analysis, or scattering and EMP studies [Ref. 3:p. 1].

19

The integral equation approach in NEC is best suited to structures with dimensions up to several wavelengths. Three models are provided for structures over ground. First, a perfectly conducting ground is modeled by including the image field in the kernel of the integral equation. The second method, called Fresnel Plane Wave Reflection Coefficients Method, is fast but approximate for structures at least 0.1 to 0.2 wavelengths above the ground. The third method is called the Somerfield/Norton solution and is available only for wires. It uses the exact solution for the fields in the presence of ground, and requires an input file containing frequency and ground parameters. It also provides an accurate solution for elements above, below, or penetrating the ground. [Ref. 3:pp. 3-5]

B. HFDF SSL SYSTEM ANTENNA ELEMENT

The HFDF SSL system modeled in this thesis consists of nine identical model 632 sleeve monopoles. In a sleeve monopole the exterior acts as a radiating element and the interior of the sleeve acts as the outer conductor of the feed coaxial transmission line. Sleeve monopoles have wider bandwidth than ordinary monopoles, with the sleeve dimensions affecting the impedance more than the pattern. Current distributions depend not only on the overall length but on the position of the coaxial junction as well. The input impedance of the sleeve monopole with ground wires can be changed by

adjusting the length, inclination angle, and the position of the ground wires.

The input impedance properties of a sleeve monopole can be summarized [Ref. 24:pp. 1-7] as:

a) As the length of the exterior sleeve increases, the ratio l/λ increases, the input resistance of the sleeve antenna also increases and its reactance can change from capacitive to inductive.

b) The variation of input impedance can be decreased by connecting radial ground wires to the sleeve monopole. As the length of radials increase, the result is a larger input resistance and a more inductive reactance. The input impedance is very sensitive to the position of ground wires.

The shape of each monopole used in the SSL array is shown in Figure 4, and has the following characteristics:

a) Antenna type :   Sleeve monopole

b) Polarization :   Vertical

c) Frequency range :   2-32 MHz

d) Feed :   Type N 50 Ω input z

e) Size :   4 m in height

f) Base :   Adjustable tripod mount

g) Screen radials :   4 meter radials every 60^0
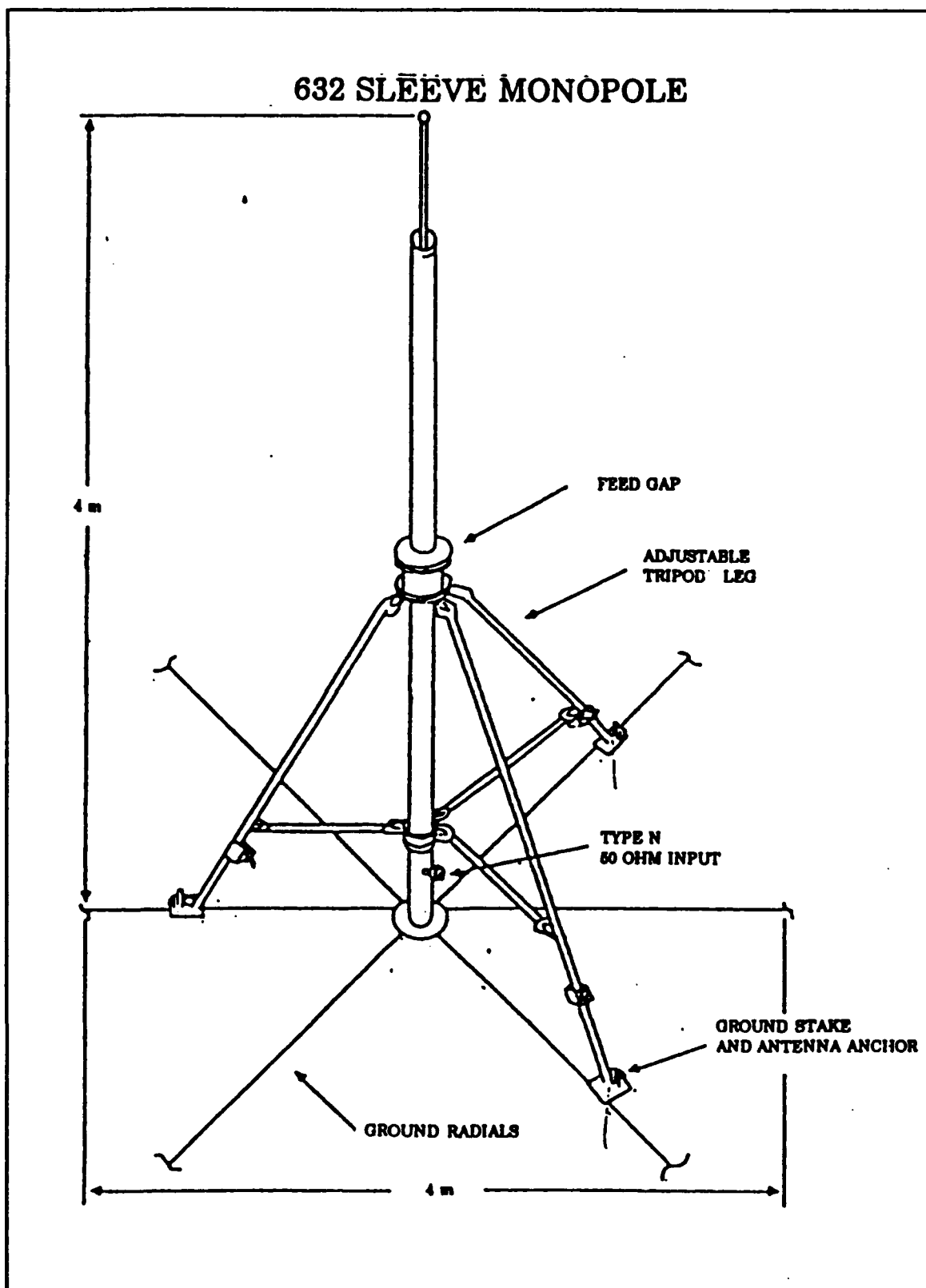
h) Radial wire diameter : 0.01 m.

Figure 4. Pictorial Drawing of 632 Sleeve Monopole.

22

C. COMPUTER ANTENNA ELEMENT MODEL DEVELOPMENT

The first step in developing the antenna array model is to define the geometry of the elements and their physical locations within the array. The second step, is selecting the length of the wire segments which form the antenna element within modeling guidelines of NEC.

The segment length Δ, should be less than about 0.1 λ at the desired frequency, but not less than about 10^{-4} λ [Ref. 3:p. 5]. The size of the segments determines the resolution when solving for the current on the model since the current is computed at the center of each segment.

The segment length limits were calculated for operating frequencies of 2-32 MHz while observing the constrains detailed above, and presented in the following Table I.

Table I. SEGMENT LENGTH LIMITS

FREQUENCY	WAVELENGTH	MAX. LENGTH	MIN. LENGTH
2 MHz	150.00 m	< 15.0 m	0.015 m
8 MHz	37.50 m	< 3.75 m	0.00375 m
16 MHz	18.75 m	< 1.875 m	$187.5 \cdot 10^{-5}$ m
32 MHz	9.375 m	< 0.9375 m	$93.75 \cdot 10^{-5}$ m

The accuracy of the numerical solution is dependent on the ratio of segment length to radius, Δ/a. For errors of less than 1% the ratio Δ/a must be greater than 8 and for the NEC model of the sleeve monopole, the smallest ratio used was $\Delta/a=9.36$, which gave good accuracy.

A large radius change between connecting segments may decrease accuracy, especially with a small Δ/a ratio. This problem may be reduced by making the radius change in steps over several segments [Ref. 3:p. 5]. Also, a segment is required at every point where a connection or a voltage source is located.

The element used in the NEC model was adjusted to meet all the above considerations for 2-32 MHz. The maximum segment length was 0.775 m which at 32 MHz was less than the guideline value of 0.1λ. The minimum segment length was 0.1013 m, which at 2 MHz was larger than the minimum acceptable value of $10^{-4}\lambda$. The NEC model of the sleeve monopole over finite ground with six, 4 meter underground radials, is shown in Figure 5.

D. HFDF SSL SYSTEM ANTENNA ARRAY

The DF array, consists of nine sleeve monopole antennas arranged in an "X" pattern on the site centerline, with $90°$ ($\pm 5°$) separation between each leg. A tenth or test antenna, is located on the site centerline 23.6 meters from the center of the array and is used for system calibration. The monopoles are connected to the mission complex by ten, 170 meter (557.7 ft.), phase matched ($\pm 3°$), RG-214 coaxial cables.

The array configuration is shown in Figure 6 and the associated NEC model is shown in Figure 7 [Ref. 17:pp. F1-16].

NUMERICAL MODEL OF SLEEVE MONOPOLE
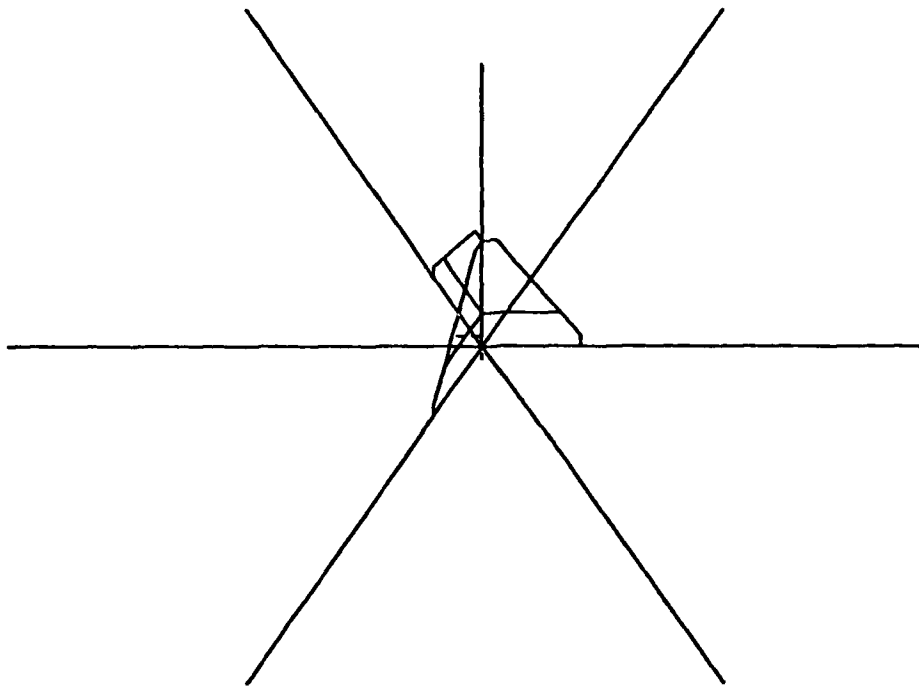
THETA = 35.00   PHI = 90.00   ETA = 90.00

Figure 5. Numerical Model of 632 Sleeve Monopole.

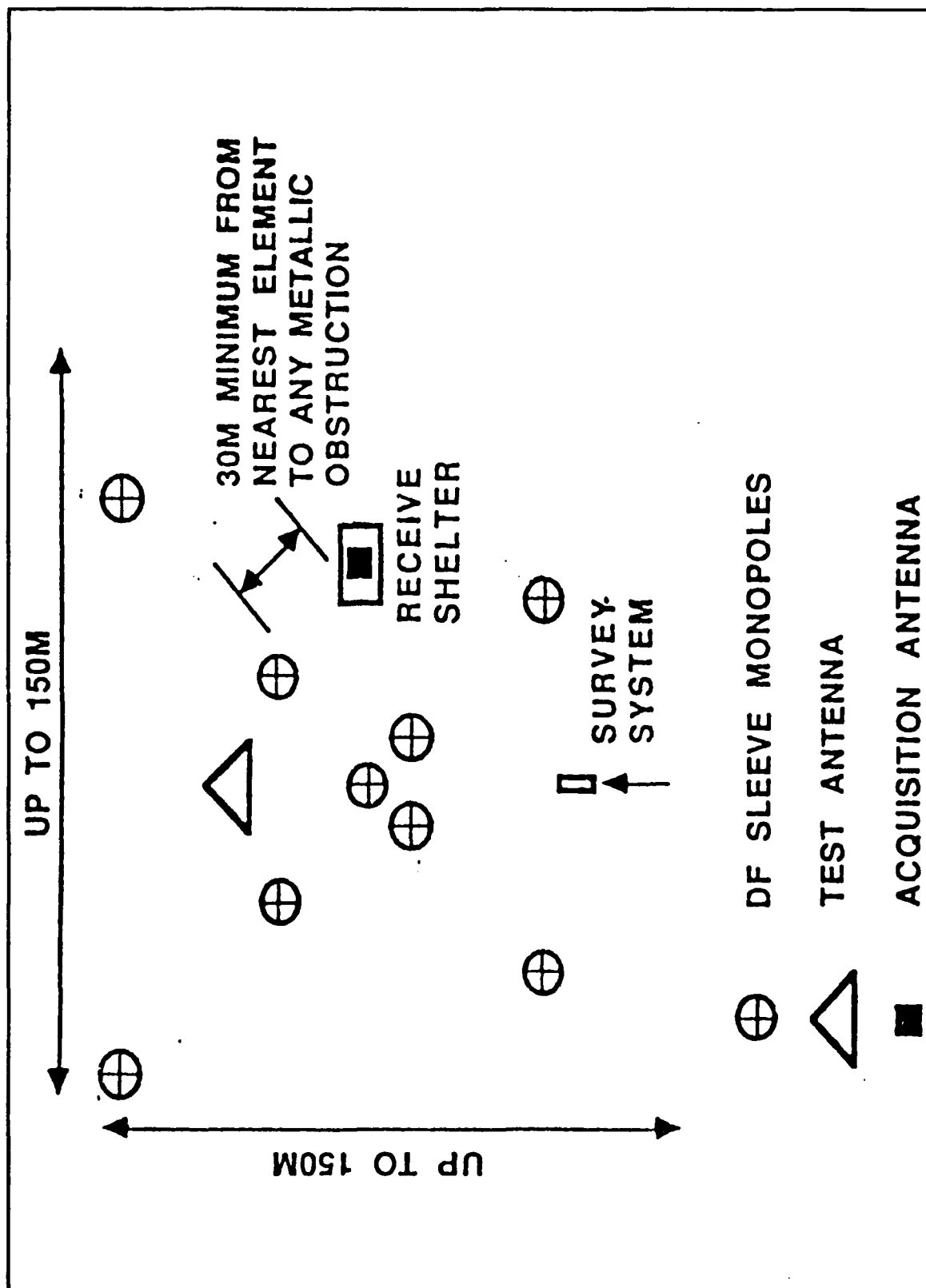**Figure 6.** DF Antenna Array Deployment Layout.

26

NUMERICAL MODEL OF SSL ARRAY

DISTANCES

1-2=1-3=4.5 m

1-4=1-5=13 m

1-6=1-7=37.8 m

1-8=1-9=104 m

$\phi = 0$

THETA = 0.00 PHI = 0.00 ETA = 0.00
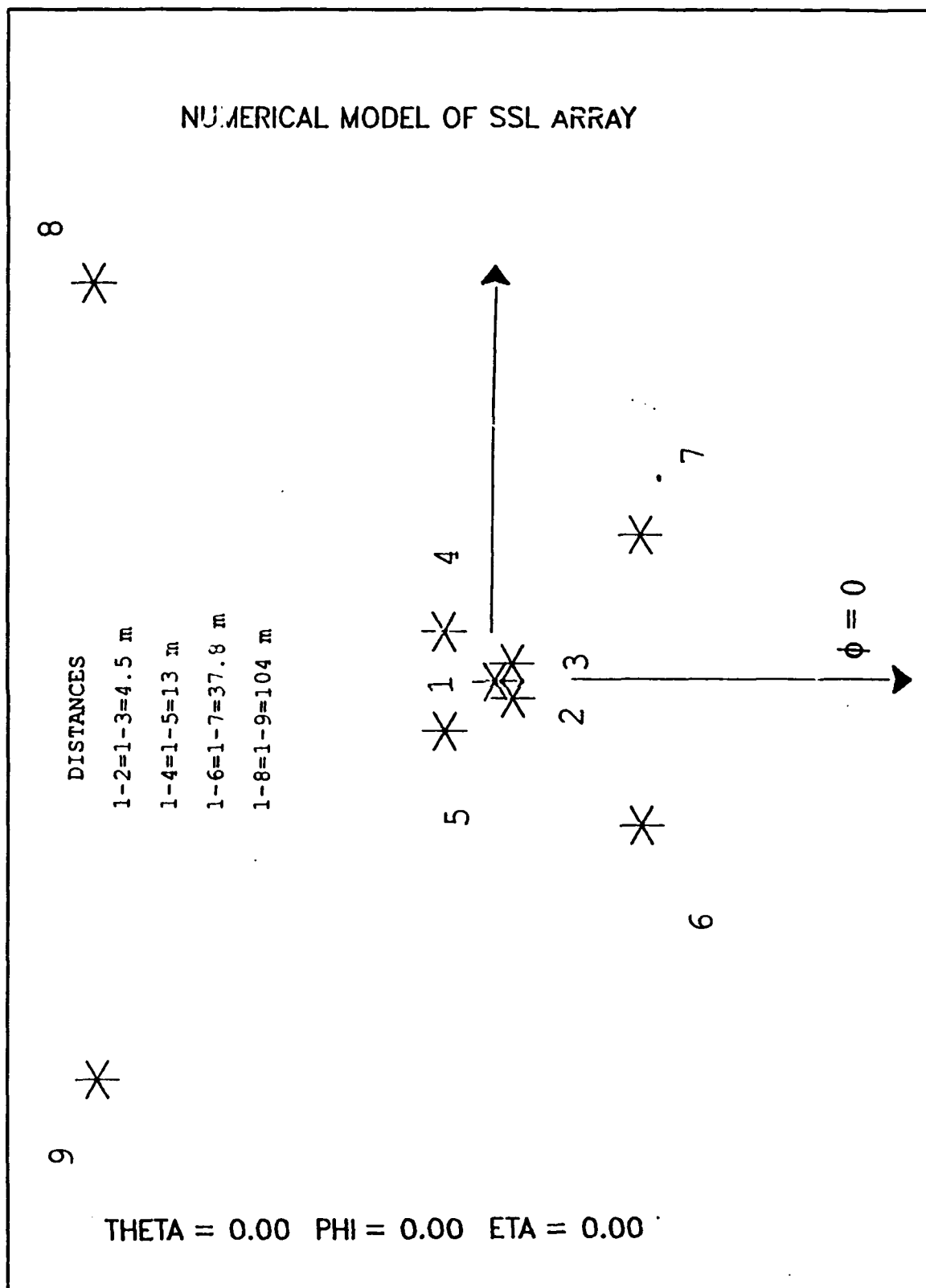
Figure 7. Numerical Model of SSL Antenna Array.

27

E. NUMERICAL MODEL OF SSL ARRAY

In addition to perfect ground, good and poor ground parameters (TABLE II) were used for receiving current calculations.

Table II. FINITE GROUND CONSTANTS

Ground	Relative Dielectric constant ϵ_r	Conductivity σ (S/m)
Good	30	0.01
Poor	5	0.001

The NEC dataset developed for the HFDF SSL antenna array is listed in Appendix C.

IV. PERFORMANCE OF THE ANTENNA

A. AVERAGE POWER GAIN

One parameter used to measure the validity of an antenna numerical model is the average power gain, defined as the antenna power gain per unit solid angle [Ref. 5:pp. 37-43]:

$$G_{avg} = \frac{P_F}{P_I} \qquad (11)$$

where:

G_{avg} = Average Power Gain

P_F = Total Radiated Power in the far field

$$P_F = \frac{r^2}{2} \lim_{r \to \infty} \int_{4\pi} Re[\vec{E} \times \vec{H}] \, \hat{r} d\Omega \qquad (12)$$

P_I = Input Power of the Antenna

$$P_I = \frac{1}{2} Re[V_I \cdot I_I^*] \qquad (13)$$

where: V_I = input voltage in volts and

I_I = complex conjugate of input current in amperes.

Lossless antennas in free space, radiate power in all directions of the far-field sphere. Antennas operated over perfect ground, radiate power only over half space. Thus for

29

antennas operating in free space, the average power gain should be 1, and for antennas operating over perfect ground, the average power gain should be 2.

Gain measurements over perfect ground for the sleeve monopole from 2 to 32 MHz were computed, and are presented in Figure 8 and Table XVI in Appendix B. The average power gain over perfect ground varied from 2.194 to 2.180, within ±10% of theoretical.
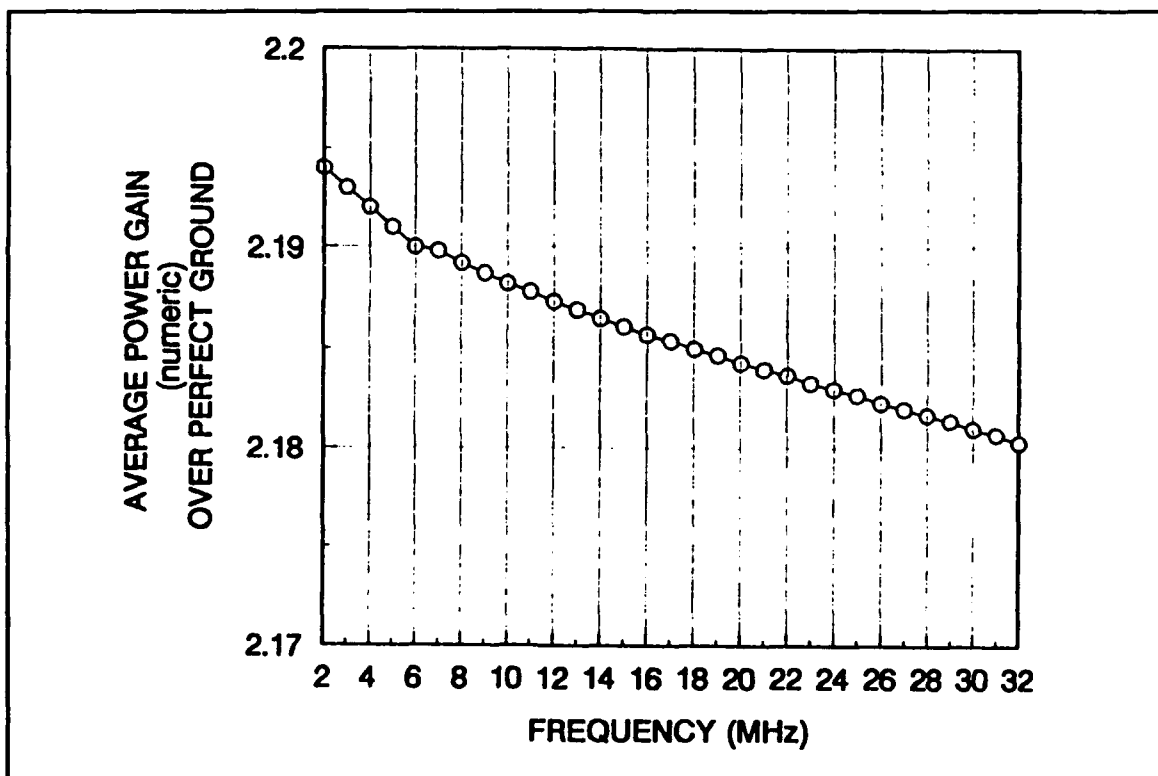

Figure 8. Average Power Gain vs Frequency Over Perfect Ground

For finite ground operation the above model was modified by the addition of six, 4 meter radial wires, 60° apart, forming a ground screen. The screen was placed 5" below the surface of the ground. The ground constants, shown in Table

30

II, were included in the Sommerfeld solution for NEC. The average power gain for lossy ground, was computed and the results for good and poor ground are presented in Figure 9 and numerically in Tables XVII and XVIII in Appendix B. The average power gain over good ground varied from 0.119 to 0.613, and from 0.014 to 0.335 over poor ground. This was expected because lossy ground was absorbing most of the incident power.
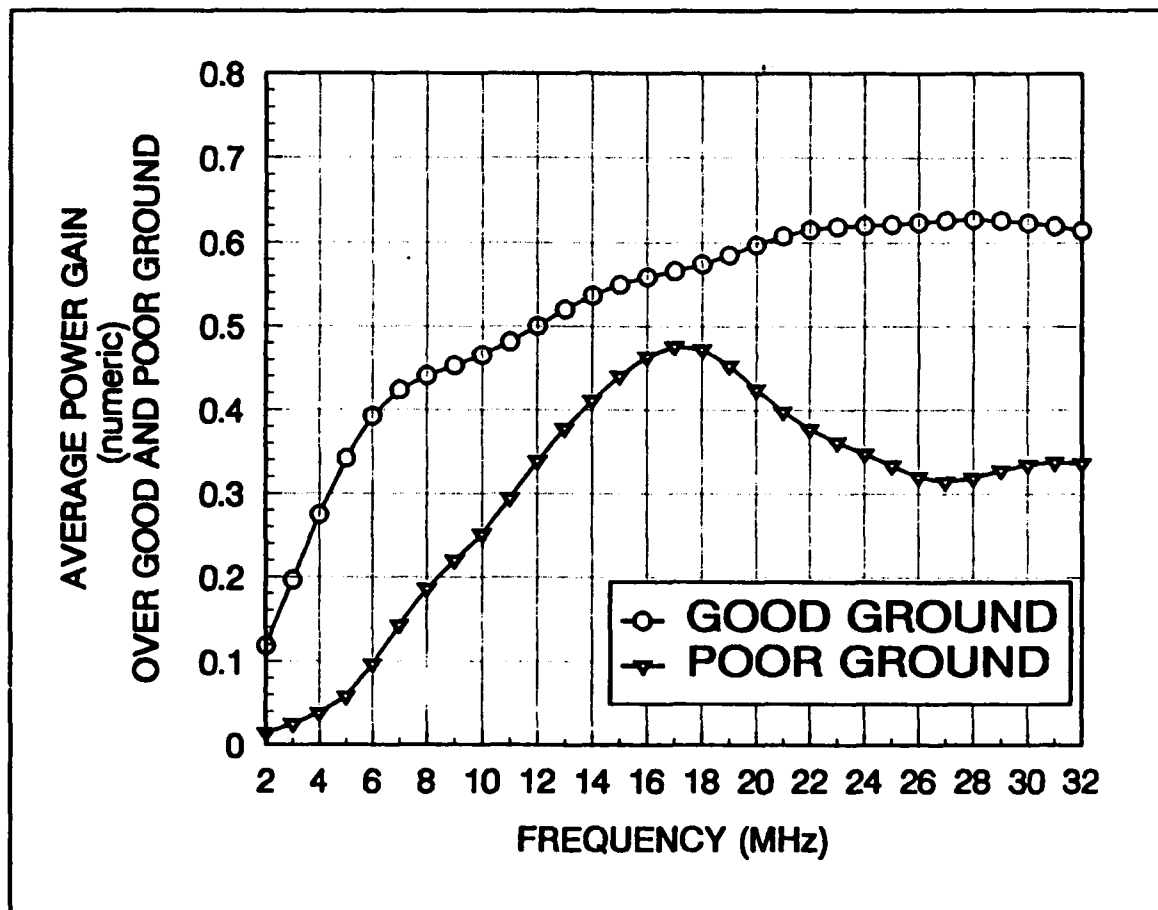

Figure 9. Average Power Gain vs Frequency Over Good and Poor Ground.

B. ANTENNA INPUT IMPEDANCE

For the model shown in Figure 4, the input impedance results for perfect, good, and poor ground, for the frequency range 2-32 MHz, are presented in Tables XIX-XXI in Appendix B. The input impedance varied considerably in all three cases, as frequency was varied, with high input reactance at long wavelengths where the monopole is electrically small.

Smith Chart displays of NEC-generated impedance for 2-32 MHz, over perfect, good, and poor ground are shown in Figures B-1, and B-3 in Appendix B. The normalization for impedance is 50 Ω. The input impedance data vary smoothly, with clockwise rotation, as frequency is increased over the operating range.

C. RADIATION PATTERNS

Azimuth and elevation radiation patterns were calculated for the sleeve monopole over perfect, good, and poor ground conditions, 2, 8, 16, and 32 MHz. The patterns are shown in Appendix B (Figures B-4 through B-9).

V. HFDF SSL ERRORS

Single Site Location System accuracy is affected by three kinds of errors. First there are errors in the measurement of the azimuth angle of arrival, (AAOA). The second kind of error is in the measurement of the elevation angle of arrival using vertical triangulation. This results in range estimation error, given a correct AAOA. The third kind is mutual coupling errors, instrumentation errors and imperfect ground effects [Ref. 8:pp. (39-24)-(39-31)].
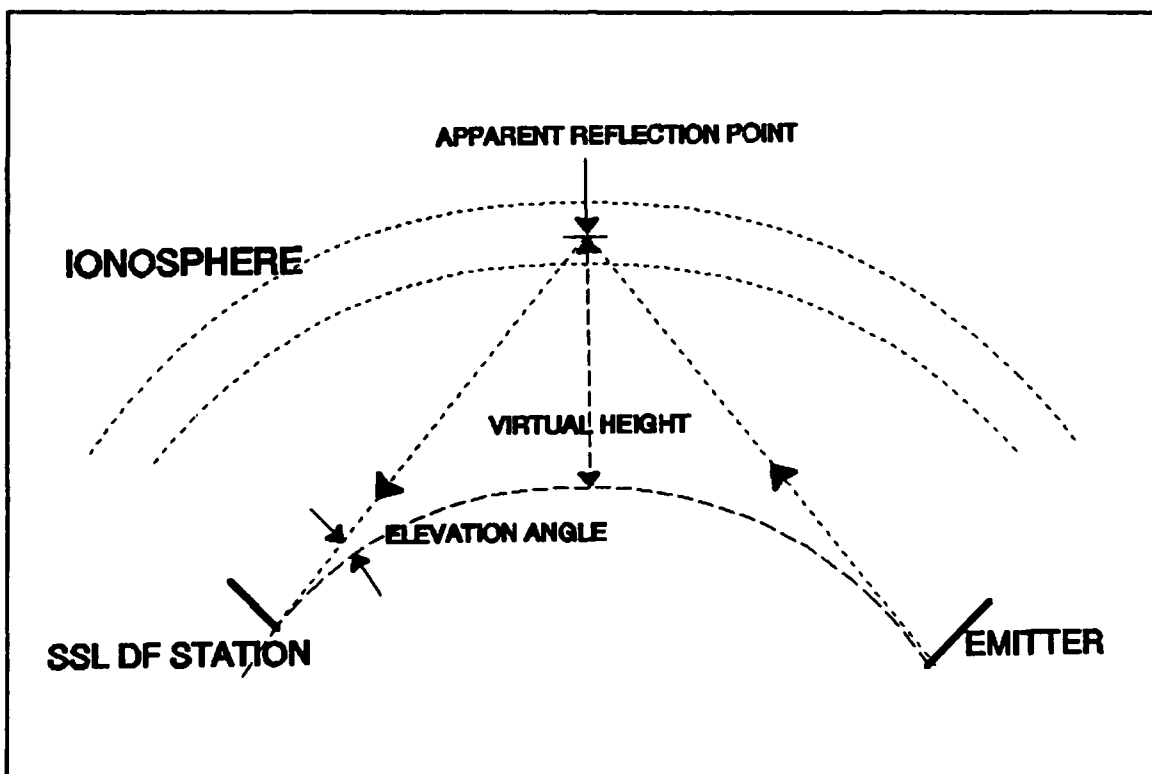

Figure 10. Vertical Triangulation (Single Station Location).

DF bearings are subject to both systematic and random errors. The magnitude of these errors depends on time of day, season, operator, and receiving equipment [Ref. 18:pp. 762-770]. There are two different types of systematic errors. First, is the systematic error whose value is known for each bearing observation and is fixed. The second type is error which is not known but affects all observations, for example, errors due to inaccurate calibration.

A. SSL BEARING AND RANGE ERROR

Angular error is the difference between the measured and the true direction of arrival of a signal transmitted from the target. It is divided into bearing and range error. Bearing error is defined as location error (perpendicular to measured azimuth), at the true distance [Ref. 8:p. 39-27]. SSL distance error is defined as range error at the true bearing.

SSL distance error depends on the elevation error and on the ability of the SSL system to trace the direction of the arriving ray backward through its zone of ionospheric refraction to the location of the transmitter. For distances greater than about 200 Km, (and a 300-Km ionospheric layer height) distance error is more sensitive to a given angle of arrival error than the bearing error [Ref. 8:p. 39-28].

Well-designed HFDF systems can measure elevation angles as accurately as azimuth angles except at very low elevation

angles. This is because the projected vertical aperture of most systems approaches zero.

SSL bearing and range errors are caused from: a) direction of arrival error, b) ionospheric error, and c) ray tracing algorithm errors.

1. Direction of Arrival Error

Direction of arrival error is caused by antenna pattern distortion, noise, and interference. Errors are also caused by unequal transmission line lengths, attenuation, and phase match of transmission lines between antennas and the SSL equipment.

For a well designed large aperture system, the total direction of arrival error should not exceed 0.1 to 0.5°. Direction of arrival error causes both bearing and range errors.

2. Ionospheric Effects Which Produce Errors

Certain ionospheric conditions affect both bearing and range errors. Examples are traveling ionospheric disturbances and ionospheric tilts, which occur with seasonal and hourly variation. Ionospheric induced errors vary with geographic location of an SSL site and change with bearing and range.

The path from the SSL system to the emitter is theoretically two straight lines in the same plane, with a reflection point at the ionosphere in the middle of the path, if the ionosphere is both spherical and geocentric. The

ionosphere consists of several non-spherical, ionized layers which change the incoming signal ray so the measured emitter position will be different from the true position.

Ionospheric effects which affect incoming waves fall into three categories: a) polarization rotation, b) multipath interference, and c) ionospheric tilts, however only ionospheric tilts affect SSL location errors.

The ionosphere is not always spherical but varies with geographical position, especially near sunrise and sunset. These distortions of the ionosphere are called "ionospheric tilts" [Ref. 6:pp. 273-295]. Tilts depend on layer and ray path geometry and cause bearing deviation of rays such that incoming signals do not arrive from a bearing angle along the great circle path. Tilts cause random errors which change slowly during several minutes, in both azimuth and elevation angles. Long-period observations of tilts can be summarized: i) at sunrise and sunset, frequencies which are affected most are near the MUF, ii) tilts at F-layer produce more severe errors than the tilts at the E-layer, and iii) single hop propagation paths suffer less error than multiple hop paths.

3. Ray Tracing Algorithm Errors

The ability of HFDF systems to trace the direction of the arriving ray backward to the emitter location, depends on the accuracy of ionospheric data, and the ray-tracing algorithm. Ray tracing errors affect the SSL range accuracy.

4. Mutual Coupling

In a DF system, antenna element mutual coupling can affect the values of relative phase observed between array elements. Because the relative phase is used to determine the angle of arrival of the incoming signal in an interferometer system, mutual coupling can result in angle-of-arrival errors.

Factors effecting mutual coupling between elements include: frequency, element separation, and geometry of elements, especially around the feedpoint [Ref. 6:pp. 92-93]. When an array system operates over a wide frequency range, mutual coupling effects can cause significant errors at low frequencies where electrical spacing is a minimum. Studies indicate [Ref. 2:p. 118] that element interaction is low if the spacing between elements is greater than 0.3λ. As the baseline in wavelengths increases the error decreases. When two adjacent elements are far enough from each other, the effect of mutual coupling can be negligible. The use of short monopoles or dipoles as array elements minimizes coupling effects. Empirical results indicate that the use of active couplers in an array can reduce currents created by mutual coupling between elements. Also, element interaction can be reduced by increasing element load impedance, but at a reduction in system sensitivity.

The magnitude of mutual coupling effects is not easily measured, but a good indication of the value can be obtained by measuring input impedance at each antenna terminal.

In an interferometer-based direction finding system (i.e. the nine element "X" shaped array used in this thesis), because of multiple baselines and different element separations, the bearing error due to mutual coupling cannot be ignored. The system operating frequency range is 2-32 MHz, so at 2 MHz, $D_{min} = 0.3\lambda = 45$ m. The distance between elements which are used for measuring phase differences (#1, #8, and #9) as shown in Figure 7, is $D_{18} = D_{19} = 104$ m $> D_{min} = 45$ m, and the interaction among these three elements is small. But even in this case the mutual coupling has to be taken into account, because there are four elements (#2, #3, #4, and #5) close to center antenna #1, and their presence affects the received phases at element #1.

5. Factors which Produce Site Errors

Site selection is one of the critical parameters in SSL systems accuracy. Site-induced errors affect the system accuracy more than equipment errors do. In practice it is found that over an oblique path corresponding to a range of 700 Km, azimuth bearings can be measured with an accuracy of about 1° while elevation angles can be measured within about 1.5° [Ref. 12:pp. 294]. Site effects can easily increase these minimums.

Site selection depends on many different factors as technical requirements, physical security of the operating system, and land availability [Ref. 11:p. 61].

There are two physical areas of interest in considering site errors [Ref. 12:p. 295]. The first area is close to the SSL array system (within a few hundred meters of the antenna) called the "near" site area. There is some corre tion between phase errors for close-spaced elements in the near site area, so the error in the observing direction is almost independent of the spacing. The second area extends from the DF system out to a distance of several kilometers where DF errors are due to random scattering of energy from reflections in this area. These are called "distant" site errors. Distant site errors cause random directional errors which vary with bearing angle, elevation angle and frequency.

Specific near and distant area site factors affecting SSL performance are [Ref. 11:p. 62]:

a. Terrain

a) The area surrounding the DF system should be flat for at least 100 meters beyond the HFDF array.

b) The site area should be higher than all the surrounding areas.

c) The soil should not be too rocky (for easy antenna and ground wire installation), and any vegetation should be short.

d) Site soil conductivity should be as uniform as possible to eliminate the requirement of installing extensive ground screen mats over the entire array area.

39

b. Obstructions

The horizon around a site should be clear of hills and mountains higher than 5° elevation angle. Urban structures must not project higher than the 5° elevation angle.

c. Local HF Transmitters and Noise Sources

The presence of strong local HF signals and nearby HF noise sources will degrade the performance of the DF system. Guidelines for minimum distances to these sources from the DF site are:

Table III. MINIMUM OBSTACLE DISTANCES FROM DF SYSTEMS

Obstacles	Distance
Scattered small buildings :	200 m
Scattered trees and vegetation :	200 m
Smoke stacks and water towers :	300 m
Wire fences :	300 m
Railroad tracks :	500 m
Shorelines :	1 Km
Cliffs :	2 Km
Overhead high-voltage power lines :	3 Km
Mountains or hills :	5 Km
5 KW HF transmitters :	20 Km
High-powered microwave and radar :	21 Km
10-40 KW HF transmitters :	25 Km

d. *Signal Path*

To prevent changes in the direction of arrival of signals the following must be considered:

a) Metal objects one-half wavelength or more at the highest frequency can act as signal re-radiators and distort incoming wavefronts, and must be eliminated.

b) Ground waves bend (refract) as they pass over boundaries with different conductivities, so the DF arrays should not be placed close to a shoreline.

e. *Site Installation Details*

a) If the DF site includes additional support system antennas such as communication antennas, or sounder antennas, those have to be installed at least 100 meters from the nearest DF array element.

b) Exact element spacing is important for proper DF operation so the antenna field layout must be according to designated dimensions to prevent errors.

VI. SITE EFFECTS ON HFDF SSL ERROR

A. CALCULATION OF SSL SITE EFFECTS USING NEC

In this thesis, both perfectly conducting and lossy ground conditions are used in the SSL array analysis in order to investigate the performance of the antenna system and to determine the amount of AOA (bearing and range) error introduced by different ground conditions.

The first step in developing the NEC array model was to define the geometry of one of the array elements. Then the model was evaluated over perfect ground. The average power gain and the element input impedance were calculated for 2-32 MHz. These results are given in Chapter IV and in Appendix B. The perfect ground study indicated the validity of the NEC model because the average power gains were close to the theoretical value of 2. The input impedance varied with frequency as expected, because the length of the sleeve monopole was small compared to a wave length.

The second step in modeling the array elements was the introduction of finite ground with a ground screen of six radials wires 5" under the ground. The finite ground calculations in NEC used the Sommerfeld solution. The patterns calculated for all grounds are shown in Appendix B.

42

The next step was developing the 9-element interferometer array, using the locations of Figure 7. Two array models were built, one over perfect ground and the second over finite ground. The NEC input data cards used for the finite ground model are listed in Appendix C, and the wire array model is shown in Figure 7.

The interferometer compares phases between two elements at a time and the center element of nine (#1) was selected as the reference antenna. The distances between the reference antenna and each one of the other eight are called interferometer baselines as explained in Chapter II and listed in Table IV:

Table IV. LENGTHS OF INTERFEROMETER BASELINES

Antenna Pairs		Distance
#1 - #2	#1 - #3	4.5 m
#1 - #4	#1 - #5	13.0 m
#1 - #6	#1 - #7	37.8 m
#1 - #8	#1 - #9	104.0 m

Each arm of the "X" interferometer has two baselines, a "short-baseline", and a "long-baseline". The two pairs of baselines around $\phi=0°$ are shorter than the two pairs around $\phi=180°$, as it shown in Figure 7. The long baseline was used for phase measurements and the other baselines were used to resolve ambiguity problems.

After the NEC wire model was complete, the array excitation was specified. The excitation is from a plane wave incident on the structure for a defined set of angles of arrival. The array is symmetrical only along the plane at $\phi=0°$ so the set of azimuth angles of arrival were selected to be from $\phi=0°$ to $\phi=180°$, in steps of $2°$. For the elevation plane which corresponds to $\beta=90°-\theta$ in spherical coordinates, four elevation angles were selected: $\beta=15°$, $30°$, $45°$, and $60°$. The operating frequency range is 2-32 MHz and four different frequencies were selected. The lower $f_{min}=2$ MHz, the higher $f_{max}=32$ Mhz, the middle frequency $f_{mid}=16$ MHz, and the geometric mean frequency $f_{gmn}=8$ MHz. The conditions selected for different NEC runs were:

Frequency: 2, 8, 16, 32 MHz

Ground conditions: Perfect, Good, Poor ground

Antenna pairs: Longest baselines (1-8, 1-9)

Azimuth angles: 0°-180°, every 2°

Elevation angles: 15°, 30°, 45°, 60°

Calculations were made to investigate the effects of ground parameters on interferometer system accuracy for perfect, good, and poor ground. NEC calculated currents at every antenna feed point, for chosen elevation and azimuth angles and stored the magnitude and phase in output files. The SSL system used was an interferometer system, so only the current phase values at each feed point were of interest. The phase differences between different array elements were

44

calculated and stored for each baseline. From theoretical formulas of McNamara [Ref. 1:p. 150] (equations 8, 9, and 10) and the calculated phase differences, the angles of arrival of incoming signals were determined. Differences between the predicted angles of arrival over perfect and good, and perfect and poor ground were calculated, for $\phi=0°$-$\phi=180°$, and for $\beta=15°$, 30°, 45°, and 60°. Next the azimuth angles for maximum azimuth and elevation errors were found and the array illuminated by plane waves at those particular azimuth angles and for three additional elevation angles ($\beta=20°$, 40°, 50°).

For all frequencies and the three different ground conditions, the azimuth error at $\phi=0°$ and $\phi=180°$ was zero. This shows symmetry of the incident wave with respect to the arms of the interferometer.

Figure A-2 and Figure A-3 in Appendix A show elevation and azimuth error for poor ground conditions, at 2 MHz. Maximum elevation error occurred for 15° elevation at an azimuth angle of $\phi=0°$. The maximum azimuth error was observed for 60° elevation angle and $\phi=48°$ azimuth angle. Figure A-1 and Table VIII in Appendix A show variations of elevation and azimuth errors versus elevation angle, at the azimuth angles where maximum error occurs. The effect of good ground is shown in Figures A-4 and Table IX in Appendix A and the elevation and azimuth errors are shown in Figures A-5, and A-6 in Appendix A. The above analyses show that maximum elevation error for both poor and good ground conditions occurred at 0° azimuth

45

angle. The value of error over poor ground was larger than the error over good ground. The maximum azimuth error occurred in both cases at the highest elevation angle, 60°.

At 8 MHz and for poor ground, as it shown in Figures A-7, A-8, and Table X, the maximum elevation error occurred again at 15° elevation and $\phi=0°$ azimuth, the same as for 2 MHz. Maximum azimuth error occurred at $\phi=40°$ and for 60° elevation angle, as shown in Figure A-9. For good ground, both errors were smaller than for poor ground, as shown in Figure A-10 and Table XI. Maximum elevation error occurred at 66° azimuth and 15° elevation, and is presented in Figure A-11. Maximum azimuth error was at 58° azimuth and 60° elevation, and is presented in Figure A-12.

Figures A-13, A-14 and A-15 together with Table XII in Appendix A demonstrate elevation and azimuth error over poor ground at 16 MHz. Figures A-16, A-17 and A-18 with the Table XIII present the errors over good ground. In both ground cases the maximum elevation error occurred at 15° elevation and the maximum azimuth error at 30° elevation angle.

Figures A-19, A-20 and A-21 with Table XIV in Appendix A show the SSL azimuth and elevation errors for 32 MHz over poor ground. Figures A-22, A-23, and A-24 with Table XV in Appendix A are for good ground conditions. Maximum elevation error in both ground cases was observed at 15° elevation and the maximum azimuth error at 60° elevation. The magnitude of

46

elevation and azimuth error over good ground was always smaller than over poor ground.

The differences between perfect and finite ground measurements represent additional bearing and elevation errors in angles of arrival of the incoming signals which were attributed to different ground conditions.

The effects of changing the ground conditions from good to poor, for all the four frequencies always caused larger azimuth and elevation errors.

From the analysis it is observed that the ground conditions play an important role in SSL interferometer system accuracy, and in general the poorer the ground the larger the errors.

B. HFDF ERROR AND FOOTPRINT

The effect of ground on SSL accuracy, is measured by comparing the predicted transmitter location, for an SSL system placed over perfect ground, to the predicted locations for an SSL system over poor and good ground, respectively. Transmitter position errors can be observed using the sky wave transmission chart of Figure 11 [Ref. 25:p. 2-13]. As described in Chapter V, azimuth error in angle of arrival produces a bearing error, and the error in elevation angle of arrival produces a range error. The combination of these two errors form the SSL "footprint". The footprint is usually elliptical in shape with the size of the minor axis determined

47
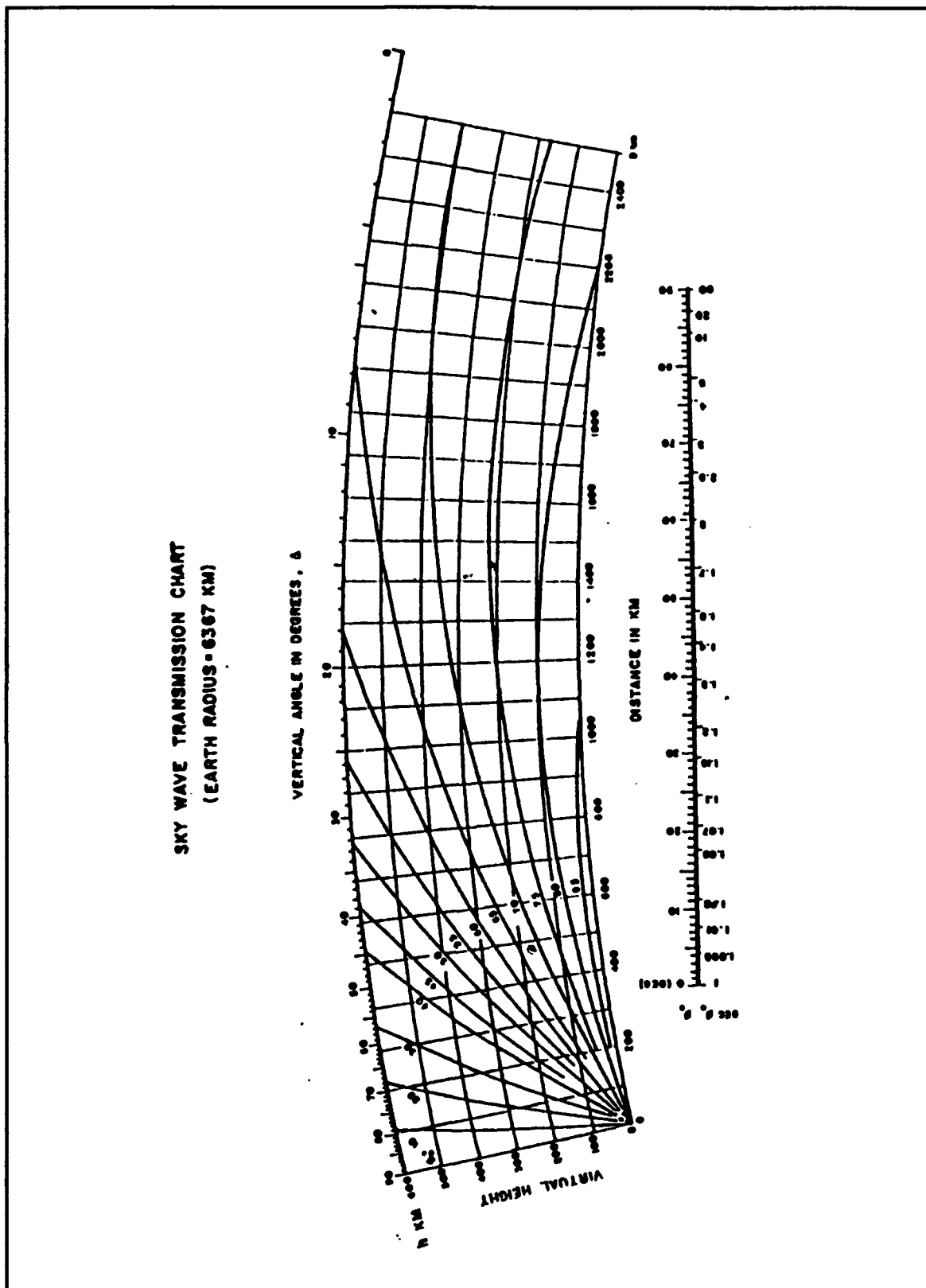
Figure 11. Sky Wave Transmission Chart.

48

by bearing error, while the major axis is proportional to the range error.

The size of the minor and major axis can be determined using the calculated worst case errors for azimuth and elevation angles provided by NEC outputs (Tables VIII through XV) and the sky wave transmission chart. The minor and major axis of footprints were determined for three different ionospheric cases and for good and poor ground conditions. In the first case the reflection takes place from the E-layer at an altitude 110 Km, in the second case the reflection is from the F_1-layer at 200 Km and in the third the reflection is at the F_2-layer at 320 Km altitude. The calculated results for each case are presented in Tables V, VI, and VII. Figures 12, 13, 14, and 15 show the footprint errors for 2, 8, 16, and 32 MHz, over poor and good ground for reflection from the F_2-layer. The footprint error increased in proportion to the altitude at which reflection took place. The smallest error occurred for the E-mode and the largest for the F_2-mode. For all frequencies larger elevation error and worst case range error occurred at 15° elevation. For 2, 8, and 32 MHz larger bearing error occurred at 60° elevation. At 16 MHz the greatest bearing error was at 30° elevation.

Maximum range error at 2 MHz was 60 Km for the E-mode, 100 Km for the F_1-mode, and 130 Km for the F_2-mode. At 8 MHz it was 180 Km for the E-mode, 210 Km for the F_1-mode and 260 Km for the F_2-mode.

49

For 16 MHz the maximum range error was 70 Km for E- mode, 110 Km for F_1-mode, and 160 Km for F_2-modes. And at 32 MHz the maximum range error was 120 Km for the E-mode, 140 Km for the F_1, and 180 Km for the F_2-mode.

From previous observations, the worst range error is seen to occur when the SSL array is operated over poor ground at all four frequencies, emphasizing the role played by the ground in the accuracy of the SSL system.

Table V. E-MODE PROPAGATION SSL FOOTPRINT ERRORS

Propagation Mode = E (Average Height 110 Km)					
Ground	Freq. (MHz)	Worst case Azimuth Error		Worst case Elevation Error	
		Range Error Major Axis	Bearing Error Minor Axis	Range Error Major Axis	Bearing Error Minor Axis
Poor Ground ϵ_r=5 σ=0.001 (S/m)	2	20 Km (range) 140 Km	3 Km	30 Km (range) 700 Km	0
	8	2 Km (range) 140 Km	14 Km	180 Km (range) 700 Km	0
	16	20 Km (range) 360 Km	25 Km	70 Km (range) 700 Km	14 Km
	32	12 Km (range) 140 Km	4.5 Km	120 Km (range) 700 Km	6 Km
Good Ground ϵ_r=30 σ=0.01 (S/m)	2	8 Km (range) 140 Km	2 Km	60 Km (range) 700 Km	0
	8	2 Km (range) 140 Km	2 Km	70 Km (range) 700 Km	2.5 Km
	16	10 Km (range) 360 Km	9.5 Km	40 Km (range) 700 Km	0
	32	6 Km (range) 140 Km	2 Km	60 Km (range) 700 Km	3.5 Km

51

Table VI. F_1-MODE PROPAGATION SSL FOOT PRINT ERRORS

Propagation Mode = F_1 (Average Height 200 Km)					
Ground	Freq. (MHz)	Worst case Azimuth Error		Worst case Elevation Error	
		Range Error Major Axis	Bearing Error Minor Axis	Range Error Major Axis	Bearing Error Minor Axis
Poor Ground $\epsilon_r = 5$ $\sigma = 0.001$ (S/m)	2	24 Km (range) 240 Km	5 Km	40 Km (range) 1220 Km	0
	8	2 Km (range) 240 Km	24 Km	210 Km (range) 1220 Km	0
	16	30 Km (range) 640 Km	45 Km	110 Km (range) 1220 Km	24 Km
	32	16 Km (range) 240 Km	7.7 Km	140 Km (range) 1220 Km	10 Km
Good Ground $\epsilon_r = 30$ $\sigma = 0.01$ (S/m)	2	8 Km (range) 240 Km	3.2 Km	100 Km (range) 1220 Km	0
	8	2 Km (range) 240 Km	1.9 Km	60 Km (range) 1220 Km	4.3 Km
	16	20 Km (range) 640 Km	16.7 Km	80 Km (range) 1220 Km	0
	32	12 Km (range) 240 Km	3.5 Km	70 Km (range) 1220 Km	6.2 Km

Table VII. F_2-MODE PROPAGATION SSL FOOTPRINT ERRORS

Propagation Mode = F_2 (Average Height 320 Km)					
Ground	Freq. (MHz)	Worst case Azimuth Error		Worst case Elevation Error	
		Range Error Major Axis (Km)	Bearing Error Minor Axis (Km)	Range Error Major Axis (Km)	Bearing Error Minor Axis (Km)
Poor Ground $\epsilon_r = 5$ $\sigma = 0.001$ (S/m)	2	30 Km (range) 350 Km	6.9 Km	60 Km (range) 1790 Km	0
	8	2 Km (range) 350 Km	35 Km	260 Km (range) 1790 Km	0
	16	70 Km (range) 970 Km	68 Km	160 Km (range) 1790 Km	35.3 Km
	32	22 Km (range) 350 Km	11.2 Km	180 Km (range) 1790 Km	14.4 Km
Good Ground $\epsilon_r = 30$ $\sigma = 0.01$ (S/m)	2	10 Km (range) 350 Km	4.7 Km	130 Km (range) 1790 Km	0
	8	2 Km (range) 350 Km	2.8 Km	80 Km (range) 1790 Km	6.2 Km
	16	40 Km (range) 970 Km	25.2 Km	130 Km (range) 1790 Km	0
	32	16 Km (range) 350 Km	5.1 Km	110 Km (range) 1790 Km	9.1 Km

53
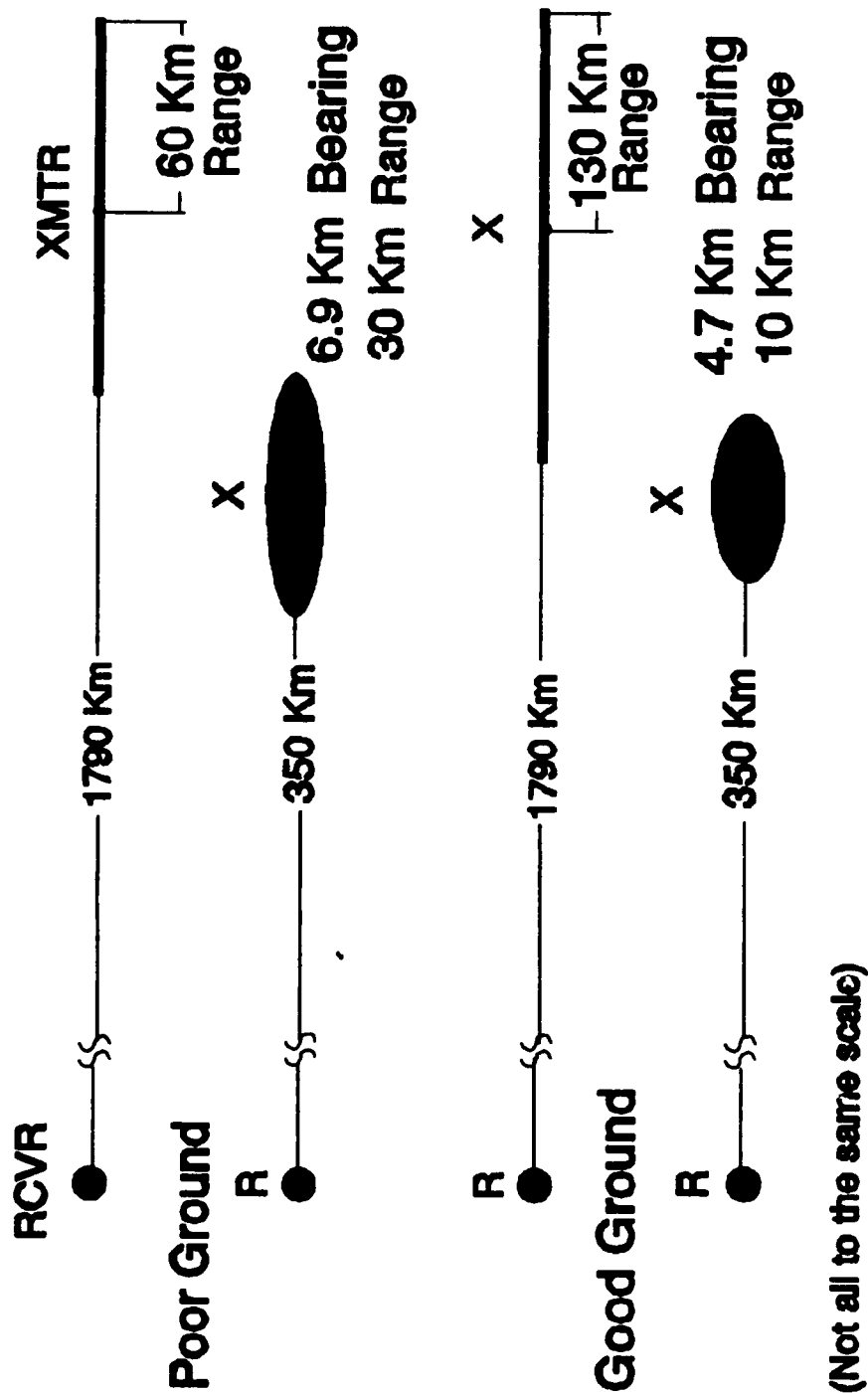
Figure 12. Worst Case SSL Footprint Errors at 2 MHz.
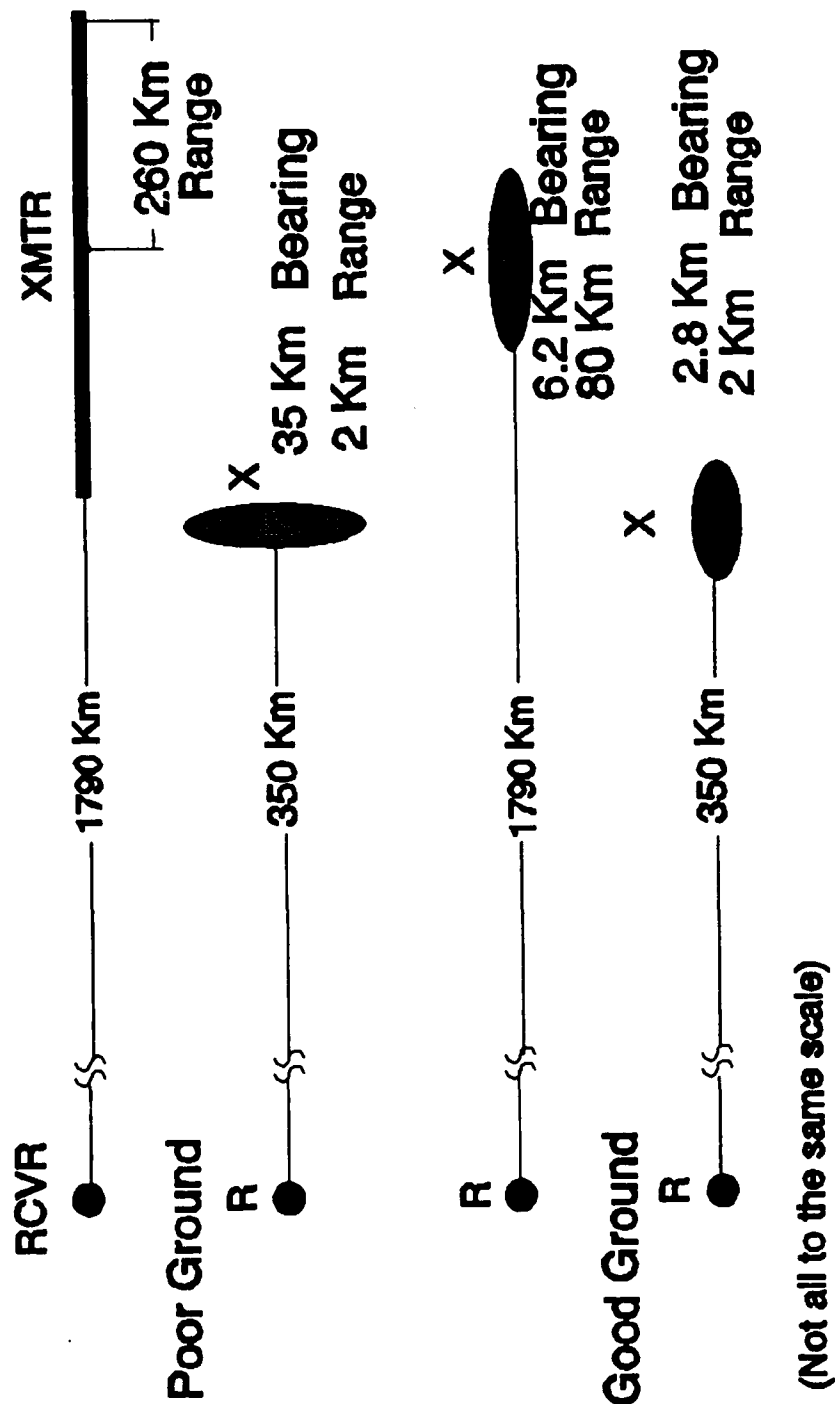
Figure 13. Worst Case SSL Footprint Errors at 8 MHz.

55
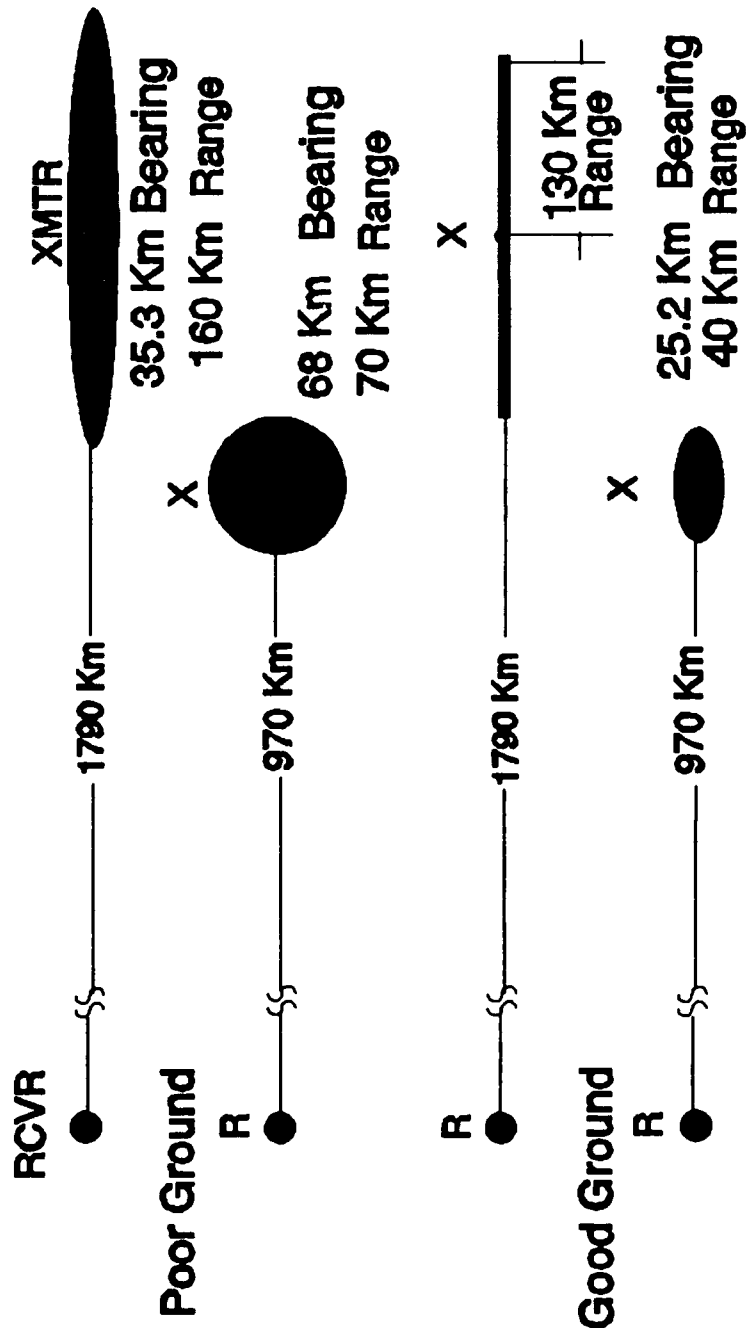
Figure 14. Worst Case SSL Footprint Errors at 16 MHz.

56
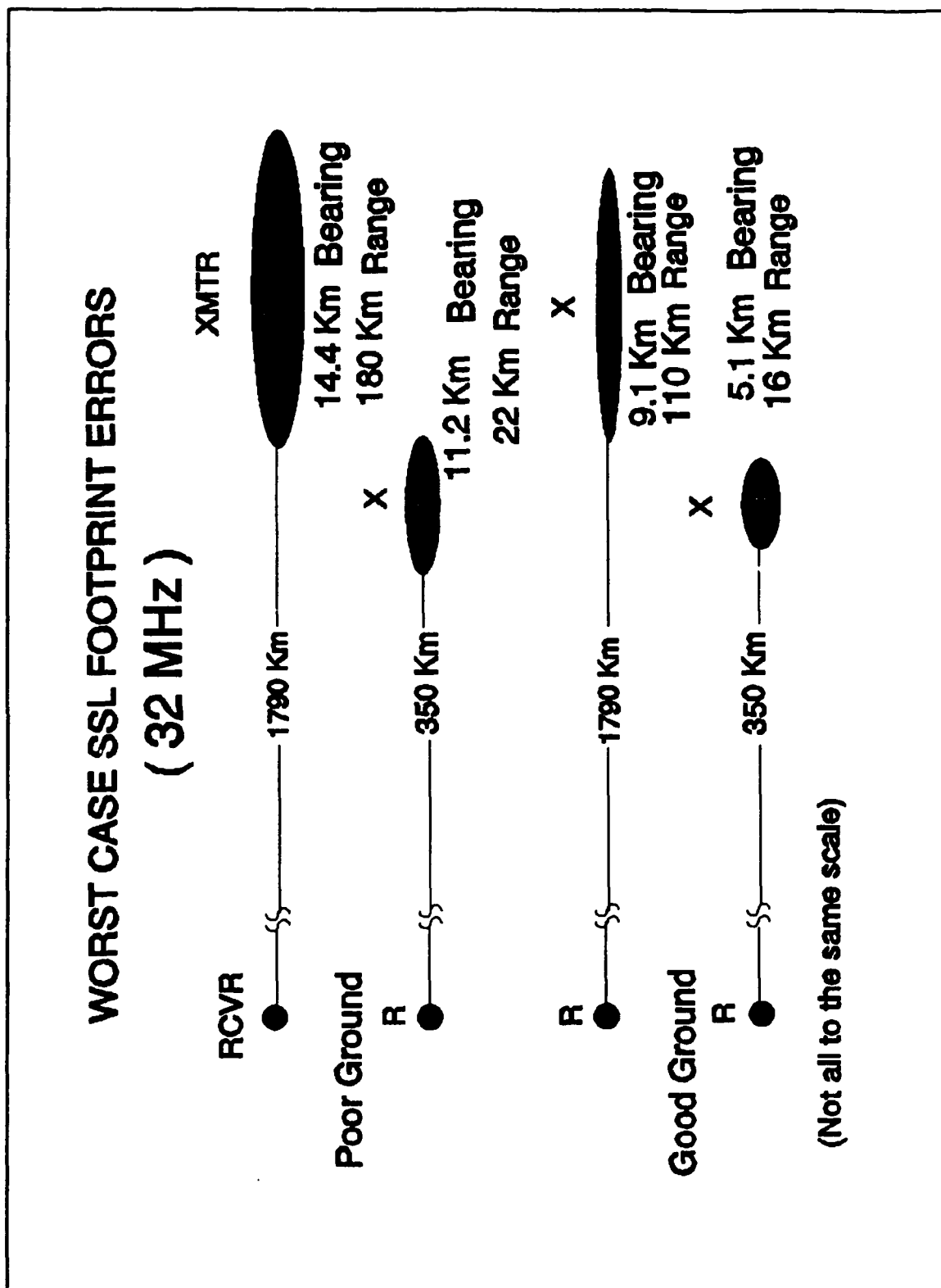
Figure 15. Worst Case SSL Footprint Errors at 32 MHz.

VII. CONCLUSIONS AND RECOMMENDATIONS

A. CONCLUSIONS

The performance of a 9-element "X" shaped interferometer SSL system was examined. The analysis was limited to the investigation of the effects of (1) perfect, good and poor ground conditions and (2) mutual coupling between elements of the array. All results were referenced to the perfect ground case. Test frequencies of 2, 8, 16, and 32 MHz were used.

Using interferometer theory and calculated phase differences between elements, errors in angle of arrival of incoming signals due to finite ground effects were determined. The lowest elevation and azimuth errors were consistently obtained for the good ground case. Larger elevation and azimuth errors were obtained for poor ground, with maximum elevation and azimuth errors of about 2 degrees obtained for some conditions.

Elevation and azimuth errors were translated into lateral and range distance errors using a sky-wave transmission chart. The largest errors at all frequencies occurred when the SSL array was operated over poor ground and when signals were received over an F_2 propagation mode. The largest error was at 8 MHz. The smallest errors occurred with the array over

good ground and with signals arriving over a 1-hop E-mode. The lowest error was at 16 MHz.

Range location errors up to 260 km were found along with lateral errors up to 68 km due to ground effects.

While the study investigated important sources of location errors in SSL systems, other sources also exist and cannot be ignored in operational systems. Examples of other sources of errors are the accuracy of the layout of the array, discontinuities in ground conditions within and near the array, conducting objects within and near the array, ionospheric tilts, ionospheric layer movements, multipath propagation effects, radio interference, signal-to-noise ratio, and imperfect equipment parameters.

B. RECOMMENDATIONS

The results of the work described in this thesis suggest a number of additional studies and analyses of the accuracy of SSL systems. Examples follow: a) An important extension of this work would be the comparison of actual measured results with the theoretical calculations provided. b) Results for a larger number of elevation angles would be useful, especially at elevation angles higher than 60 degrees. c) Results for additional examples of poor ground would be useful. d) An examination of the impact of the additional items identified as affecting target location accuracy are necessary to provide a full understanding of the capabilities of the SSL systems.

APPENDIX A.

SSL ERRORS OVER FINITE GROUND.

Table VIII. WORST CASE ERROR AT 2 MHZ OVER POOR GROUND

Frequency= 2 MHz			
Poor Ground (ϵ_r= 5, σ= 0.001 S/m)			
Worst Case Azimuth Error at Azimuth Angle ϕ=48°	Elevation Angle	Azimuth Error	Elevation Error
	15°	-0.29°	-0.96°
	20°	-0.31°	-0.75°
	30°	-0.37°	-0.57°
	40°	-0.45°	-0.52°
	45°	-0.55°	-0.50°
	50°	-0.72°	-0.51°
	60°	-1.13°	-0.56°
Worst Case Elevation Error at Azimuth Angle ϕ=0°	Elevation Angle	Azimuth Error	Elevation Error
	15	0°	-1.84°
	20	0°	-1.60°
	30	0°	-1.14°
	40	0°	-1.08°
	45	0°	-1.03°
	50	0°	-1.10°
	60	0°	-1.24°
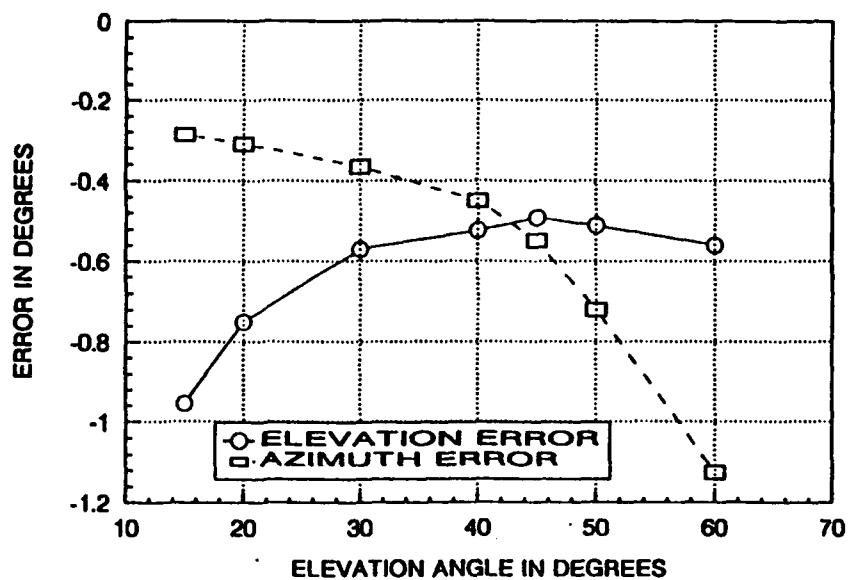
Figure A-1. SSL Azimuth and Elevation Error at 2 MHz Over Poor Ground.

61
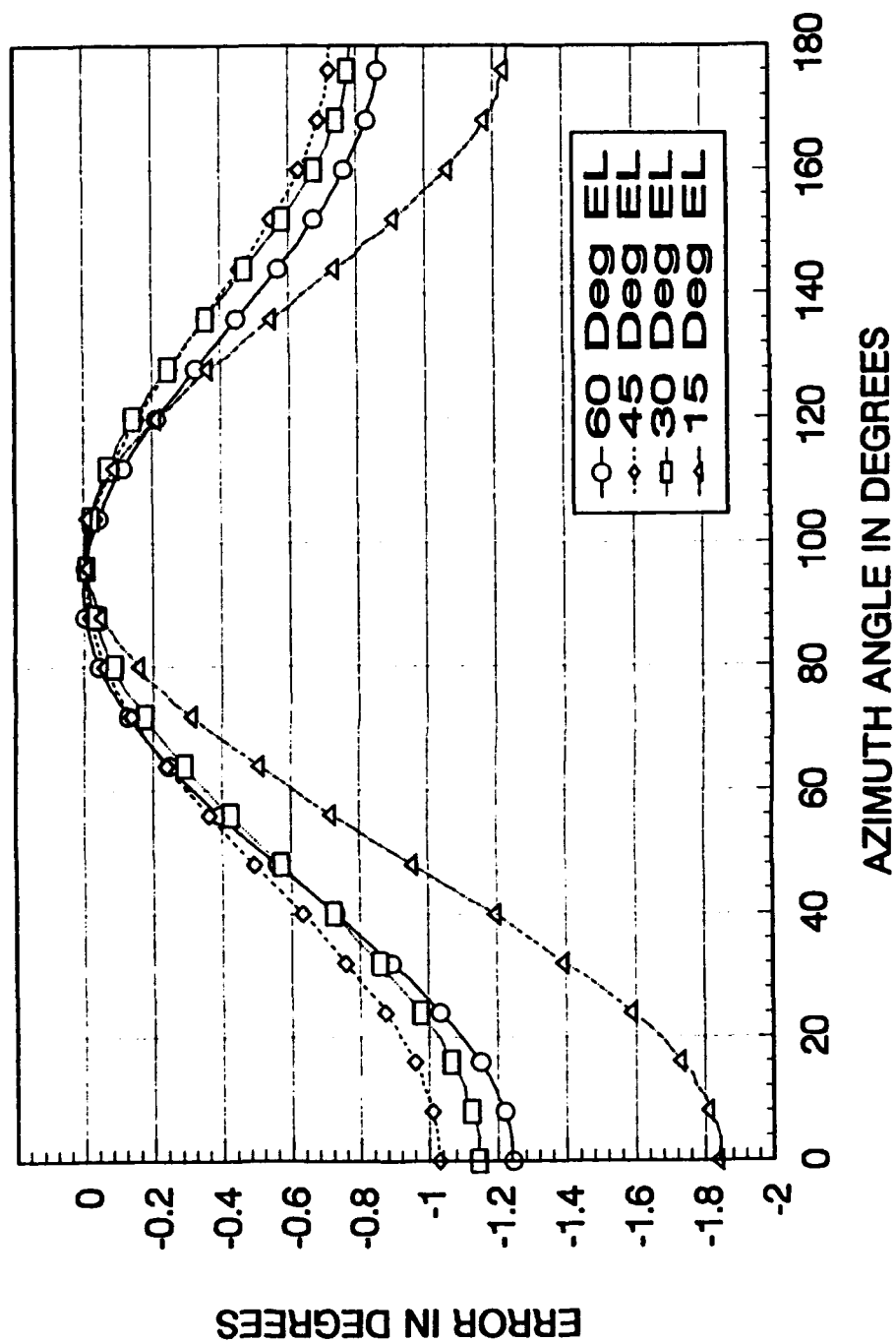
Figure A-2. SSL Elevation Error at 2 MHz Over Poor Ground.
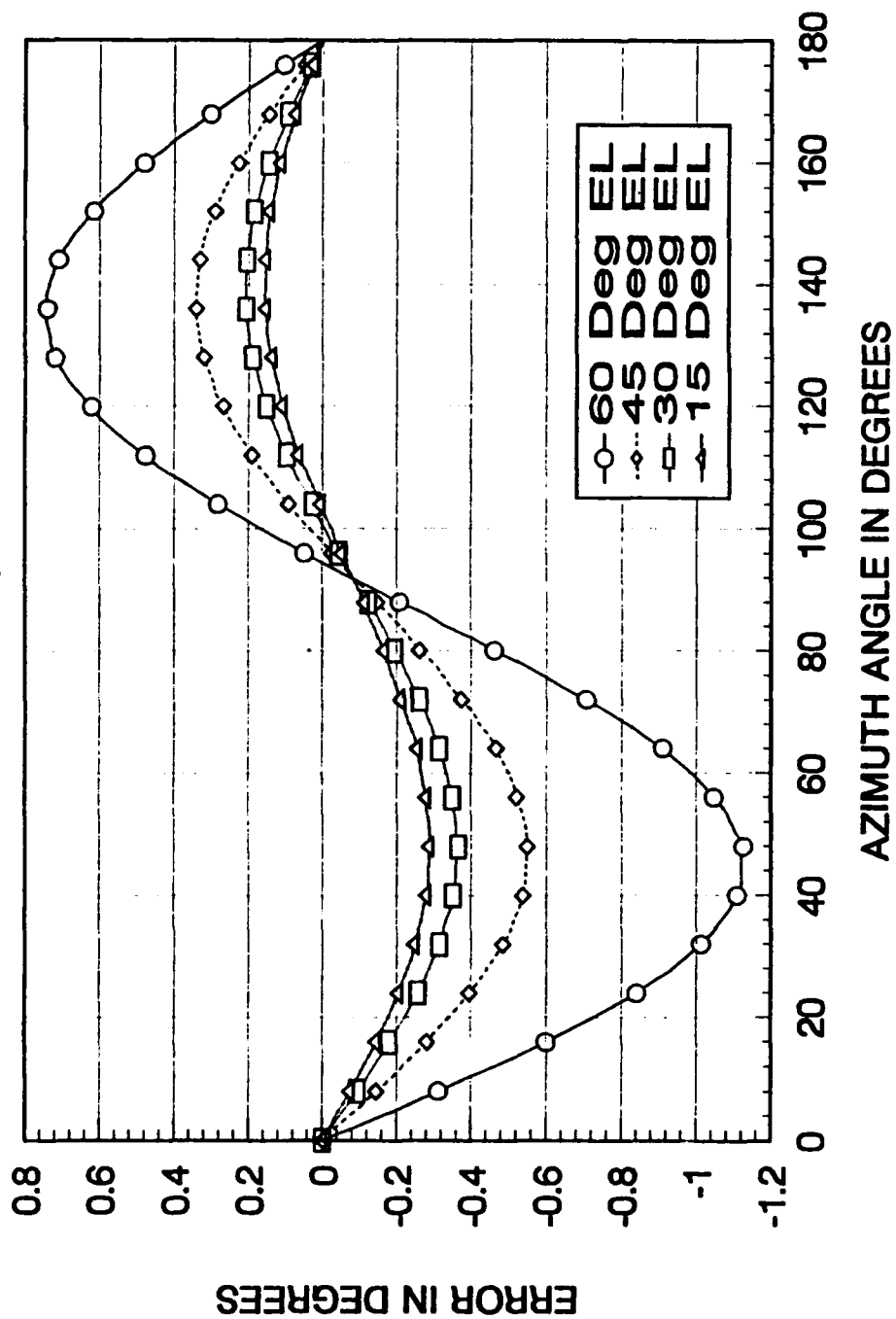
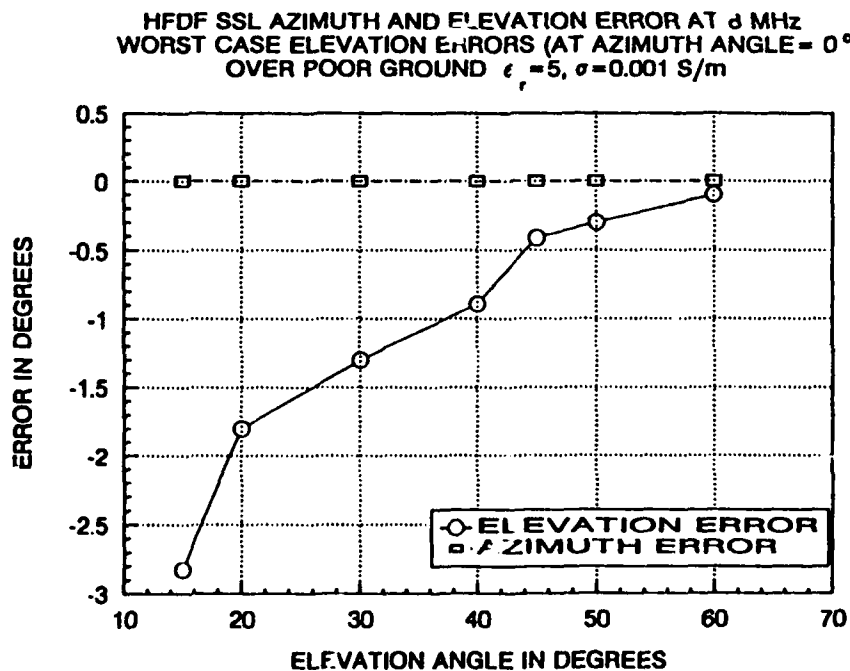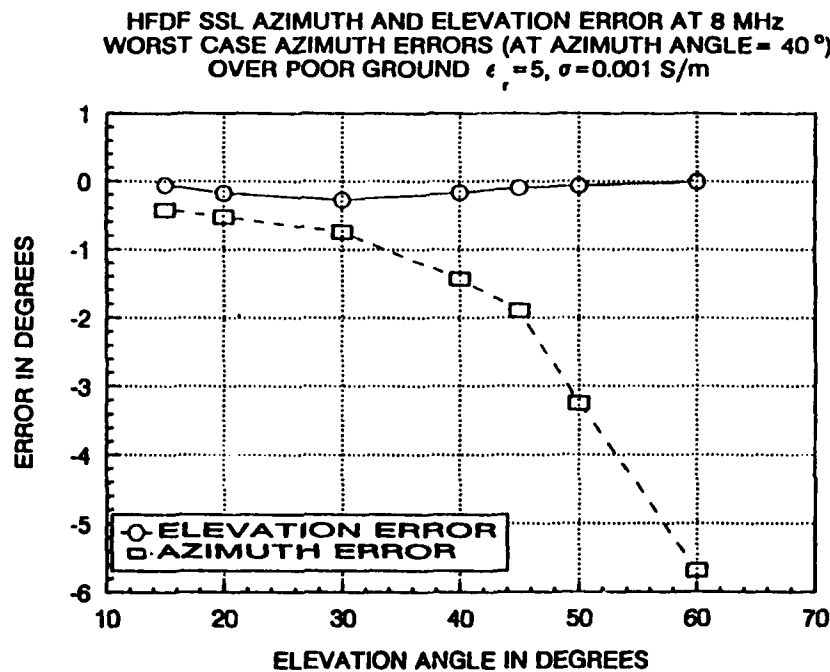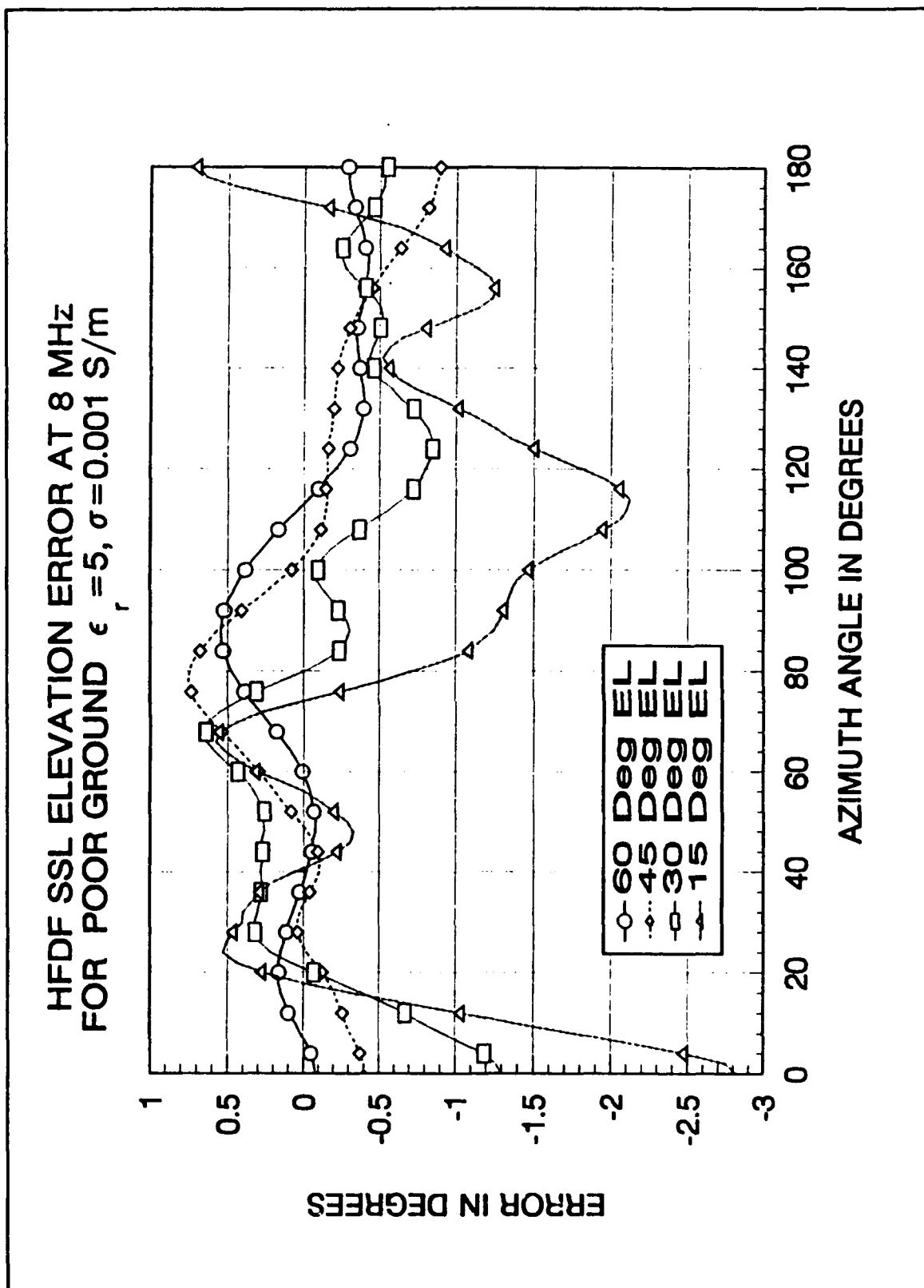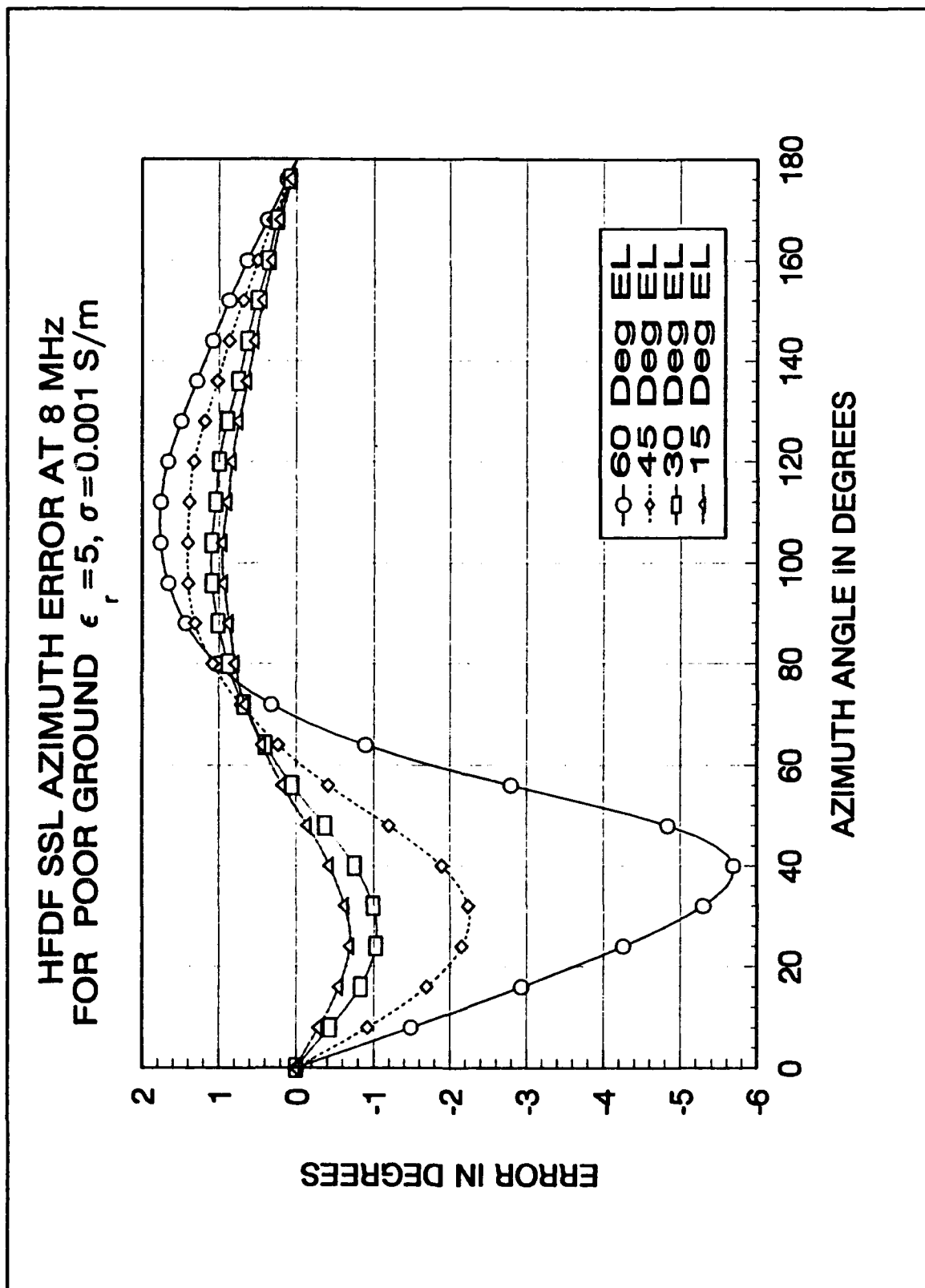**Figure A-3.** SSL Azimuth Error at 2 MHz Over Poor Ground.

Table IX. WORST CASE ERROR AT 2 MHZ OVER GOOD GROUND

Frequency= 2 MHz			
Good Ground (ϵ_r= 30, σ= 0.01 S/m)			
Worst Case Azimuth Error at Azimuth Angle ϕ=46°	Elevation Angle	Azimuth Error	Elevation Error
	15°	-0.20°	0.72°
	20°	-0.23°	0.62°
	30°	-0.26°	0.42°
	40°	-0.33°	0.38°
	45°	-0.38°	0.37°
	50°	-0.48°	-0.39°
	60°	-0.77°	0.44°
Worst Case Elevation Error at Azimuth Angle ϕ=0°	Elevation Angle	Azimuth Error	Elevation Error
	15°	0°	1.61°
	20°	0°	1.40°
	30°	0°	0.90°
	40°	0°	0.84°
	45°	0°	0.78°
	50°	0°	0.85°
	60°	0°	0.91°

64
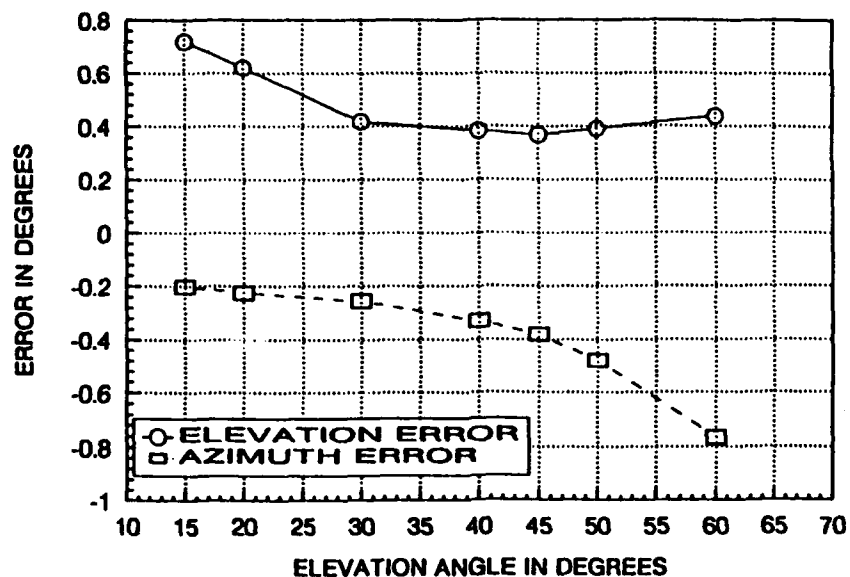
Figure A-4. SSL Azimuth and Elevation Error at 2 MHz Over Good Ground.
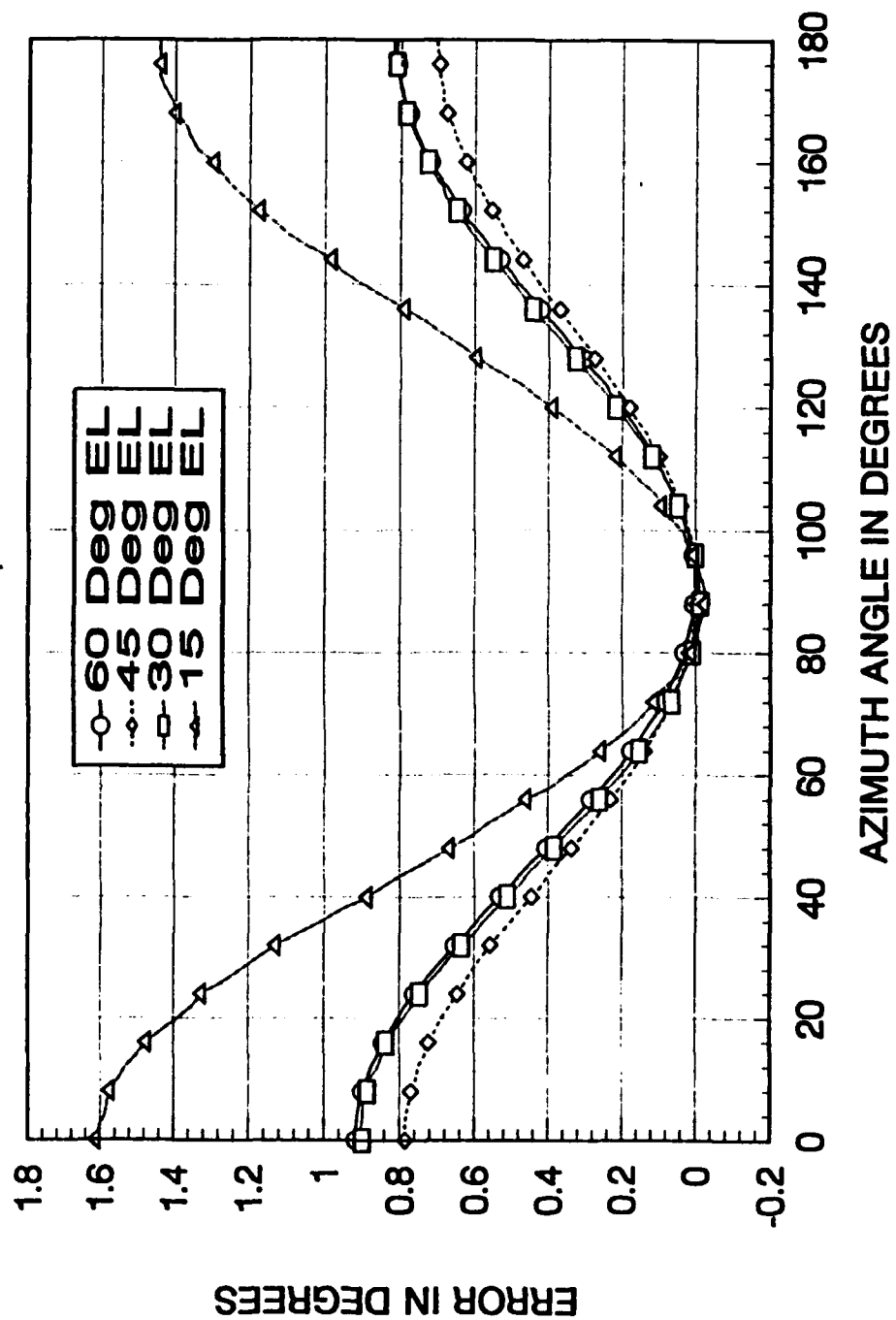
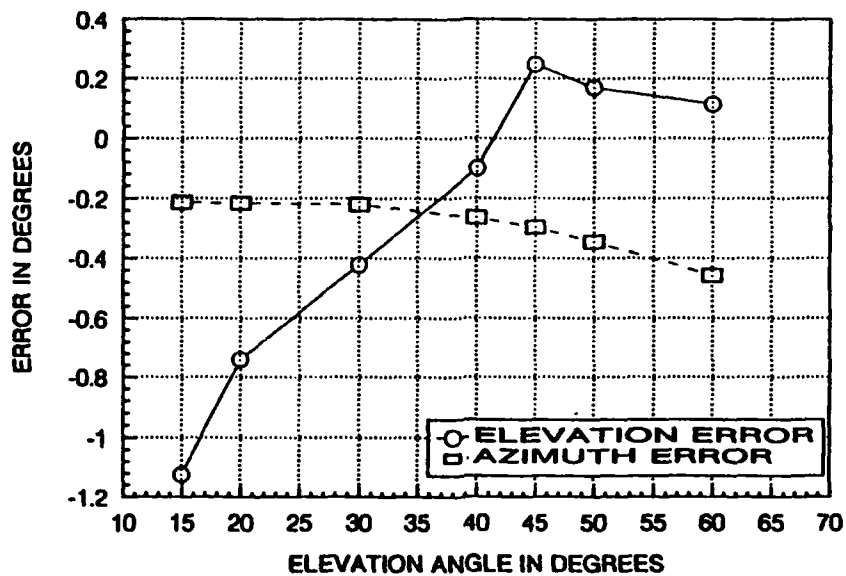**Figure A-5**. SSL Elevation Error at 2 MHz Over Good Ground.
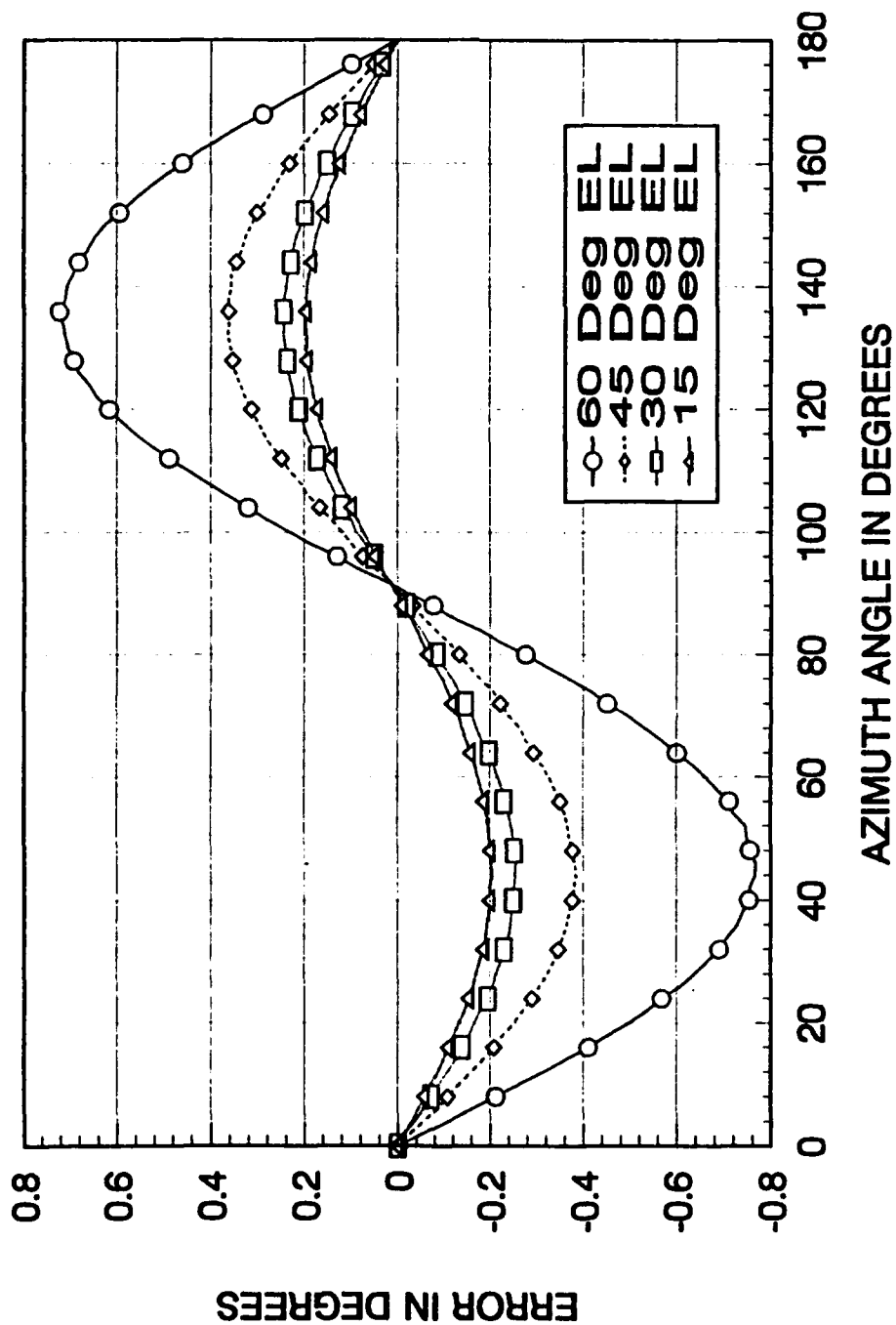
Figure A-6. SSL Azimuth Error at 2 MHz Over Good Ground.

67

Table X. WORST CASE ERROR AT 8 MHZ OVER POOR GROUND

Frequency= 8 MHz			
Poor Ground (ϵ_r= 5, σ= 0.001 S/m)			
Worst Case Azimuth Error at Azimuth Angle ϕ=40°	Elevation Angle	Azimuth Error	Elevation Error
	15°	−0.43°	−0.1°
	20°	−0.53°	−0.2°
	30°	−0.75°	−0.3°
	40°	−1.43°	−0.2°
	45°	−1.90°	−0.1°
	50°	−3.24°	−0.1°
	60°	−5.69°	−0.1°
Worst Case Elevation Error at Azimuth Angle ϕ=0°	Elevation Angle	Azimuth Error	Elevation Error
	15°	0°	−2.8°
	20°	0°	−1.8°
	30°	0°	−1.3°
	40°	0°	−0.9°
	45°	0°	−0.4°
	50°	0°	−0.3°
	60°	0°	−0.1°

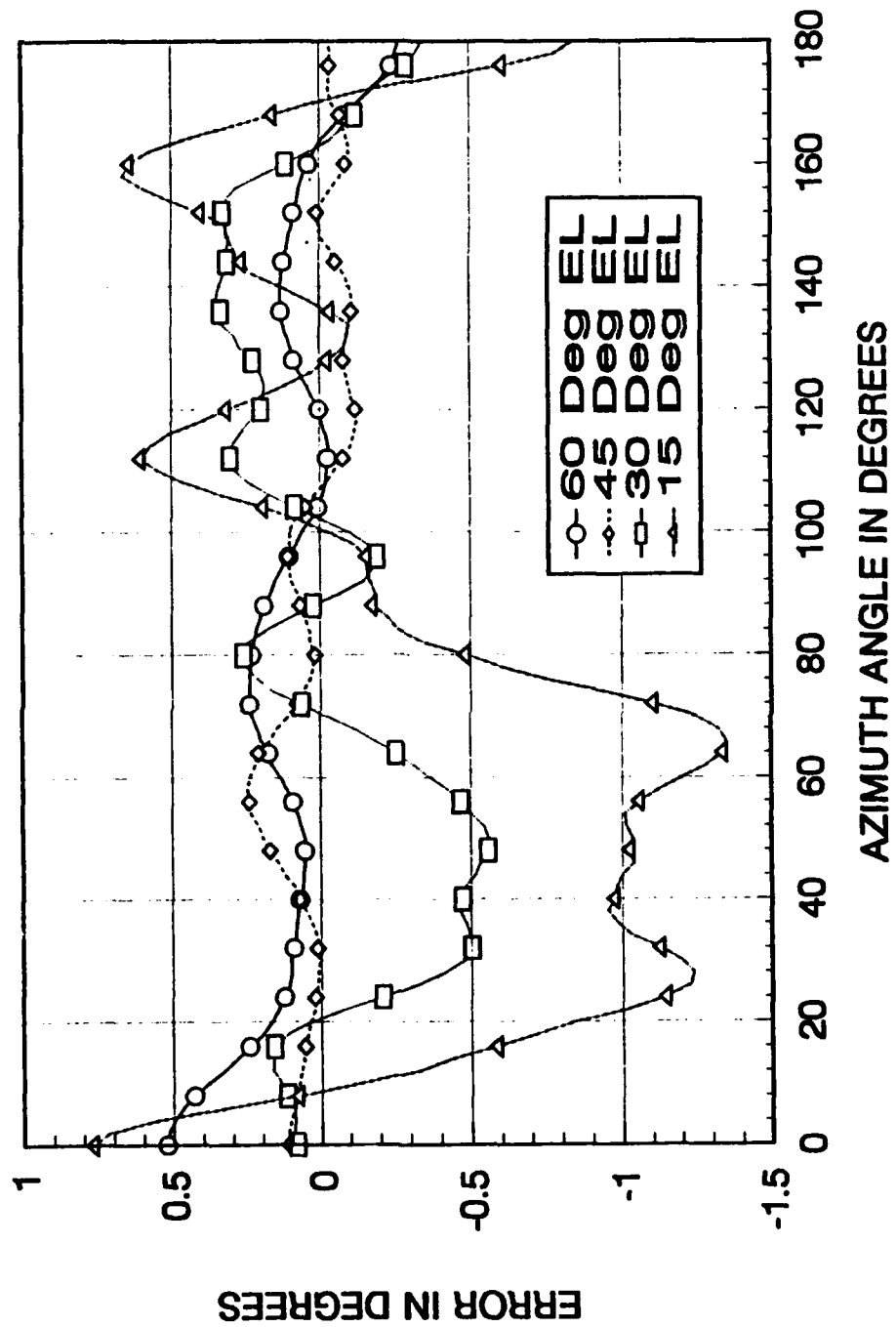Figure A-7. SSL Azimuth and Elevation Error at 8 MHz Over Poor Ground.

Figure A-8. SSL Elevation Error at 8 MHz Over Poor Ground.

Figure A-9. SSL Azimuth Error at 8 MHz Over Poor Ground.

Table XI. WORST CASE ERROR AT 8 MHZ OVER GOOD GROUND

Frequency= 8 MHz			
Good Ground (ϵ_r= 30, σ= 0.01 S/m)			
Worst Case Azimuth Error at Azimuth Angle ϕ=58°	Elevation Angle	Azimuth Error	Elevation Error
	15°	−0.21°	−1.1°
	20°	−0.21°	−0.8°
	30°	−0.22°	−0.4°
	40°	−0.26°	−0.1°
	45°	−0.30°	0.2°
	50°	−0.35°	0.2°
	60°	−0.46°	0.1°
Worst Case Elevation Error at Azimuth Angle ϕ=66°	Elevation Angle	Azimuth Error	Elevation Error
	15°	−0.20°	−1.4°
	20°	−0.17°	−0.8°
	30°	−0.15°	−0.2°
	40°	−0.18°	0.1°
	45°	−0.19°	0.2°
	50°	−0.24°	0.2°
	60°	−0.38°	0.2°

72

Figure A-10. SSL Azimuth and Elevation Error at 8 MHz Over Good Ground.

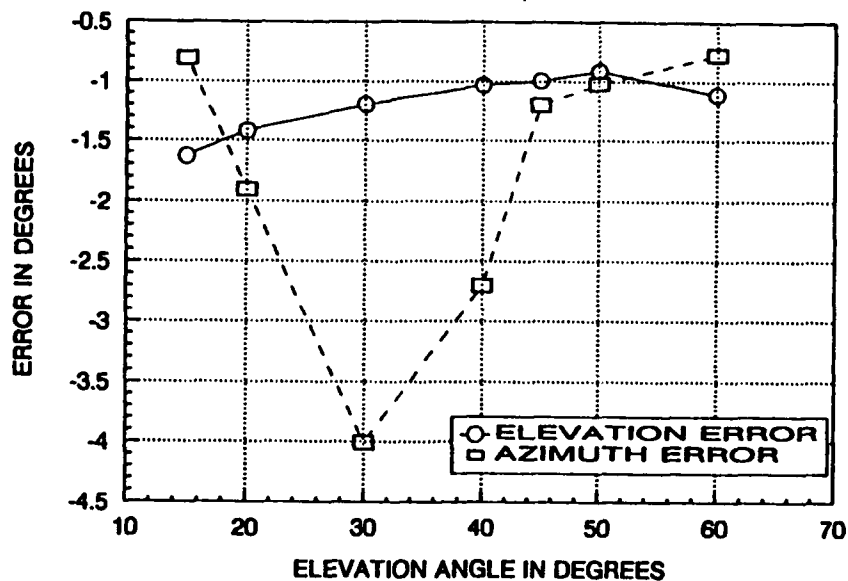**Figure A-11**. SSL Elevation Error at 8 MHz Over Good Ground.
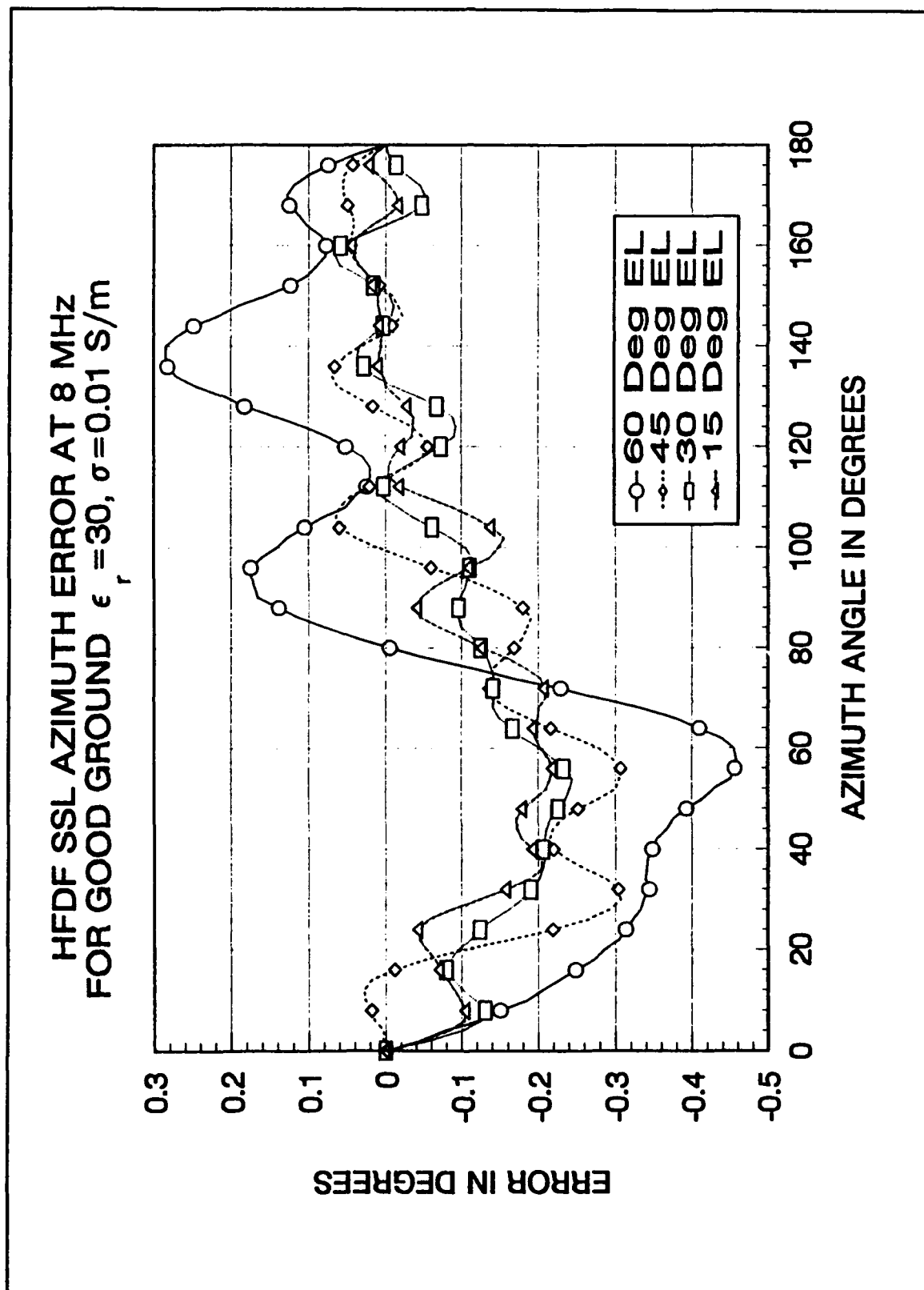
Figure A-12. SSL Azimuth Error at 8 MHz Over Good Ground.

Table XII. WORST CASE ERROR AT 16 MHZ OVER POOR GROUND

Frequency= 16 MHz			
Poor Ground (ϵ_r= 5, σ= 0.001 S/m)			
Worst Case Azimuth Error at Azimuth Angle ϕ=4°	Elevation Angle	Azimuth Error	Elevation Error
	15°	-0.80°	-1.63°
	20°	-1.90°	-1.42°
	30°	-4.01°	-1.20°
	40°	-2.70°	-1.03°
	45°	-1.20°	-0.99°
	50°	-1.02°	-0.91°
	60°	-0.78°	-1.11°
Worst Case Elevation Error at Azimuth Angle ϕ=38°	Elevation Angle	Azimuth Error	Elevation Error
	15°	-1.13°	-2.02°
	20°	-1.08°	-1.53°
	30°	-1.02°	-0.78°
	40°	-1.71°	-0.75°
	45°	-1.85°	-0.81°
	50°	-2.37°	-0.84°
	60°	-3.01°	-0.91°

76
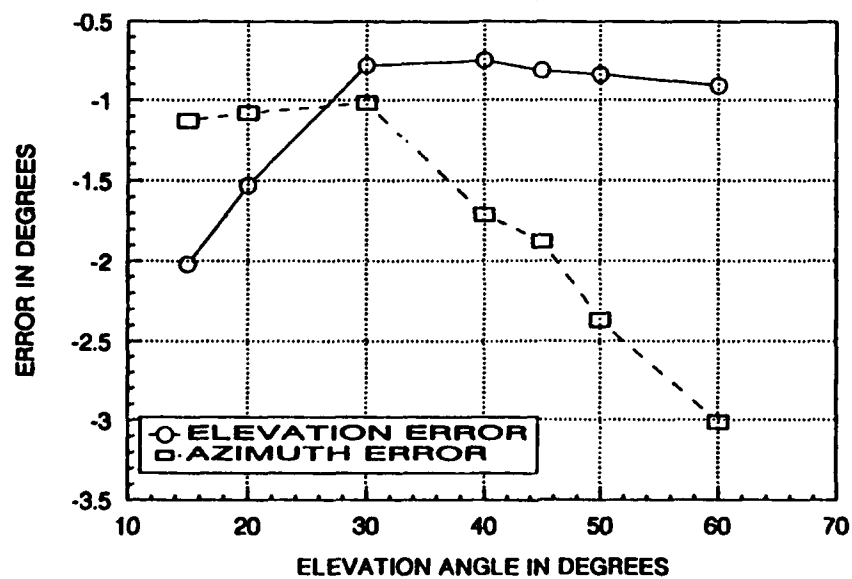
Figure A-13. SSL Azimuth and Elevation Error at 16 MHz Over Poor Ground.
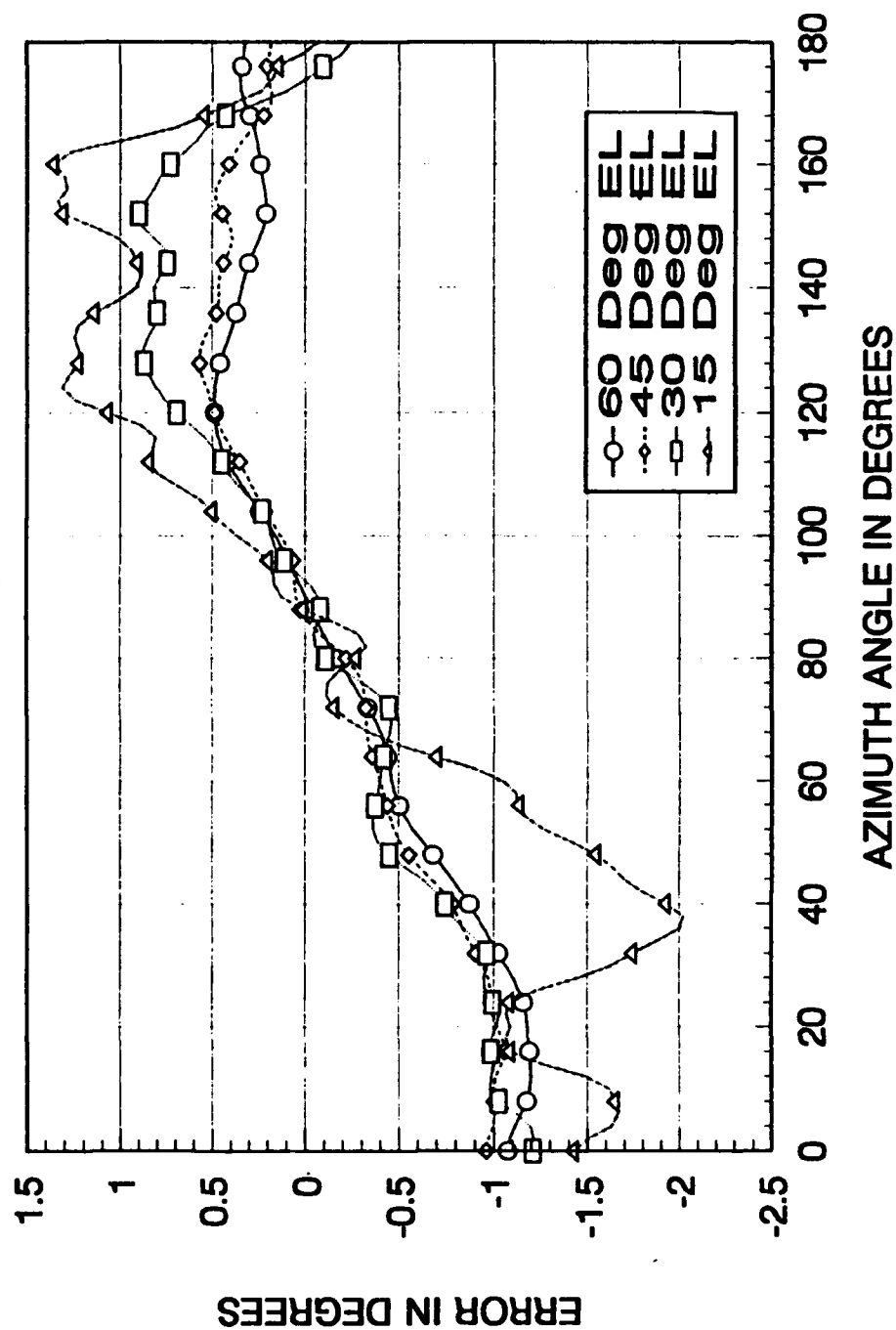
Figure A-14. SSL Elevation Error at 16 MHz Over Poor Ground.

78

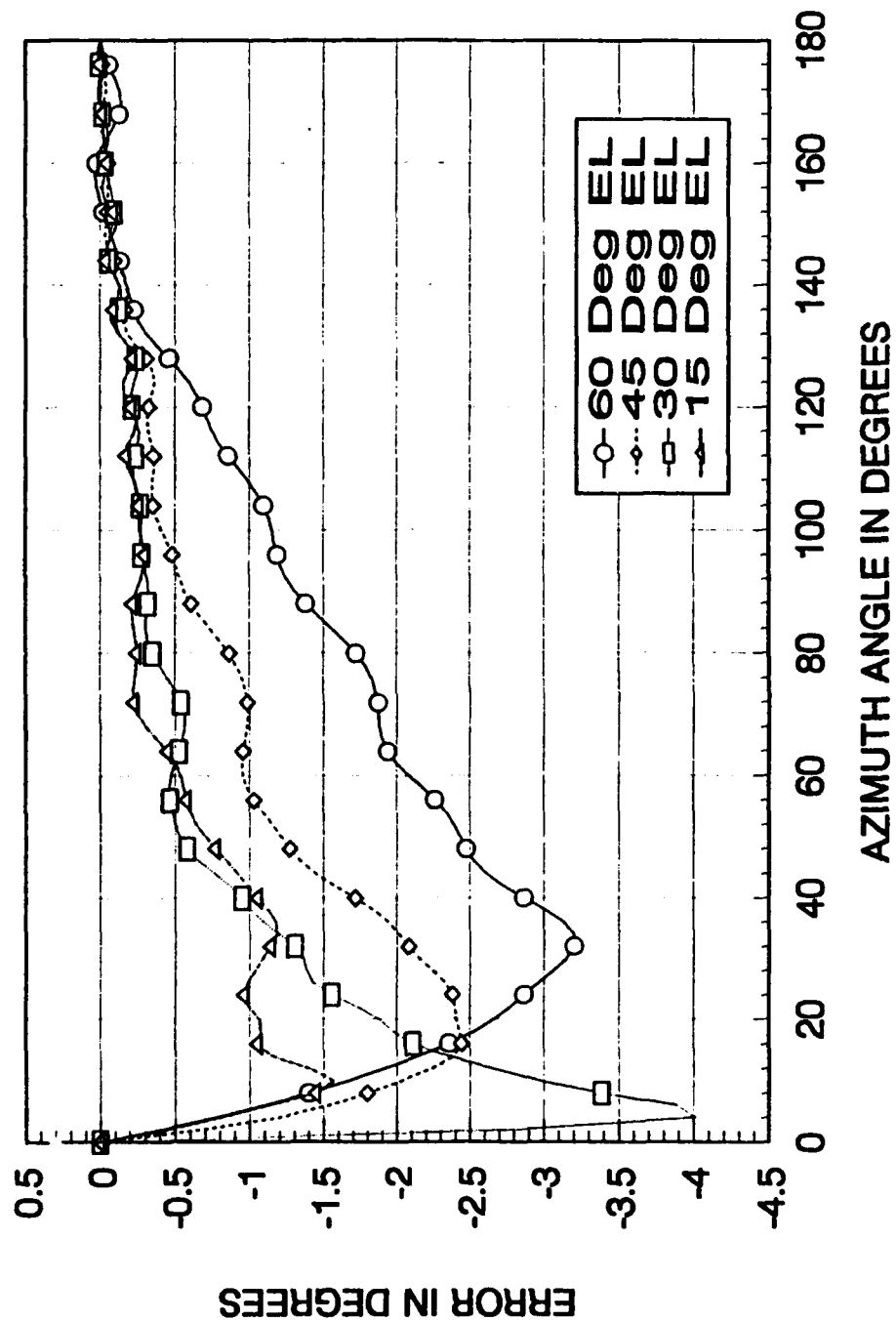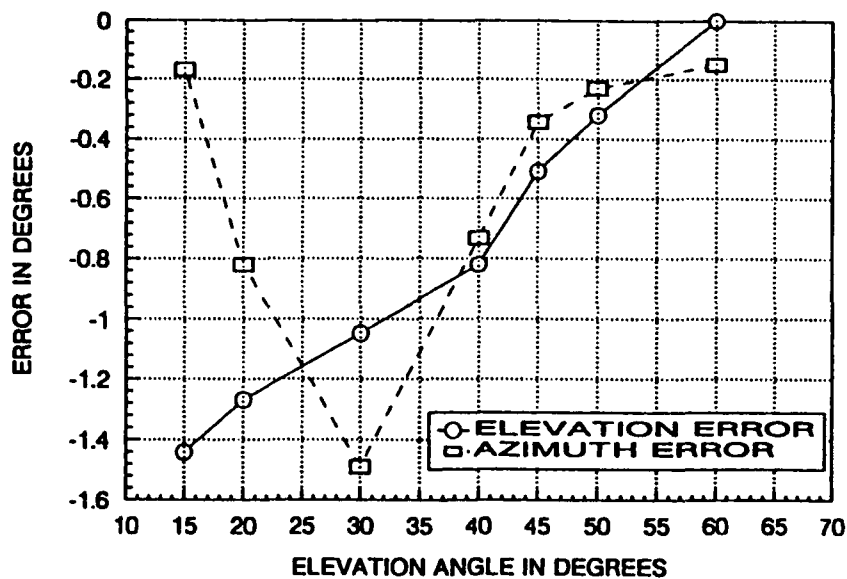**Figure A-15.** SSL Azimuth Error at 16 MHz Over Good Ground.

Table XIII. WORST CASE ERROR AT 16 MHZ OVER GOOD GROUND

Frequency= 16 MHz			
Good Ground (ϵ_r= 30, σ= 0.01 S/m)			
Worst Case Azimuth Error at Azimuth Angle ϕ=4°	Elevation Angle	Azimuth Error	Elevation Error
	15°	-0.17°	-1.44°
	20°	-0.82°	-1.27°
	30°	-1.49°	-1.05°
	40°	-0.73°	-0.82°
	45°	-0.34°	-0.51°
	50°	-0.23°	-0.32°
	60°	-0.15°	-0.01°
Worst Case Elevation Error at Azimuth Angle ϕ=0°	Elevation Angle	Azimuth Error	Elevation Error
	15°	0°	-1.66°
	20°	0°	-1.43°
	30°	0°	-1.21°
	40°	0°	-0.87°
	45°	0°	-0.54°
	50°	0°	-0.26°
	60°	0°	-0.02°

Figure A-16. SSL Azimuth and Elevation Error at 16 MHz Over Good Ground.

81
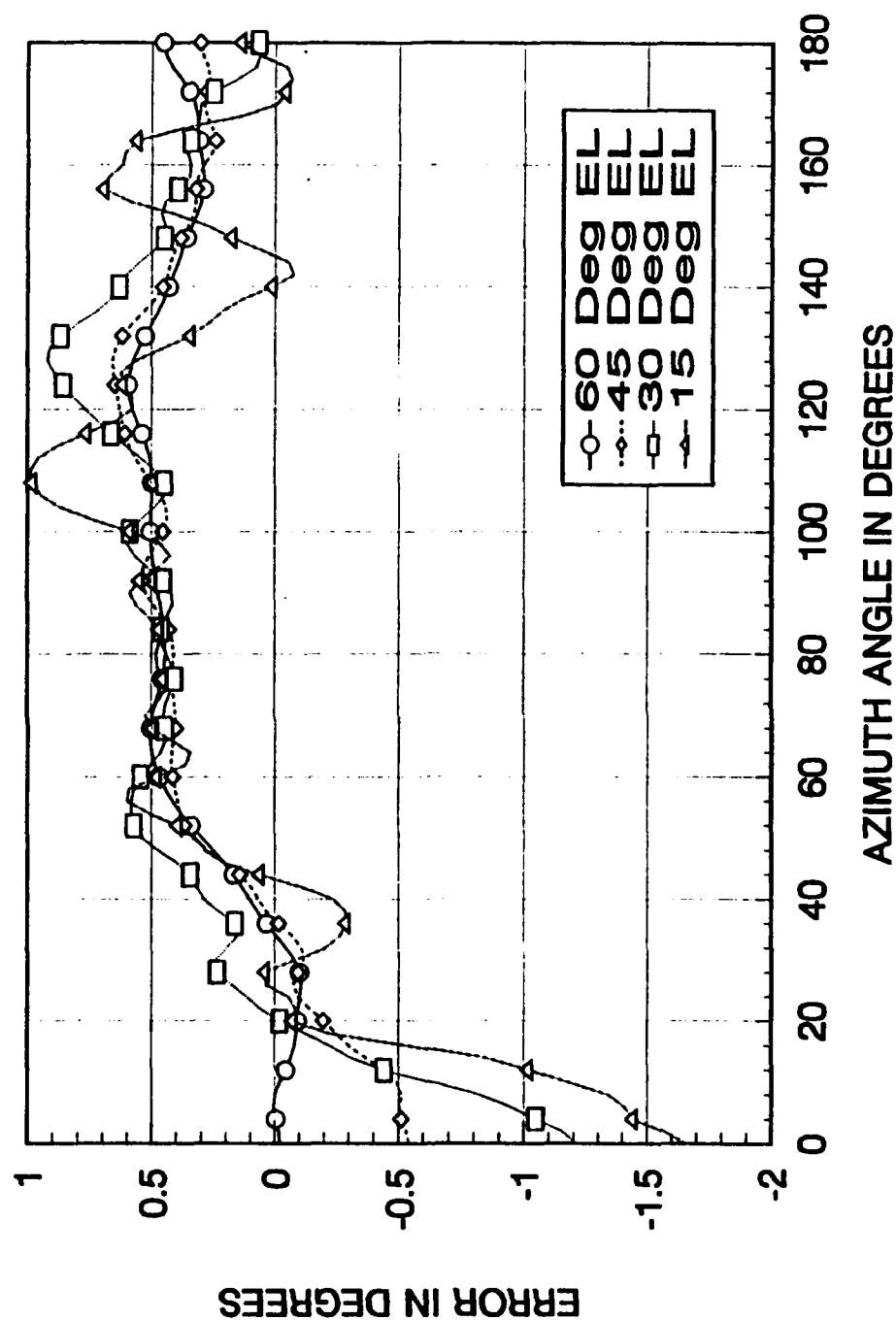
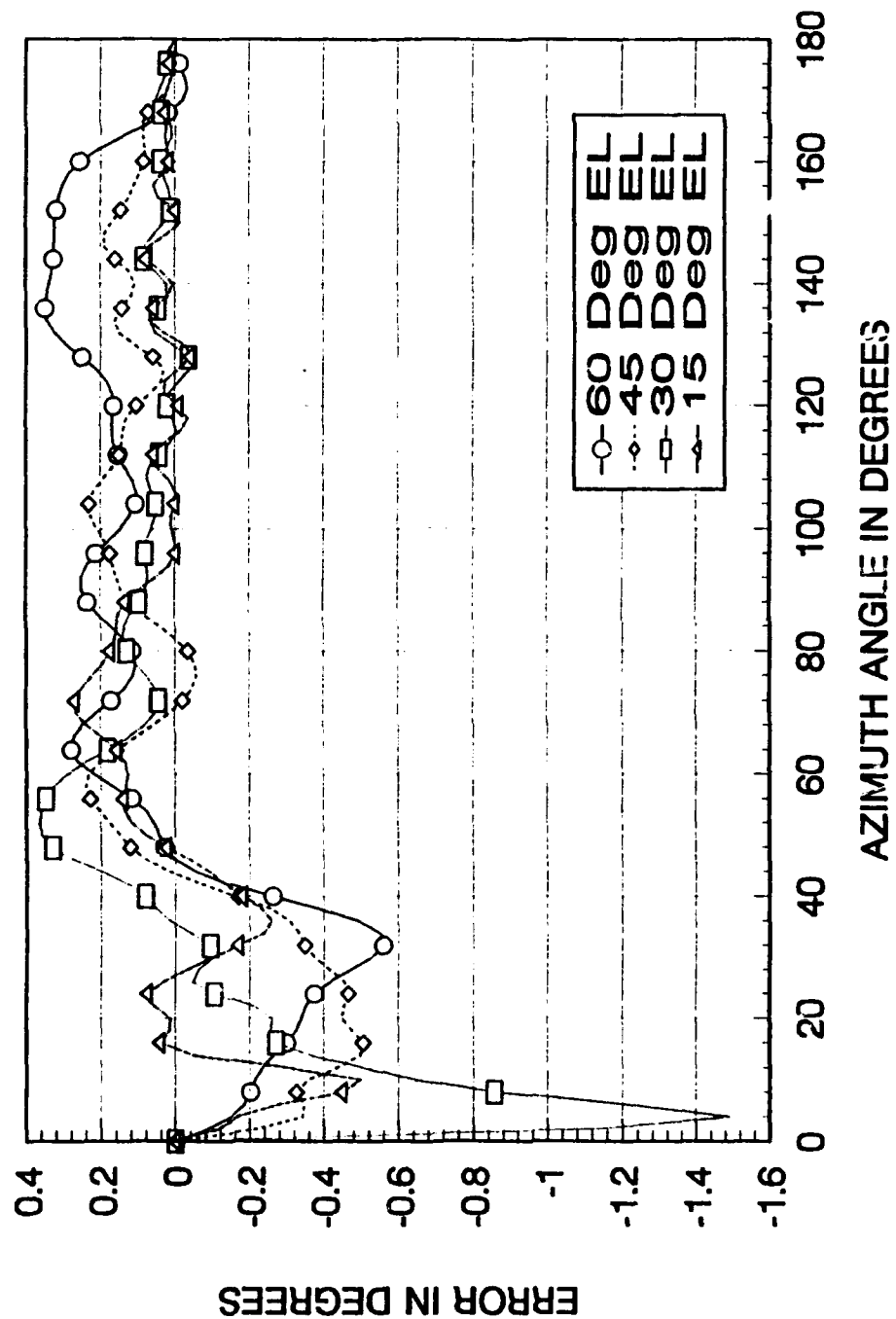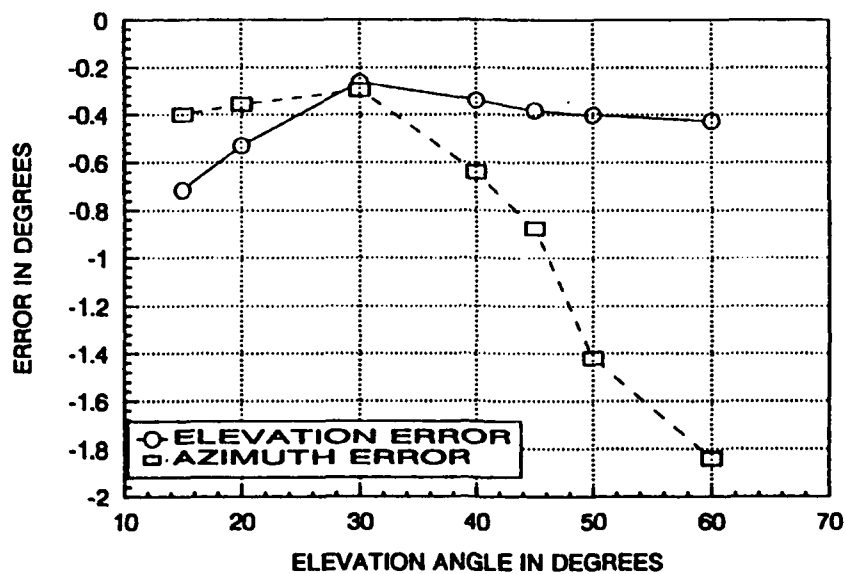**Figure A-17**. SSL Elevation Error at 16 MHz Over Good Ground.

82

Figure A-18. SSL Azimuth Error at 16 MHz Over Good Ground.

Table XIV. WORST CASE ERROR AT 32 MHZ OVER POOR GROUND

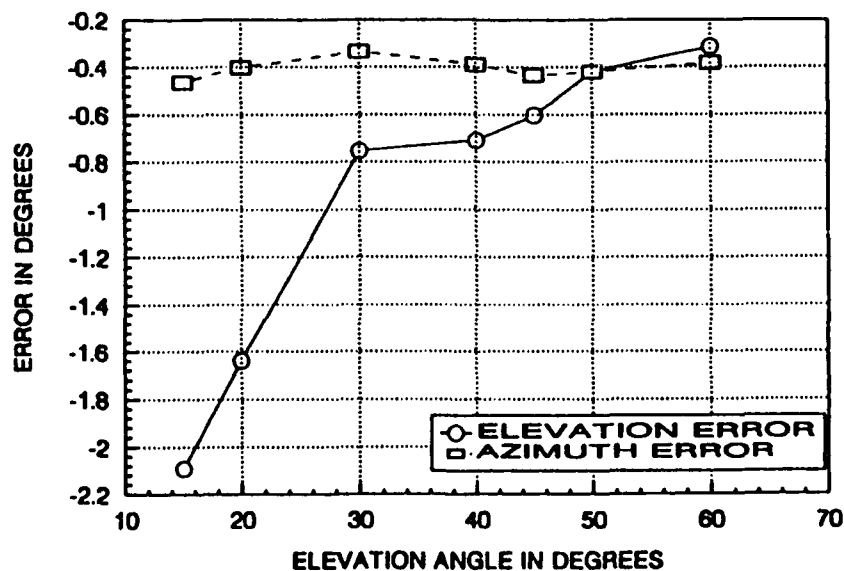| Frequency= 32 MHz			
Poor Ground (ϵ_r= 5, σ= 0.001 S/m)			
Worst Case Azimuth Error at Azimuth Angle ϕ=22°	Elevation Angle	Azimuth Error	Elevation Error
	15°	-0.40°	-0.76°
	20°	-0.36°	-0.53°
	30°	-0.30°	-0.26°
	40°	-0.64°	-0.34°
	45°	-0.88°	-0.38°
	50°	-1.42°	-0.40°
	60°	-1.84°	-0.43°
Worst Case Elevation Error at Azimuth Angle ϕ=4°	Elevation Angle	Azimuth Error	Elevation Error
	15°	-0.46°	-2.09°
	20°	-0.40°	-1.64°
	30°	-0.33°	-0.75°
	40°	-0.39°	-0.71°
	45°	-0.44°	-0.60°
	50°	-0.42°	-0.42°
	60°	-0.38°	-0.31°

Figure A-19. SSL Azimuth and Elevation Error at 32 MHz Over Poor Ground.

85
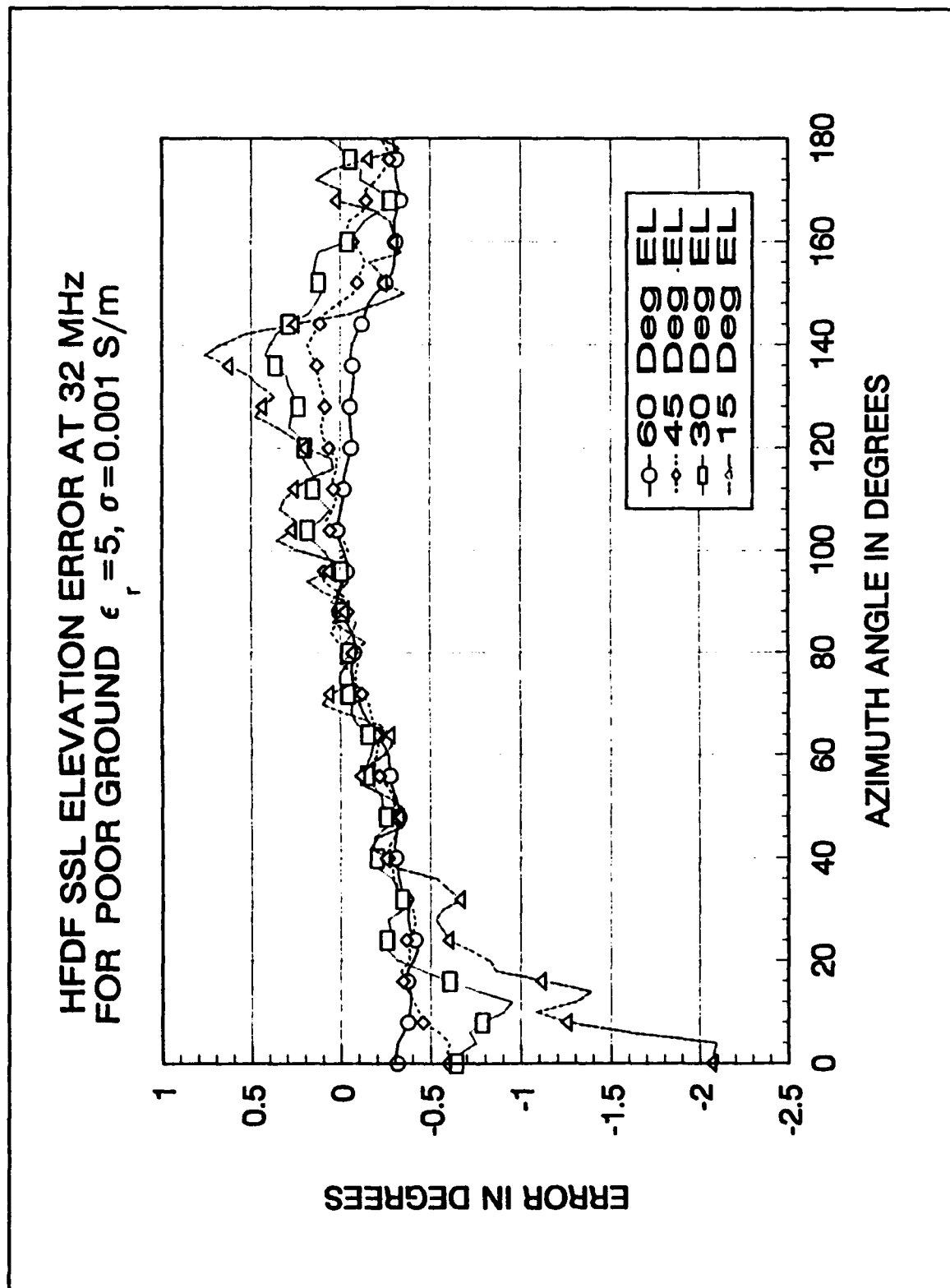
Figure A-20. SSL Elevation Error at 32 MHz Over Poor Ground.
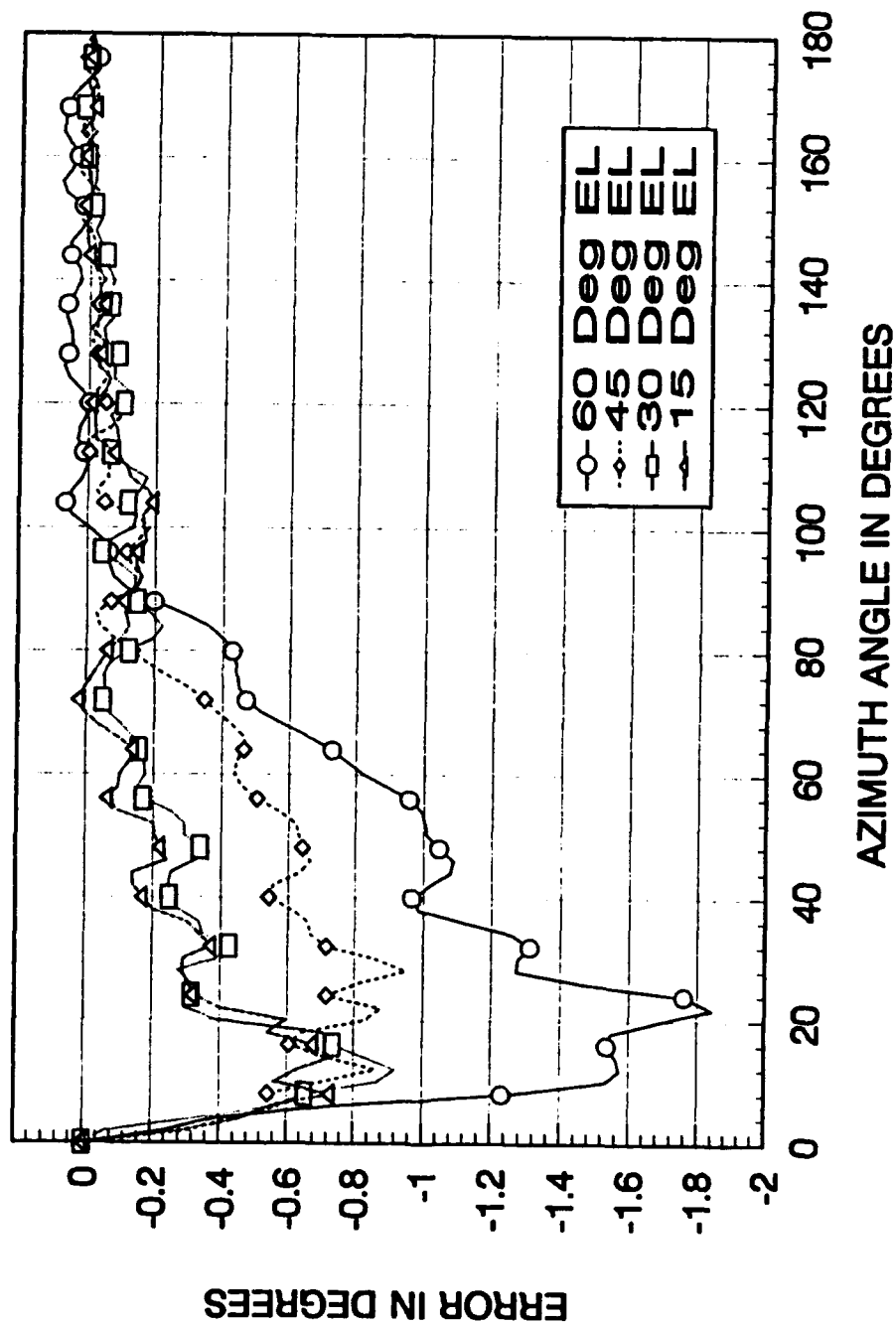
Figure A-21. SSL Azimuth Error at 32 MHz Over Poor Ground.

Table XV. WORST CASE ERROR AT 32 MHZ OVER GOOD GROUND

Frequency= 32 MHz			
Good Ground (ϵ_r= 30, σ= 0.01 S/m)			
	Elevation Angle	Azimuth Error	Elevation Error
Worst Case Azimuth Error at Azimuth Angle ϕ=22°	15°	-0.26°	-0.48°
	20°	-0.17°	-0.32°
	30°	-0.10°	-0.11°
	40°	-0.36°	-0.17°
	45°	-0.47°	-0.19°
	50°	-0.63°	-0.19°
	60°	-0.84°	-0.19°
	Elevation Angle	Azimuth Error	Elevation Error
Worst Case Elevation Error at Azimuth Angle ϕ=4°	15°	-0.29°	-1.44°
	20°	-0.24°	-0.86°
	30°	-0.19°	-0.45°
	40°	-0.23°	-0.40°
	45°	-0.24°	-0.35°
	50°	-0.12°	-0.23°
	60°	0.07°	-0.07°
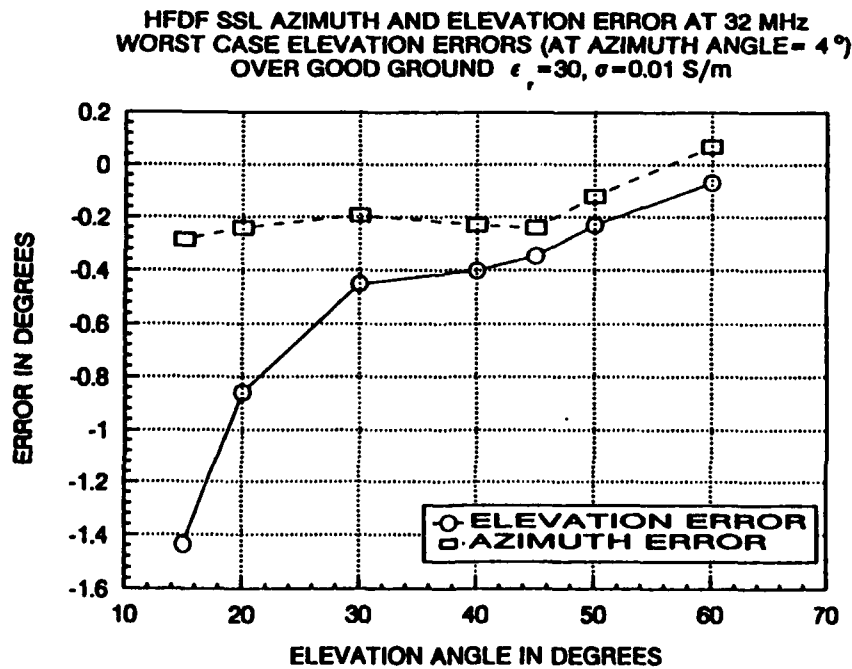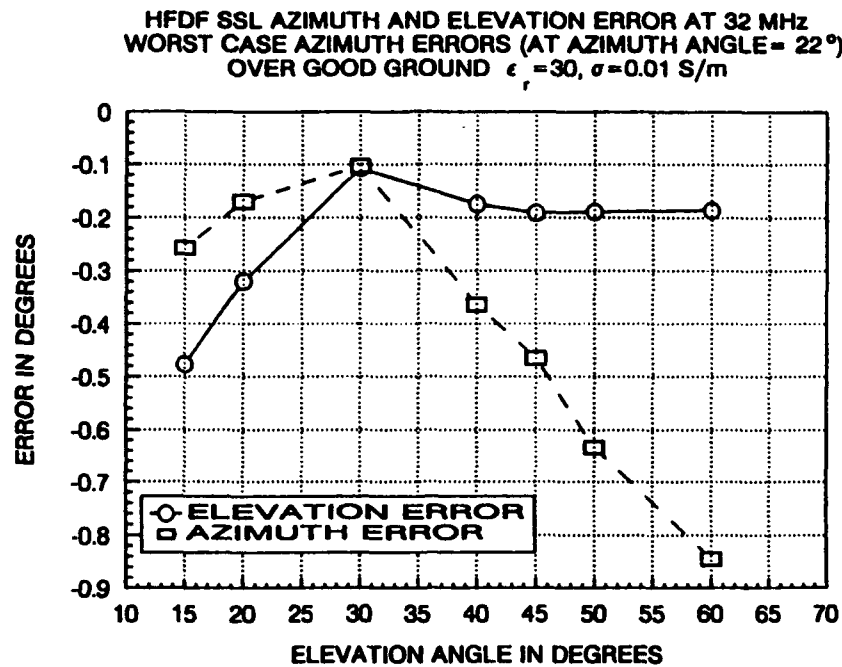
Figure A-22. SSL Azimuth and Elevation Error at 32 MHz Over Good Ground.

89
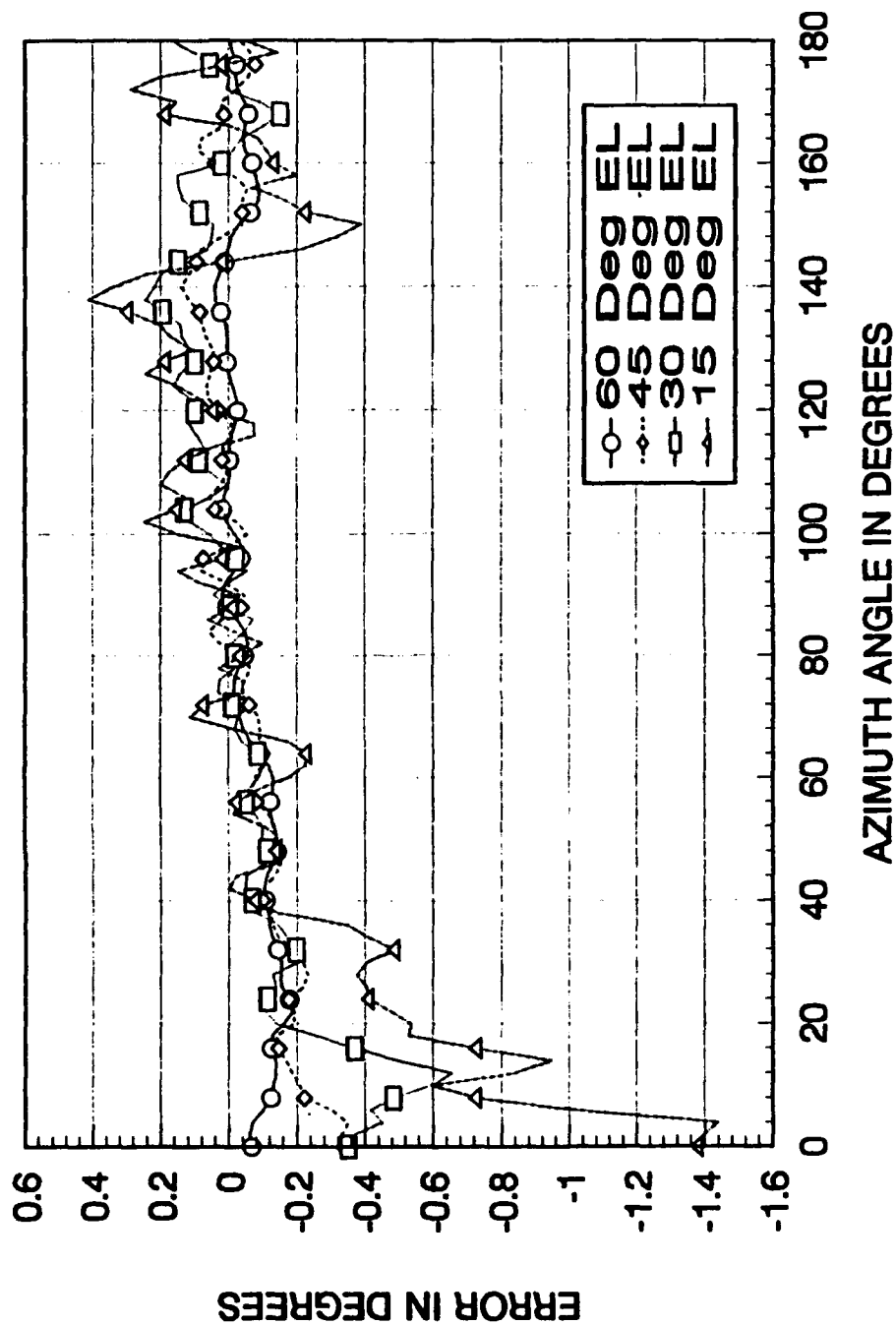
Figure A-23. SSL Elevation Error at 32 MHz Over Good Ground.
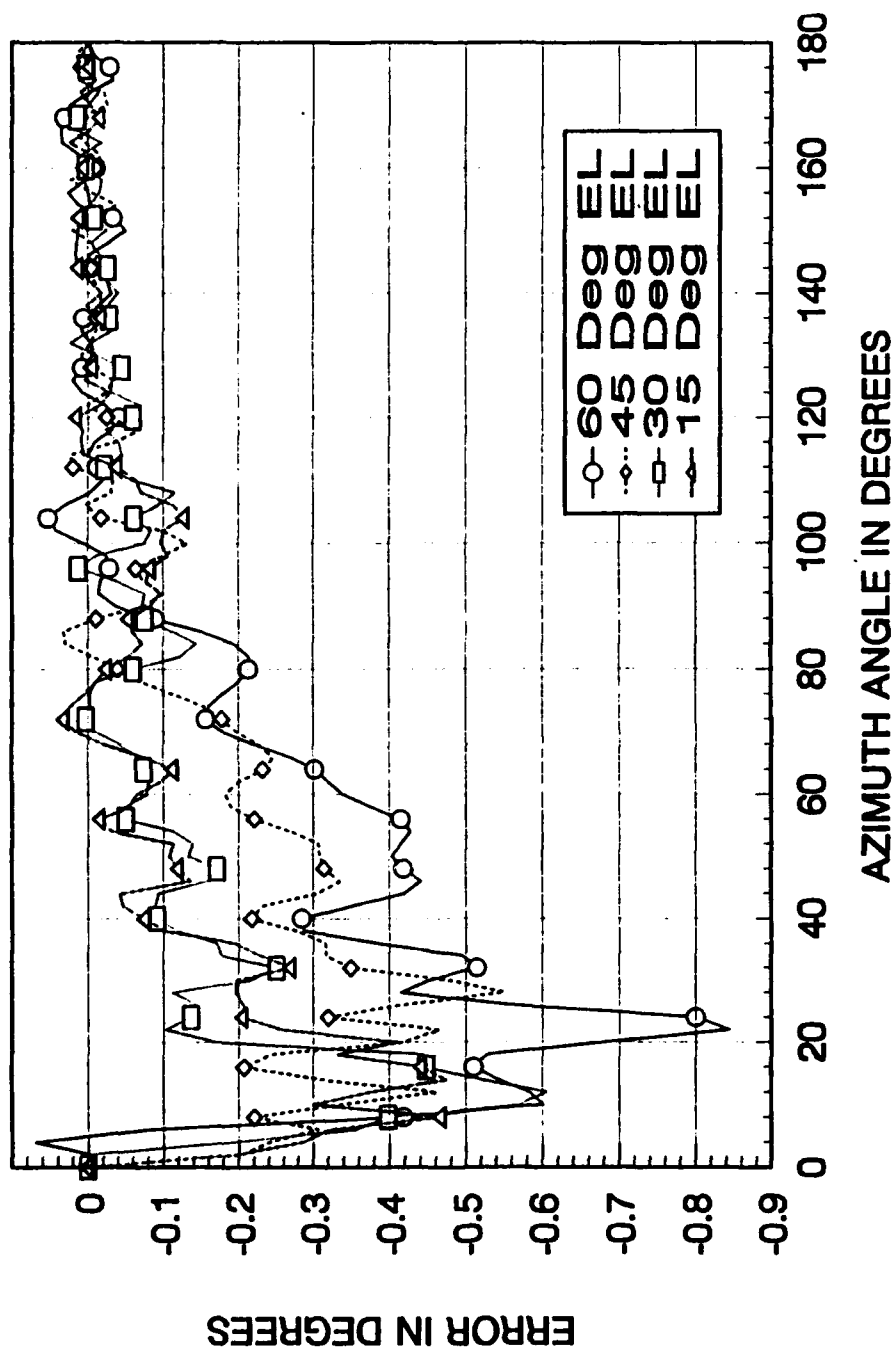
Figure A-24. SSL Azimuth Error at 32 MHz Over Good Ground.

91

APPENDIX B.

AVERAGE POWER GAIN AND INPUT IMPEDANCE.

Table XVI. AVERAGE POWER GAIN OVER PERFECT GROUND

FREQUENCY	AVERAGE POWER GAIN	FREQUENCY	AVERAGE POWER GAIN
2	2.194	18	2.185
3	2.193	19	2.185
4	2.192	20	2.184
5	2.191	21	2.184
6	2.190	22	2.184
7	2.190	23	2.183
8	2.189	24	2.183
9	2.189	25	2.183
10	2.188	26	2.182
11	2.188	27	2.182
12	2.187	28	2.182
13	2.187	29	2.181
14	2.186	30	2.181
15	2.186	31	2.181
16	2.186	32	2.180
17	2.185	33	2.180

Table XVII. AVERAGE POWER GAIN OVER GOOD GROUND

FREQUENCY	AVERAGE POWER GAIN	FREQUENCY	AVERAGE POWER GAIN
2	0.119	18	0.575
3	0.197	19	0.586
4	0.275	20	0.598
5	0.342	21	0.608
6	0.393	22	0.616
7	0.424	23	0.619
8	0.441	24	0.621
9	0.453	25	0.622
10	0.466	26	0.625
11	0.482	27	0.627
12	0.501	28	0.628
13	0.520	29	0.627
14	0.537	30	0.624
15	0.550	31	0.620
16	0.559	32	0.615
17	0.566	33	0.613

Table XVIII. AVERAGE POWER GAIN OVER POOR GROUND

FREQUENCY	AVERAGE POWER GAIN	FREQUENCY	AVERAGE POWER GAIN
2	0.014	18	0.473
3	0.025	19	0.453
4	0.038	20	0.425
5	0.059	21	0.398
6	0.097	22	0.378
7	0.144	23	0.362
8	0.187	24	0.348
9	0.220	25	0.334
10	0.251	26	0.321
11	0.295	27	0.315
12	0.339	28	0.319
13	0.378	29	0.328
14	0.411	30	0.335
15	0.441	31	0.338
16	0.464	32	0.336
17	0.477	33	0.335

Table XIX. INPUT IMPEDANCE FROM 2 TO 33 MHz OVER PERFECT
GROUND.

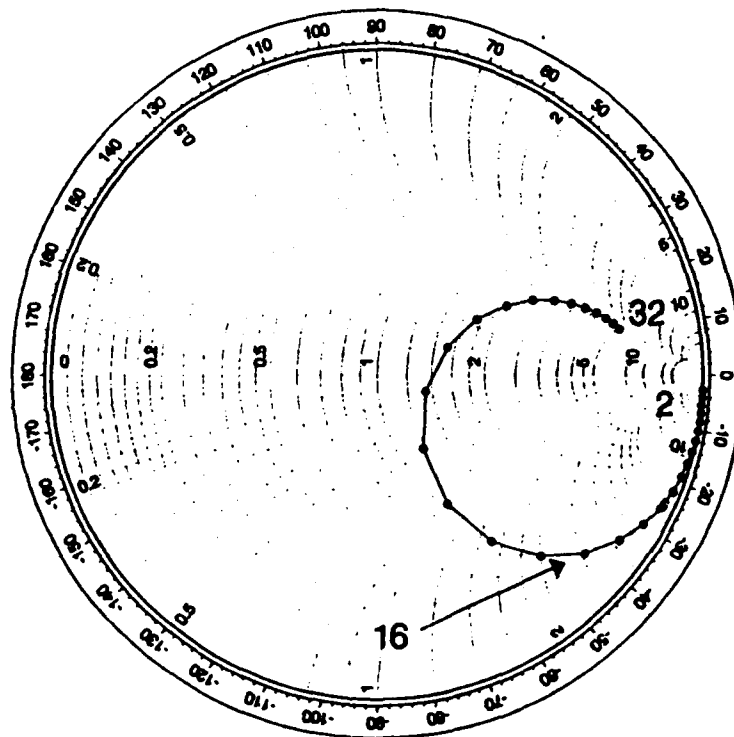| FREQUENCY	INPUT IMPEDANCE	FREQUENCY	INPUT IMPEDANCE
2	0.4-j2189	18	44.6-j75.2
3	0.9-j1445	19	51.3-j51.4
4	1.7-j1069	20	58.7-j28.7
5	2.7-j840	21	66.9-j6.9
6	3.9-j684	22	76.2+j14.1
7	5.4-j570	23	86.5+j34.1
8	7.1-j482	24	98.1+j53.5
9	9.1-j411	25	110.9+j72.2
10	11.5-j353	26	125.1+j90.1
11	14.1-j303	27	141.1+j107
12	17.1-j260	28	158.7+j123
13	20.5-j222	29	178.3+j137
14	24.3-j187	30	199.9+j150
15	28.6-j156	31	223.5+j161
16	33.3-j127	32	249.3+j170
17	38.7-j100	33	276.9+j176

SLEEVE MONOPOLE OVER PERFECT GROUND
2-32 MHz

Figure B-1. Input Impedance of Sleeve Monopole Over Perfect Ground.

Table XX. INPUT IMPEDANCE FROM 2 TO 33 MHz OVER GOOD
GROUND

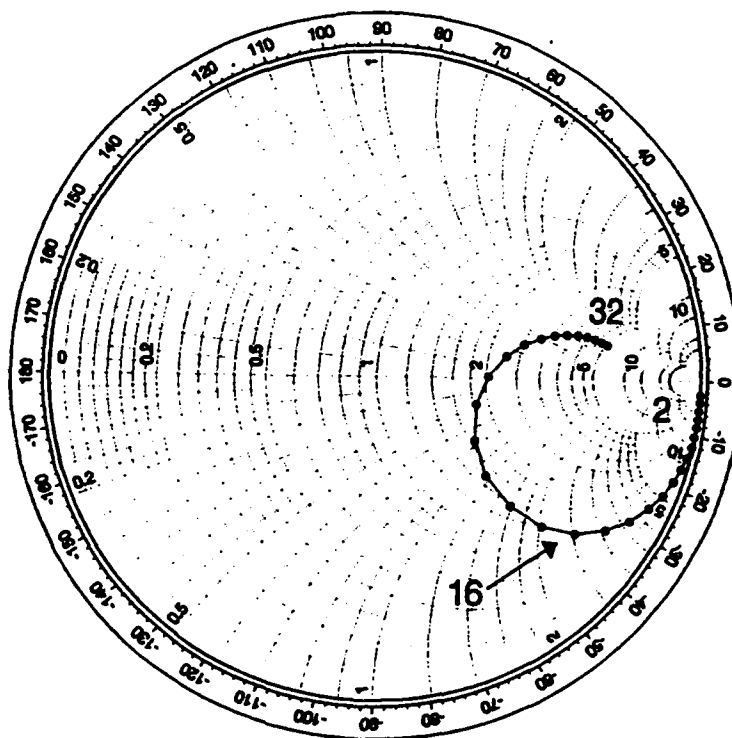| FREQUENCY	INPUT IMPEDANCE	FREQUENCY	INPUT IMPEDANCE
2	4.4-j2187	18	67.1-j79.1
3	5.4-j1444	19	74.7-j57.5
4	6.5-j1067	20	82.8-j36.9
5	7.9-j837	21	91.8-j17.3
6	9.7-j680	22	102.1+j1.2
7	12.1-j565	23	113.7+j18.3
8	15.2-j477	24	126.2+j33.7
9	18.9-j406	25	139.1+j47.6
10	22.9-j348	26	152.5+j60.4
11	27.1-j299	27	166.6+j72.4
12	31.2-j256	28	181.8+j83.3
13	35.7-j220	29	198.2+j93.1
14	40.6-j185	30	215.8+j101
15	46.3-j155	31	234.5+j107
16	52.7-j127	32	254.4+j112
17	59.7-j102	33	258.8+j118

SLEEVE MONOPOLE OVER GOOD GROUND
2-32 MHz

Figure B-2. Input Impedance of Sleeve Monopole Over Good Ground.

Table XXI. INPUT IMPEDANCE FROM 2 TO 33 MHz OVER POOR GROUND.

| FREQUENCY	INPUT IMPEDANCE	FREQUENCY	INPUT IMPEDANCE
2	18.6-j2192	18	68.3-j45.3
3	20.9-j1452	19	94.3-j17.2
4	22.8-j1078	20	125-j2.1
5	22.3-j853	21	150-j0.6
6	19.1-j698	22	165-j3.4
7	17.5-j582	23	173-j3.9
8	17.7-j492	24	179-j1.6
9	19.3-j420	25	185+j1.2
10	21.1-j361	26	188+j3.3
11	22.3-j310	27	189+j7.3
12	23.8-j265	28	190+j16.1
13	26.2-j224	29	193+j28.2
14	29.5-j186	30	200+j40.6
15	34.1-j150	31	210+j52.2
16	40.7-j114	32	223+j62.8
17	51.2-j79.3	33	227+j68.1
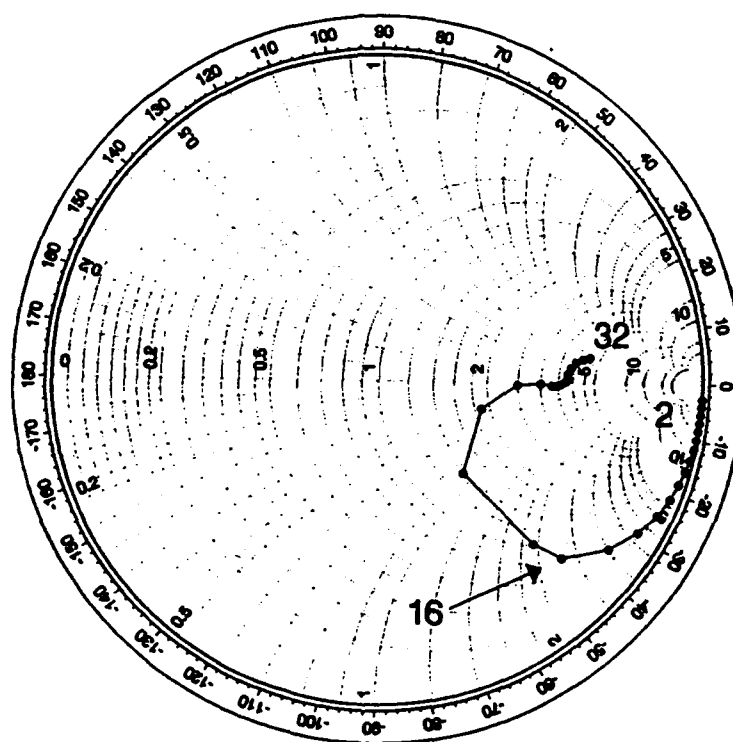
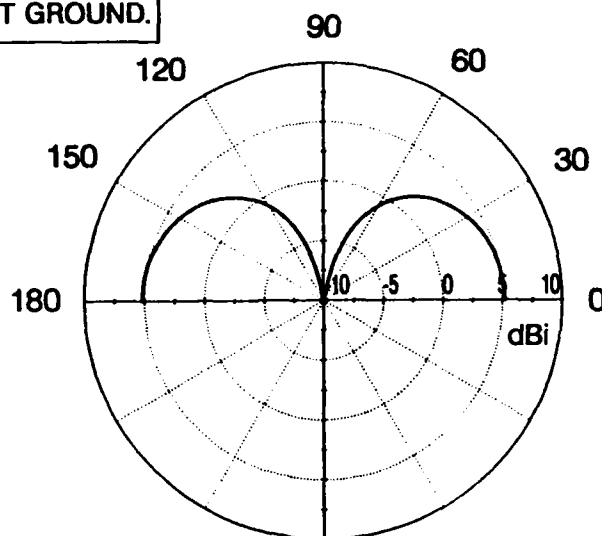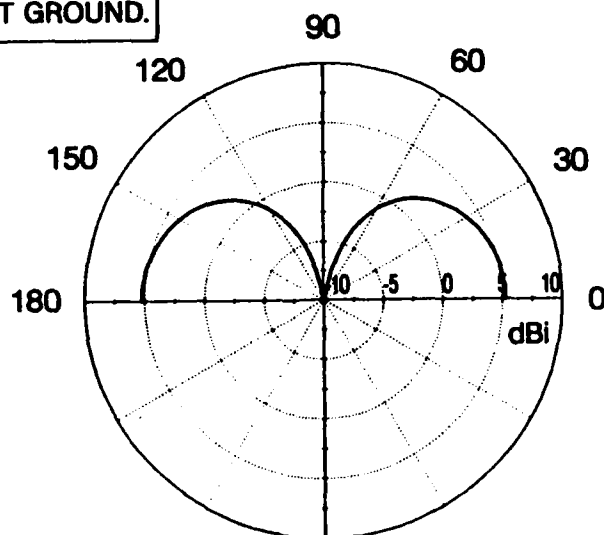**Figure B-3.** Input Impedance of Sleeve Monopole Over Poor Ground.

2 MHz ELEVATION PLANE PATTERN
FOR THE SLEEVE MONOPOLE
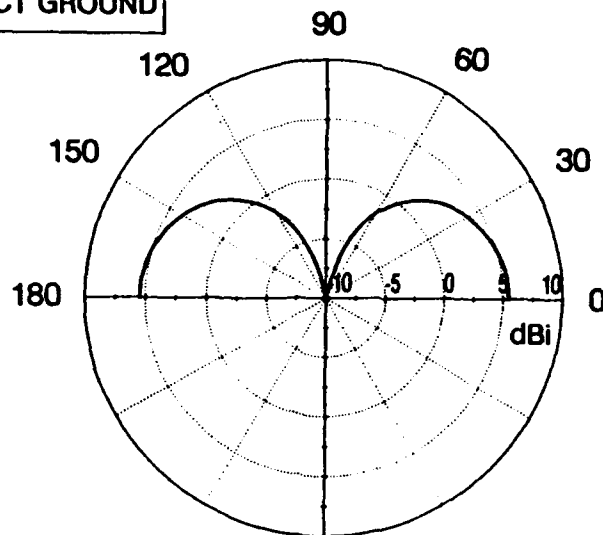OVER PERFECT GROUND.

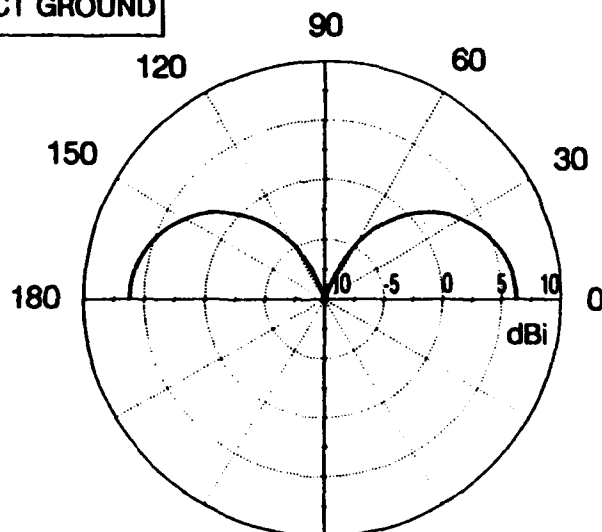8 MHz ELEVATION PLANE PATTERN
FOR THE SLEEVE MONOPOLE
OVER PERFECT GROUND.

Figure B-4. 2 and 8 MHz Elevation Pattern Over Perfect Ground.

**16 MHz ELEVATION PLANE PATTERN
FOR THE SLEEVE MONOPOLE
OVER PERFECT GROUND.**

**32 MHz ELEVATION PLANE PATTERN
FOR THE SLEEVE MONOPOLE
OVER PERFECT GROUND.**

Figure B-5. 16 and 32 MHz Elevation Pattern Over Perfect
Ground.
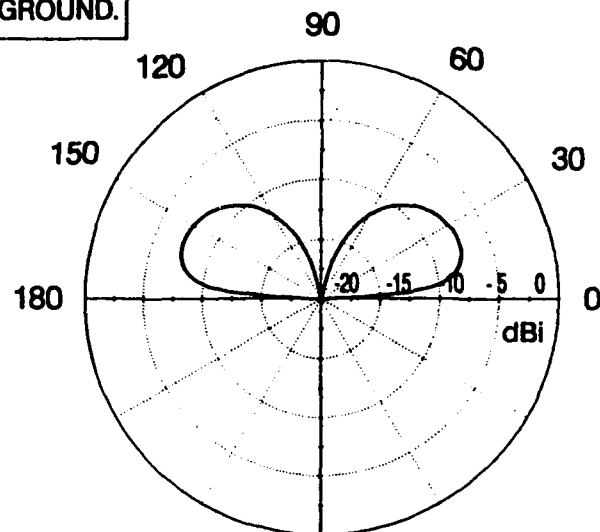
**2 MHz ELEVATION PLANE PATTERN
FOR THE SLEEVE MONOPOLE
OVER GOOD GROUND.**
$\epsilon_r =30$, $\sigma =0.01$ (Siemens/meter)

**8 MHz ELEVATION PLANE PATTERN
FOR THE SLEEVE MONOPOLE
OVER GOOD GROUND.**
$\epsilon_r =30$, $\sigma =0.01$ (Siemens/meter)

Figure B-6. 2 and 8 MHz Elevation Pattern Over Good Ground.

16 MHz ELEVATION PLANE PATTERN
FOR THE SLEEVE MONOPOLE
OVER GOOD GROUND.
$\epsilon_r = 30$, $\sigma = 0.01$ (Siemens/meter)

32 MHz ELEVATION PLANE PATTERN
FOR THE SLEEVE MONOPOLE
OVER GOOD GROUND.
$\epsilon_r = 30$, $\sigma = 0.01$ (Siemens/meter)

Figure B-7. 16 and 32 MHz Elevation Pattern Over Good Ground.

104

2 MHz ELEVATION PLANE PATTERN
FOR THE SLEEVE MONOPOLE
OVER POOR GROUND.
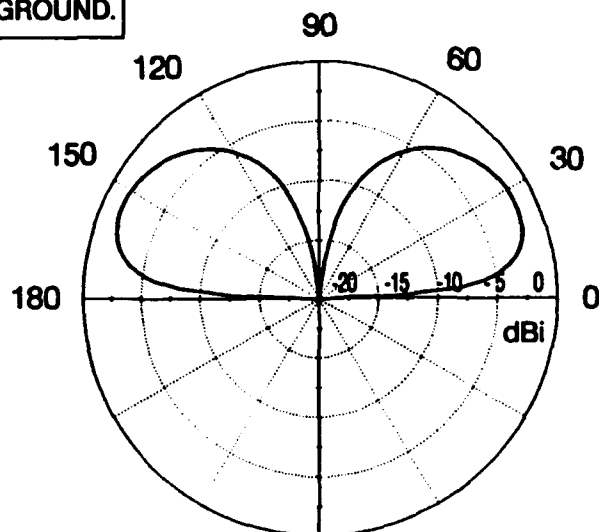$\epsilon_r = 5$, $\sigma = 0.001$ (Siemens/meter)

8 MHz ELEVATION PLANE PATTERN
FOR THE SLEEVE MONOPOLE
OVER POOR GROUND.
$\epsilon_r = 5$, $\sigma = 0.001$ (Siemens/meter)

Figure B-8. 2 and 8 MHz Elevation Pattern Over Poor Ground.
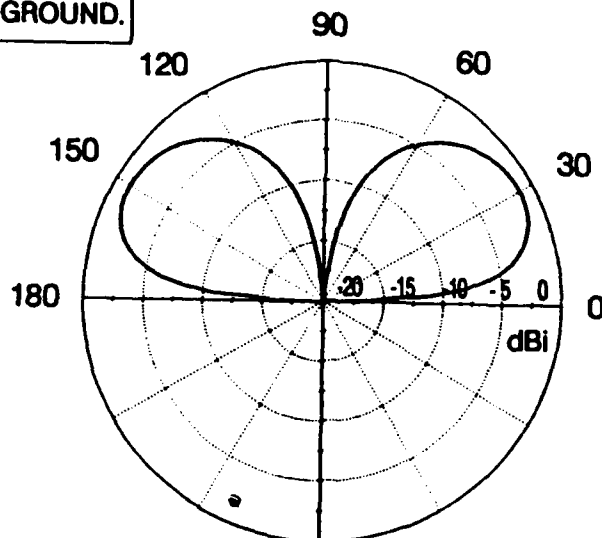
**16 MHz ELEVATION PLANE PATTERN
FOR THE SLEEVE MONOPOLE
OVER POOR GROUND.**
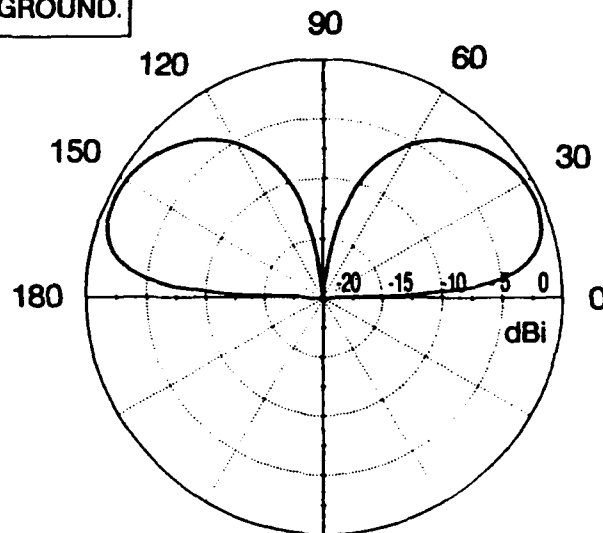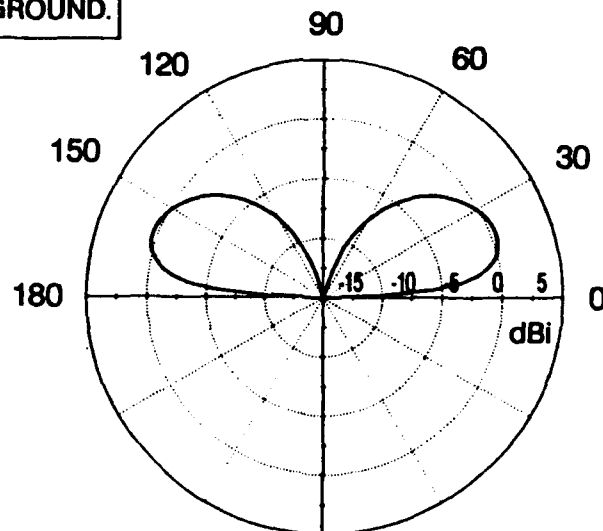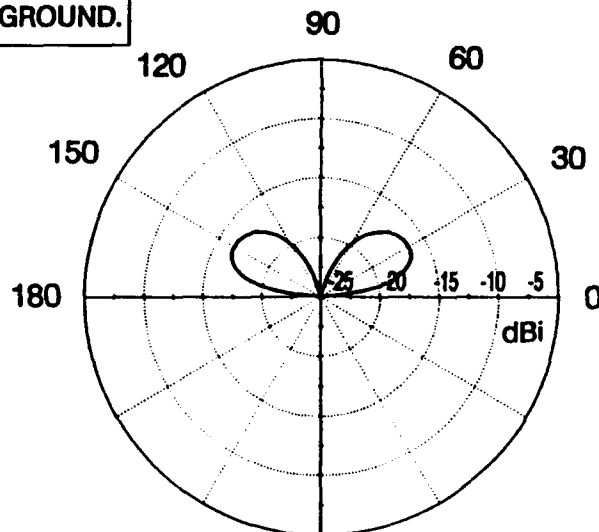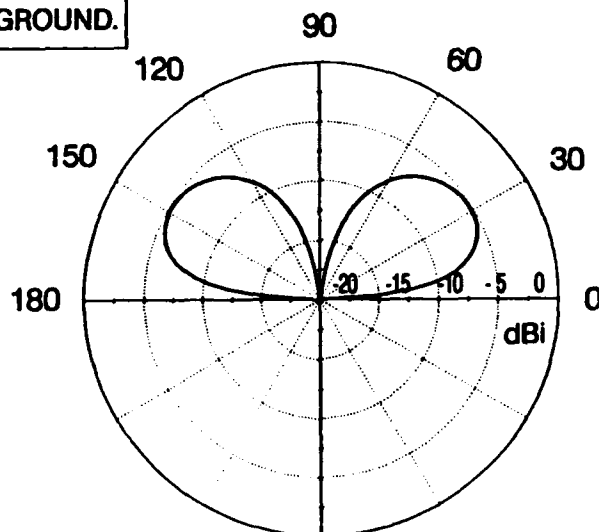$\epsilon_r = 5$, $\sigma = 0.001$ (Siemens/meter)
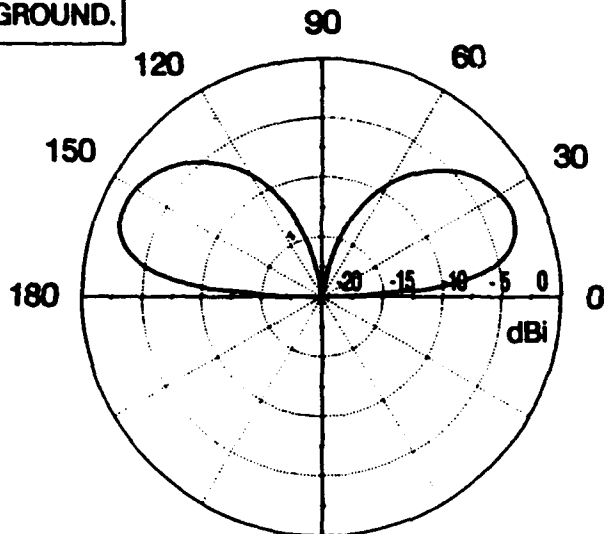
**32 MHz ELEVATION PLANE PATTERN
FOR THE SLEEVE MONOPOLE
OVER POOR GROUND.**
$\epsilon_r = 5$, $\sigma = 0.001$ (Siemens/meter)

Figure B-9. 16 and 32 MHz Elevation Pattern Over Poor Ground.

APPENDIX C.

NEC DATASETS.

```
CM

CM      HFDF SSL ARRAY OF 9 OFF 632 SLEEVE MONOPOLES

CM       WITH SIX 4 METERS GROUND WIRES 6" UNDERGROUND

CM                   OVER FINITE GROUND

CM                   FREQUENCY 2-32 MHZ

CM

CE

            BEGIN TRIPOD GEOMETRY

GW 7,2,-0.8189,0.,0.,-0.6482,0.,0.3414,0.0127

GW 10,3,-0.6482,0.,0.3414,0.,0.,0.3414,0.0127

GW 13,4,-0.6482,0.,0.3414,-0.1189,0.,1.40,0.0127

GW 16,1,-0.1189,0.,1.40,0.,0.,1.40,0.0127

            BEGIN UNDERGROUND WIRE GEOMETRY

GW 20,2,0.0,0.0,-0.1524,-0.8189,0.0,-0.1524,0.01

GW 23,6,-0.8189,0.0,-0.1524,-4.0,0.0,-0.1524,0

GC 0,0,1.5,0.01,0.01

GW 26,1,-0.8189,0.0,-0.1524,-0.8189,0.0,0.0,0.01

GW 29,2,0.0,0.0,-0.1524,0.8189,0.0,-0.1524,0.01

GW 32,6,0.8189,0.0,-0.1524,4.0,0.0,-0.1524,0
```

```
GC 0,0,1.5,0.01,0.01
                  STRUCTURE TO BE ROTATED 3 TIMES
GR 0,3
                  BEGIN SLEEVE MONOPOLE GEOMETRY
GW 1,5,0.,0.,^.8316,0.,0.,3.9905,0.0127
GW 2,5,0.,0.,1.6378,0.,0.,2.8316,0.0254
GW 3,1,0.,0.,1.5013,0.,0.,1.6378,0.0254
GW 4,1,0.,0.,1.40,0.,0.,1.5013,0.01905
GW 5,5,0.,0.,0.3414,0.,0.,1.40,0.01905
GW 6,2,0.,0.,0.,0.,0.,0.3414,0.0127
                  END #1 ANTENNA GEOMETRY
GW 19,1,0.0,0.,-0.1524,0.0,0.0,0.0,0.0127
                  CREATE ANTENNA # 2
GM 200,1,0.,0.,0.,3.182,-3.182,0.,001.032
                  CREATE ANTENNA # 3
GM 300,1,0.,0.,0.,3.182,+3.182,0.,001.032
                  CREATE ANTENNA # 4
GM 400,1,0.,0.,0.,-9.191,+9.191,0.,001.032
                  CREATE ANTENNA # 5
GM 500,1,0.,0.,0.,-9.191,-9.191,0.,001.032
                  CREATE ANTENNA # 6
GM 600,1,0.,0.,0.,+26.725,-26.725,0.,001.032
                  CREATE ANTENNA # 7
GM 700,1,0.,0.,0.,+26.725,+26.725,0.,001.032
                  CREATE ANTENNA # 8
GM 800,1,0.,0.,0.,-73.54,+73.54,0.,001.032
```

CREATE ANTENNA # 9

GM 900,1,0.,0.,0.,-73.54,-73.54,0.,001.032

GOOD GROUND CONDITIONS

GE -1

GN 2,0,0,0,20.00,0.030   (E=30,S=0.01 S/M)

FR 0,1,0,0,16.00,0.,0

PT 8,3,1,0   RECEIVING CURRENTS IN ANTENNA # 1

EX 1,1,91,0,45.,0.,0.,0.,2.,0.,

XQ

PT 8,203,1,0   RECEIVING CURRENTS IN ANTENNA # 2

EX 1,1,91,0,45.,0.,0.,0.,2.,0.,

XQ

PT 8,303,1,0   RECEIVING CURRENTS IN ANTENNA # 3

EX 1,1,91,0,45.,0.,0.,0.,2.,0.,

XQ

PT 8,403,1,0   RECEIVING CURRENTS IN ANTENNA # 4

EX 1,1,91,0,45.,0.,0.,0.,2.,0.,

XQ

PT 8,503,1,0   RECEIVING CURRENTS IN ANTENNA # 5

EX 1,1,91,0,45.,0.,0.,0.,2.,0.,

XQ

PT 8,603,1,0   RECEIVING CURRENTS IN ANTENNA # 6

EX 1,1,91,0,45.,0.,0.,0.,2.,0.,

XQ

PT 8,703,1,0   RECEIVING CURRENTS IN ANTENNA # 7

EX 1,1,91,0,45.,0.,0.,0.,2.,0.,

```
XQ

PT 8,803,1,0                    RECEIVING CURRENTS IN  ANTENNA # 8

EX 1,1,91,0,45.,0.,0.,0.,2.,0.,

XQ

PT 8,903,1,0                    RECEIVING CURRENTS IN  ANTENNA # 9

EX 1,1,91,0,45.,0.,0.,0.,2.,0.,

XQ

EN                                        END NEC DATASET
```

LIST OF REFERENCES

1. Leo F. McNamara, *The Ionosphere: Communications, Surveillance, and Direction Finding,* Krieger Publishing Company, Malabar, Florida, 1991.

2. Hernodon H. Jenkins, *Small-Aperture Radio Direction Finding,* Artech House Inc., Norwood, MA, 1991.

3. *The Numerical Electromagnetics Engineering Design System,* Version 2.0, Distributed by: The Applied Computational Electromagnetics Society, June 1989.

4. *Additions for NPS Versions of NEC,* Technical Document 116, Volume 2, Prepared by Lawrence Livermore Laboratory (Report UCID 18834), modified by Prof. R.W. Adler.

5. C.A.Balanis, *Antenna Theory - Analysis and Design,* John Wiley & Sons, New York, 1982.

6. P.J.D. Gething, *Radio Direction Finding and Superresolution,* Peter Pelegrinus Ltd., Herts, United Kingdom, 1991.

7. R.E. Franks, "Direction-Finding Antennas," in Y.T.Lo, S.W.Leo, *Antenna Handbook*, chapter 25, pp 1-26, Van Nostrand Reinold Company Inc., 1988.

8. Hugh D. Kennedy, William Wharton, "Direction-Finding Antennas and Systems," in Richard C. Johnson, Henry Jasik, *Antenna Engineering Handbook,* chapter 39, pp 2-33, McGraw-Hill Book Company, New York, 1961.

9. David W. Horner, "Specification, Calibration and Testing of Phase Interferometers," *Microwave Journal*, pp 139-155, February 1988.

10. A.R Baron, K.P. Davis, C.P. Hofmann, "Passive Direction Finding and Signal Location," pp 59-76, *Microwave Journal*, September, 1982.

11. Richard Groller, "Single Station Location HF Direction Finding," *Journal of Electronic Defence*, pp 58-83, June 1990.

12. W. Ross, E.N. Bramley, G.E. Ashwell, "A Phase Comparison Method of Measuring the Direction of Arrival of Ionospheric Radio Waves," *The Proceedings of the Institution of Electrical Engineers*, Volume 98, Part III Number 54, pp 294-301, London, July 1951.

13. C.W. Earp, R.M. Godfrey, "Radio Direction Finding by the Cyclical Differential Measurement of Phase," *The Journal of the Institution of Electrical Engineers*, Volume 94, Part IIIA. Radiocommunication, pp 705-721, London, 1947.

14. David Louis Prisaznick, *Technical Evaluation of a Radio Direction Finding System Utilizing Complementary Sequence Phase Coding of Incident Signals,* M.S. Thesis, pp 13-22, Naval Postgraduate School, Monterey, CA, June 1973.

15. Richard Clark Todaro, *An Approach to Direction Finding Involving the Phase Coding of the Received Signal Utilizing Complementary Sequences,* M.S. Thesis, pp 8-11, Naval Postgraduate School, Monterey, CA, June 1972.

16. Harry Thornberry Schiantarelli, *Performance Analysis of High Frequency Single-Site-Location Antenna Arrays Using Numerical Electromagnetic Modeling,* M.S. Thesis, Naval Postgraduate School, Monterey, CA, September 1990.

17. Technical Manual for the AN/TSQ 161(V) SSL System, October 1990.

18. R.G. Stansfield, "Statistical Theory of D.F. Fixing," *The Journal of the Institution of Electrical Engineers*, Volume 94, Part IIIA. Radiocommunication, pp 762-770, London, 1947.

19. Richard L. Johnson, "Eigenvector Matrix Partition and Radio Direction Finding Performance," *IEEE Transactions on Antennas and Propagation*, Volume 34, No.8, pp 985-991, August 1986.

20. Ralph O. Schmidt, "Multiple Source DF Signal Processing: An Experimental System," *IEEE Transactions on Antennas and Propagation*, Volume 34, No.3, pp 281-290, March 1986.

21. Alan J. Fenn, "Theoretical and Experimental Study of Monopole Phased Array Antennas," *IEEE Transactions on Antennas and Propagation*, Volume 33, No.10, pp 1118-1126, October 1985.

22. Benjamin Friedlander, "Direction Finding in the Presence of Mutual Coupling," *IEEE Transactions on Antennas and Propagation*, Volume 39, No.3, pp 273-284, March 1991.

23. R.A. Perrott, "The Effects of Mutual Coupling on Interferometer Accuracy," *Fourth International Conference on Antennas and Propagation*, pp 273-284, University of Warwick, Coventry, UK, April 1985.

24. Mitsuo Taguchi, "Sleeve Antenna with Ground Wires," *IEEE Transactions on Antennas and Propagation*, Volume 39, No.1, pp 1-7, January 1991.

25. R.C. Fenwick, "H-F Antenna Selection," *Engineering Compendium*, pp 2-13, Collins Radio Company, Dallas, Texas, 1969.

26. D. Curtis Schleher, *Introduction to Electronic Warfare*, Artech House Inc., Norwood, MA, 1990.

INITIAL DISTRIBUTION LIST

No. Copies

1. Defense Technical Information Center   2
   Cameron Station
   Alexandria, Virginia 22304-6145

2. Library, Code 52   2
   Naval Postgraduate School
   Monterey, CA 93943-5002

3. Chairman, Code EC   1
   Department of Electrical and Computer Engineering
   Naval Postgraduate School
   Monterey, CA 93943-5000

4. Dr. Richard W. Adler, Code EC/Ab   5
   Department of Electrical and Computer Engineering
   Naval Postgraduate School
   Monterey, CA 93943-5000

5. Prof. Wilbur R. Vincent, Code EC/Ab   1
   Department of Electrical and Computer Engineering
   Naval Postgraduate School
   Monterey, CA 93943-5000

6. Commander   3
   Naval Security Group
   Attn: G40 (CDR G.K. Lott)
   3801 Nebraska Ave, N.W,
   Washington, DC 20390

7. Mr. George Hagn   1
   SRI International
   1611 Kent St
   Arlington, VA 22209-2111

8. Dr. James K. Breakall   1
   Penn State University
   306 EE East
   University Park, PA 16802

9. Mr. Robert M. Rose   1
   NCCOSC/NRaD, Code 542
   San Diego, CA 92152-5000

10. Mr. Robert Riegel   1
    SR 1778
    Ridge, MD 20680

11.   Embassy of Greece   3
      Naval Attache
      2228 Massachusetts Ave., N.W.,
      Washington D.C., 20008

12.   Lieutenant Gerasimos Dionisios Milatos   1
      29 Menelaou Str.,
      Kallithea, 17672
      Athens, GREECE